Available online at www.sciencedirect.com
SCIENCE DIRECT
Coordination Chemistry Reviews 249 (2005) 2691–2729
COORDINATION CHEMISTRY REVIEWS
www.elsevier.com/locate/ccr

Review

Design of single chain magnets through cyanide-bearing six-coordinate complexes

Rodrigue Lescouëzec [a], Luminita Marilena Toma [a], Jacqueline Vaissermann [b], Michel Verdaguer [b], Fernando S. Delgado [c], Catalina Ruiz-Pérez [c], Francesc Lloret [a], Miguel Julve [a,*]

[a] *Departament de Química Inorgánica/Instituto de Ciencia Molecular, Facultat de Química de la Universitat de València, Avda. Dr. Moliner 50, 46100-Burjassot, València, Spain*
[b] *Laboratoire de Chimie Inorganique et Matériaux Moléculaires, Unité CNRS 7071, Université Pierre et Marie Curie, 4 Place Jussieu, F75252-Paris, France*
[c] *Laboratorio de Rayos X y Materiales Moleculares, Departamento de Física Fundamental II, Facultad de Física de la Universidad de La Laguna, Avda. Francisco Sánchez s/n, 38204 La Laguna, Tenerife, Spain*

Contents

Abstract

The design and preparation of stable cyanide-bearing six-coordinate complexes of formula $[M^{III}(L)(CN)_x]^{(x+l-m)-}$ (M = trivalent transition metal ion and L = polydentate blocking ligand) are summarized here. Their use as ligands towards either fully hydrated metal ions or coordinatively

Abbreviations: bipy, 2,2′-bipyridine; phen, 1,10-phenanthroline; bpym, 2,2′-bipyrimidine; dpa, 2,2′-dipyridylamine; pyim, 2-(2-pyridyl)imidazole; ampy, 2-aminomethylpyridine; en, ethylenediamine; dmbpy, 4,4′-dimethyl-2,2′-bipyridine; Hacac, acetylacetone; terpy, 2,2′:6′,2″-terpyridine; bpca$^-$, bis(2-pyridylcarbonyl)amidate; tacn, 1,4,7-triazacyclononane; Me_3tacn, 1,4,7-trimethyltriazacyclononane; $HB(pz)_3^-$, hydrotris(1-pyrazolyl)borate; PPh_4^+, tetraphenylphosphonium; $AsPh_4^+$, tetraphenylarsonium; tach, 1,3,5-triaminocyclohexane; $B(pz)_4^-$, tetrakis(1-pyrazolyl)borate; tetren, tetraethylenepentaamine; MeOsalen^{2-}, *N*,*N*′-ethylenebis(3-methoxysalicylideneiminate); H_2L^1, 11,23-dimethyl-3,7,15,19-tetraazatricyclo[19.3.1.1^{9,13}]hexacosa-2,7,9,11,13(26),14,19,21(25),22,24-decaene-25,26-diol; dmphen, 2,9-dimethyl-1,10-phenanthroline; H_2apox, *N*,*N*′-bis(3-aminopropyl)oxamide; impy, 2-(2-pyridyl)-4,4,5,5-tetramethyl-4,5-dihydro-1H-imidazolyl-1-oxy; H_2bqm, *N*,*N*′-bis(quinolyl)malonamide; H_2pbqm, *N*,*N*′-bis(quinolyl)dibenzylmalonamide; NEt_4^+, tetraethylammonium; $NBut^+$, tetra-*n*-butylammonium; ox^{2-}, oxalate; saltmen^{2-}, *N*,*N*′-1,1,2,2-tetramethylethylenebis(salicylideneiminate); Hhfac, hexafluoroacetylcacetone; NITPhOMe, 4′-methoxyphenyl-4,4,5,5-tetramethylimidazoline-1-oxy-3-oxide; pao$^-$, pyridine-2-aldoximate; bt, 2,2′-bithiazoline; 2,4,6-tmpa^{2-}, *N*-2,4,6-trimethylphenyloxamate dianion; pbaOH^{2-}, *N*,*N*′-2-hydroxy-1,3-propylenebis(oxamate); $HPhSeO_2$, benzeneseleninic acid; 5-Brsalen^{2-}, *N*,*N*′-ethylenebis(5-bromosalicylideneiminate); 5-MeOsalen^{2-}, *N*,*N*′-ethylenebis(5-methoxysalicylideneiminate); L^2, 6-methyl-1,4,8,11-tetraazacyclotetra-decan-6-amine; L^3, 10-methyl-1,4,8,12-tetraazacyclopentadecan-10-amine

* Corresponding author. Tel.: +34 96 354 4856; fax: +34 96 3544322.
E-mail address: miguel.julve@uv.es (M. Julve).

0010-8545/$ – see front matter
doi:10.1016/j.ccr.2005.09.017

unsaturated preformed species, to afford a wide variety of low-dimensional metal assemblies whose nuclearity, dimensionality and magnetic properties can be tuned, is also reviewed. Special emphasis is put on the appropriate choice of the end-cap ligand L whose denticity determines the number of coordinated cyanide groups in the mononuclear precursors. Among the different new spin topologies obtained through this rational synthetic strategy, ferromagnetically coupled 4,2-ribbon like bimetallic chains which exhibit slow magnetic relaxation and hysteresis effects (chain as magnets) are one of the most appealing and constitute the heart of the present contribution.

Keywords: Cyanocomplexes; Preparation; Crystal structures; Polynuclear complexes; Bimetallic chains; Chains as magnets; Magnetic properties

1. Introduction

Several recent reviews have been devoted to the chemistry of cyanide-bridged metal complexes [1–5] illustrating the popularity of these old but evergreen systems. One of the keypoints of the cyanide group is its ability to link two different metal ions when acting as a bridge, a quality which is related to its asymmetric character. A large number of cyanide-bridged compounds which are known, show a wide range of applications such as catalysts [6,7], ion exchangers [8], molecular sieves [9–12], hosts for small molecules and ions [1,13,14], photosensitizers [15], room temperature magnets [16–21], electrochemically tunable magnets [22,23], photomagnetism [22,24–31] and magneto-optics [32,33]. Among this family, the Prussian blue-like phases of general formula $C_nA_p[B(CN)_6]_q{\cdot}xH_2O$ (C is a univalent cation; A and B are six-coordinate transition metal ions which are high- and low-spin ions, respectively) have caught the eyes of scientists interested in magnetic studies [34]. These compounds exhibit well known cubic phases, where A ocupies all the summits and all the centres of the faces, $[B(CN)_6]$ fills the octahedral sites and C can be inserted in some of the tetrahedral holes. Because of the high symmetry of their structures, the prediction of the nature of the exchange interaction between the A and B metal sites through the linear A–NC–B fragment which develops in the three directions is an easy task. Let us visualize the three different cases for magnetic coupling in the linear A–NC–B fragment. As only the low-lying t_{2g} orbitals are occupied for B (d^n B ion with $n > 6$ is unknown for $[B(CN)_6]$), the nature of the magnetic coupling between A and B depends on the electronic configuration of A. Three cases are possible: (i) if all the unpaired lectrons of A occupy t_{2g} type orbitals, the A–B interaction is antiferromagnetic leading to a ferrimagnet when the local magnetic moments are not compensated; (ii) if the unpaired electrons of A lie in both t_{2g} and e_g orbitals, the A–B interaction is also antiferromagnetic (ferrimagnet) but of weaker magnitude than in (i) because of the ferromagnetic contributions arising from the strict orthogonality between the t_{2g} (at B) and e_g (at A) orbitals; (iii) finally, if the unpaired electrons of A occupy e_g orbitals, the A–B interaction is ferromagnetic (case of strict orthogonality between the magnetic orbitals) and the resulting compound will be a ferromagnet. These orbital considerations were succesfully applied by Verdaguer and coworkers in long term work to push the Curie temperature (T_c) from 5.6 K in Prussian blue itself to 315 K in the compound $V^{II}_{0.42}V^{III}_{0.58}[Cr(CN)_6]_{0.86}{\cdot}2.8H_2O$ [17]. This compound is the first rationally synthesized molecule-based magnet whose T_c value is above room temperature. This temperature was later increased by improving the crystallinity of the sample or by changing the stoichiometry to increase the number of magnetic neighbours. So, following analogous recipes and using the same chemicals, Miller et al. were able to push the value of T_c up to 373 K [21]. Also Girolami et al., using a sol–gel approach, prepared a sample with a stoichiometry close to $K^I_1V^{II}_1Cr^{III}_1$ whose T_c is equal to 376 K (that is above the boiling temperature of water) [20].

Nowadays, one of the most remarkable aspects of the Prussian blue phases from a magnetic point of view lies in the fact that it is possible to predict the nature of the interaction and also to estimate the value of T_c by using simple orbital models which are based on the symmetry of the magnetic orbitals (singly occupied molecular orbitals) [35]. This is a very important point for the chemist because he needs simple tools to orient his preparative work towards the wanted products overcoming thermodynamics and kinetics that often impose their rules leading to undesired materials.

As our knowledge of Prussian blue and its analogues becomes deeper, chemists are more and more interested in lower dimensionality cyanide-bridged compounds, that is to enter into the molecular regime. In fact, the reaction of the hexacyanometallate unit $[B(CN)_6]^{(6-b)-}$ with the fully solvated species $[A(H_2O)_6]^{a+}$ affords the highly insoluble three-dimensional Prussian blue analogues. The most common problem dealing with the characterization of these compounds is their poor crystallinity and consequently, the difficulty in growing single crystals (amorphous powders are often obtained with peculiar stoichiometries). A technique for the synthesis of high quality single crystals of the Prussian blue family, which is crucial for magneto-structural correlations, has not yet been developed. In this respect, we note that the first report concerning the single crystal X-ray analysis of a $C_nA_p[B(CN)_6]_q{\cdot}xH_2O$ Prussian blue analogue with a strictly face-centered cubic lattice structure (the compound of formula $NaMn[Cr(CN)_6]$) was published in 2004 [36].

Following the demand for the rational design of clearly identified target molecules, impressive synthetic work has been performed since the 1990's tending towards the nuclearity control of the cyanide-bridged compounds. The most commonly used synthetic strategy consists of reacting the hexacyanometallate unit $[B(CN)_6]^{(6-b)-}$ (Lewis base, b being the charge of B) with a coordinatively unsaturated six-coordinate metal complex $[A(L)(H_2O)_x]^{(a-l)+}$ (Lewis acid, a and l being the charges of A and L, respectively), the number of available coordination sites and their relative position (for instance, *cis*- or *trans*- in the case of two labile sites and *mer*- or *fac*- in the case of three) around the metal ion A^{a+} being determined by the denticity and stereochemistry of the blocking ligand L. Recent reviews have outlined the impressive results obtained through

this strategy [3–5]. More recently, this rewarding chemistry has been also extended to octacyanometallate building blocks of Mo^{IV} [37–46], Mo^{V} [47–51], W^{IV} [39–43,45,52–54], W^{V} [49,50,52–54,55–59], Nb^{IV} [60,61] and Re^{V} [62] aiming at preparing metal assemblies that exhibit new and interesting magnetic or photomagnetic properties. Comparatively speaking, the heptacyanometallates which are better candidates for designing low-symmetry cyanide-bridged compounds (important characteristic when thinking at anisotropic magnetic properties) have received less attention [37,63–70]. Without being exhaustive for brevity reasons, one can cite the following results on the basis of their relevance from a magnetic point of view: (i) the rational design of heterobimetallic complexes whose nuclearity, anisotropy and ground spin state are controlled [71,72]; (ii) the preparation of discrete coordination compounds with ground-spin states as large as $S = 27/2$, 39/2 and 51/2 [47,55,71,73]; (iii) the achievement of single-molecule magnets (SMMs) [74–77], whose signature is a slow magnetic relaxation of the magnetization demonstrated by a frequency-dependent out-of-phase ac susceptibility signal and hysteretic behavior which are related to the combination of a large spin ground state and negative uniaxial anisotropy (see ref. [78] for detailed information); (iv) the isolation and characterization of the first photomagnetic high-spin heterometallic molecule where a high-spin species with ferromagnetic interaction between the spin carriers is induced by irradiation upon blue light (410–415 nm), the process being thermally reversible [79].

Another more elaborated strategy which is used by a small number of research groups consists of decreasing the number of cyanide groups of the hexacyanometallate $[B(CN)_6]^{(6-b)-}$ precursor by blocking some of its coordination sites with a polydentate ligand [13,74,80–88]. A better control of the polymerization possibilities is expected through these convergent precursors of formula $[M(L)(CN)_x]^{(x+l-m)-}$ (M = transition metal ion, x = number of cyanide ligands, l = charge of L and m = charge of M). This *bottom up* strategy is thoroughly analyzed and discussed below.

2. Synthetic strategy: choice of the precursors and analysis of the relevant parameters

One of the best methods for the rational synthesis of nuclearity tailored polynuclear complexes is the use of a stable building block which can act as ligand (complex as ligand strategy). All the tools associated with the flexibility of coordination chemistry are used in this strategy. Three of the most best rewarding examples are represented by the oxamidatocopper(II) complexes [89–93], the tris(oxalato)chromate(III) entity [5,94–99] and the hexacyanometallate family [2–4,71–73,75,76,100–102] which have provided a plethora of new extended systems with interesting magnetic properties. These precursors have in common a high solubility in water, a great stability (their nature being kept in solution), an anionic character (important parameter when thinking at their reaction with cationic species (fully solvated cations or preformed cationic complexes) and a good complexing ability (chelating and bischelating character of the oxamidate and oxalate and remarkable capability of the cyanide to act as a bridge). The cyanide group has several singularities: first, its asymmetric character makes it a very appropriate ligand for selective binding of two different metal ions; second, it is able to mediate strong magnetic interactions between the paramagnetic centres that it bridges; and third, due to the quasi linear arrangement of the M–CN–M′ entity, the nature of the magnetic coupling is easily predicted and its value tuned by choosing the metal centers M and M′ involved. A priori, this allows to predict the nature of the ground spin state of the cyanide-briged entities.

2.1. Preparation of the precursors $[M^{III}(L)(CN)_x]^{(x+l-m)-}$ (L = blocking ligand)

As mentioned above, in an attempt to extend the vast cyanide chemistry to the molecular regime, several groups have developed an alternative synthetic route which consists of using stable cyanide-bearing six-coordinate complexes of general formula $[M(L)(CN)_x]^{(x+l-m)-}$ (M = transition metal ion and L = polydentate ligand) as ligands towards either fully solvated metal ions or partially blocked metal complexes. The possibilities that these type of precursors offer and the main parameters to play with, are summarized in Scheme 1. Although bidentate and tridentate ligands (L) were considered in this scheme for simplicity reasons, the same points shown therein apply for other denticity ligands.

Let us outline briefly some of the points associated with the choice of these building blocks and their advantages. Concerning the cyanide-bearing precursor, its spin is determined by the nature and oxidation state of the metal ion M. As shown below, the early research focused on trivalent transition metal ions such as chromium(III) ($S_{Cr} = 3/2$), low-spin iron(III) ($S_{Fe} = 1/2$) and ruthenium(III) ($S_{Ru} = 1/2$). Each unpaired electron of M is defined by a magnetic orbital whose symmetry is topologically dependent. The local anisotropy of M is also a factor to be taken into account when aiming at preparing anisotropic high-spin molecules; this is one of the crucial parameters needed to obtain a single molecule magnet (SMM) [103]. As far as the peripheral ligand L is concerned, its nature is extremely important because of the variety of roles that it can play. Firstly, the charge of the precursor $[M(L)(CN)_x]^{(x+l-m)-}$ depends not only on the oxidation state of M but also on L (in general, L is a neutral species but it can be charged). Secondly, the number of the cyanide groups bound to M and their relative positions (stereochemical control of the coordinated cyanides) are fixed by the number of peripheral ligands L as well as by their denticity and conformation. So, four cyanide groups are coordinated to M and two of them are in *trans* position when L is a bidentate ligand such as bipy, phen, bpym, dpa, pyim, ampy, en or acac and only one L group is present. In the case where two bidentate L ligands are bound to M, the two cyanide groups can adopt *trans* [85a] or *cis* conformations [104] depending on the geometric constraints of L. If L is a tridentate ligand, three cyanide groups are present in the coordination sphere of M and they can exhibit the *mer* (L = terpy or bpca) or *fac* [L = Me_3tacn or $HB(pz)_3$] conformations. For L being a tetradentate ligand, *cis* and *trans* dicyanide-containing species are possible. Thirdly, when L is not only a terminal ligand (like bipy) but may act also as a bridge (case of bpym),

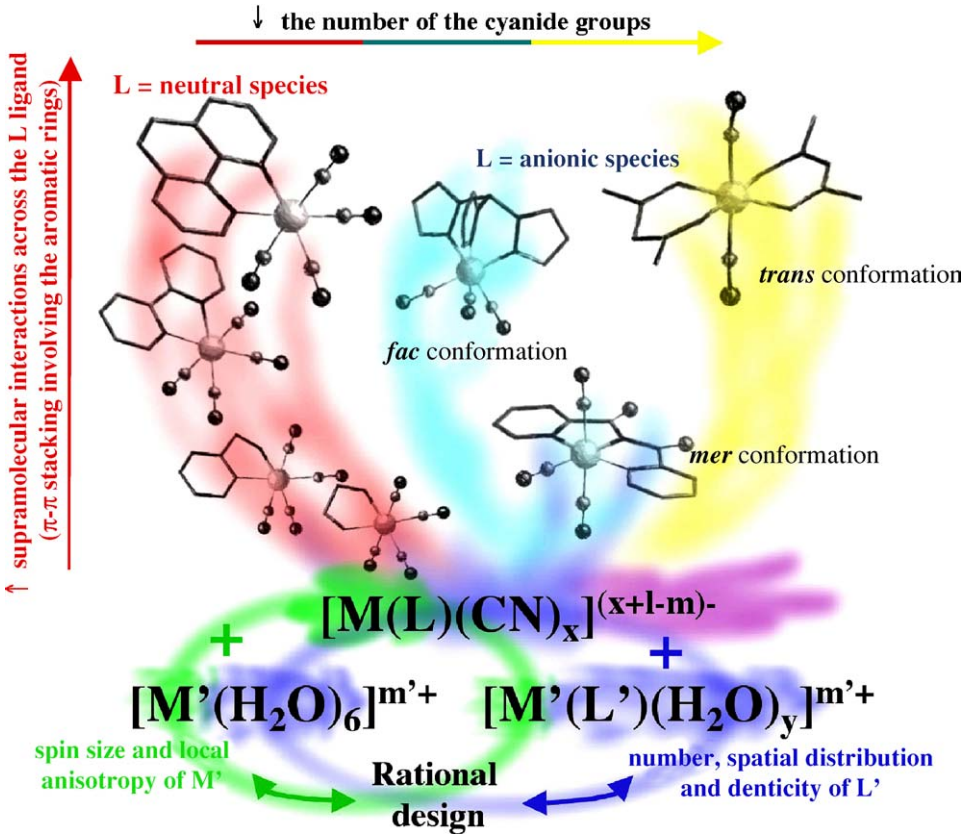

Scheme 1.

the complexing ability of the precursor is increased. Fourthly, supramolecular interactions across the L ligand are also possible: π–π stacking involving the aromatic rings from bipy or phen and hydrogen bonds using the H–N group from dpa and piym or the H–B unit from $HB(Pz)_3$, for instance. This versatility of the anionic precursor is completed by the possibilities that the cationic species can offer which can be the fully solvated $[M'(H_2O)_6]^{m'+}$ or partially blocked $[M'(L')(H_2O)_y]^{m'+}$. As previously indicated for M, the spin size and local anisotropy of M′ are dependent on its nature and its oxidation state. The number of labile coordination sites and their spatial distribution around M′ are dependent on the denticity of L′. In the light of these considerations, one can easily understand the potential richness of this synthetic route as far as the rational design of nuclearity and dimensionality controlled cyanide-bridged assemblies are concerned.

2.1.1. With a bidentate end-cap ligand

We will focus here on the preparative routes and characterization of selected examples of mononuclear precursors of formula $[M^{III}(L)(CN)_4]^-$ with M = Cr and Fe and L = bidentate nitrogen donor, that we are using in our current research work. They are quite stable paramagnetic and anionic building blocks with local spins of 3/2 (Cr^{III}) and 1/2 (low-spin Fe^{III}). In general, we use two types of cations as precipitating agents: univalent alkaline cations (lithium and potassium essentially) and bulky organic cations (tetraphenylphosphonium or tetraphenylarsonium). This allows us to isolate high purity precursors which can be solubilized in common solvents (both polar and non polar). They were characterized by chemical analysis, infrared spectroscopy, X-ray diffraction on single cystals and variable-temperature magnetic susceptibility measurements.

The source of chromium in the chromium derivatives is the air-sensitive dinuclear chromium(II) complex $[Cr_2(CH_3COO)_4(H_2O)_2]$ [105]. The preparation of the compound of formula $PPh_4[Cr(bipy)(CN)_4]\cdot 2CH_3CN\cdot H_2O$ is detailed here as a representative example of the procedure used for the other tetracyanide chromium(III) series, the bidentate ligand being phen, ampy and en. The synthetic route is outlined below (Scheme 2).

Most of the synthetic work is carried out under an inert atmosphere and in a typical experiment, a 1:1:4:1 Cr(II): bipy:CN^-:PPh_4^+ molar ratio was used [86f]. The infrared spectrum of the compound $PPh_4[Cr(bipy)(CN)_4]\cdot 2CH_3CN\cdot H_2O$ as a

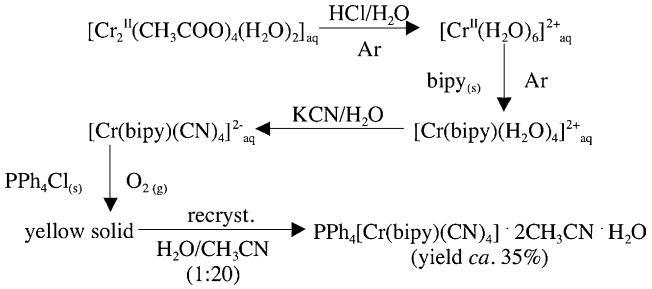

Scheme 2.

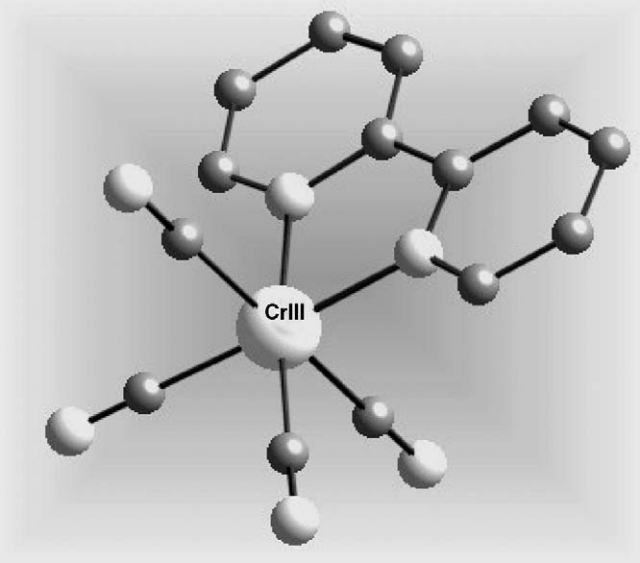

Fig. 1. Perspective view of the structure of $[Cr(bipy)(CN)_4]^-$. Adapted from Toma et al. [86f]. Copyright ©Wiley-VCH.

KBr disk exhibits two peaks in the cyanide stretching region: one at 2212w cm^{-1} (CH_3CN molecule) and the other at 2124w cm^{-1} (terminal cyanide ligand), w standing for weak. The X-ray structure of this compound (Fig. 1) shows the occurrence of the desired anionic building block $[Cr(bipy)(CN)_4]^-$ with four terminally bound cyanide groups and a bidentate bipy ligand [86f]. The anions are grouped by pairs (Fig. 2) involving the crystallization water molecule and two cyanide-nitrogen atoms from two $[Cr(bipy)(CN)_4]^-$ anions resulting in a quasi square centrosymmetric motif Cr(1)–O(1)–Cr(1a)–O(1a). The magnetic properties of this compound reveal the occurrence of the Curie law behavior for a magnetically isolated spin quadruplet with a slight decrease of the $\chi_M T$ product (χ_M is the molar magnetic susceptibility) at very low temperatures which may be attributed to the zero field splitting (D) of the chromium(III) ion, to weak antiferromagnetic intermolecular interactions or to both factors simultaneously.

The structures of the related chromium(III) complexes of formula $PPh_4[Cr(phen)(CN_4)]\cdot H_2O\cdot CH_3OH$ (Fig. 3, left) [86g], $PPh_4[Cr(ampy)(CN_4)]\cdot H_2O$ (Fig. 3, middle) [86g] and $PPh_4[Cr(en)(CN_4)]\cdot H_2O$ (Fig. 3, right) [106] show the presence

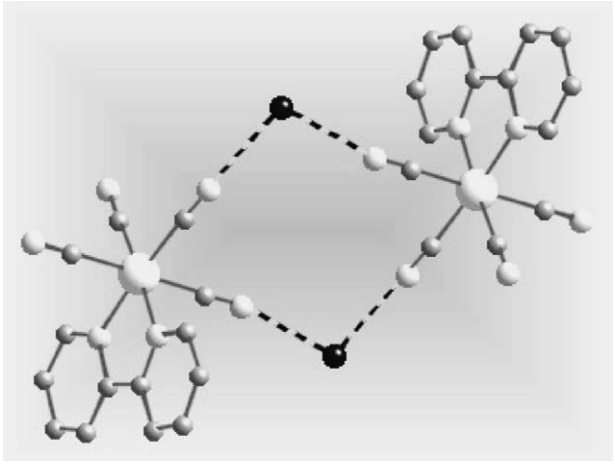

Fig. 2. A view of the hydrogen-bonded pair of $[Cr(bipy)(CN)_4]^-$.

of a distorted six-coordinate environment of the chromium atom with four terminally bound cyanide groups and the bidentate nitrogen donor. As in the preceding compound, quasi Curie law behavior of a magnetically isolated spin quadruplet is observed for this family.

Dealing with the low-spin iron(III) precursors of formula $[Fe^{III}(L)(CN)_4]^-$, the preparative route is a modification of Schildt's method [107] and is illustrated by the following synthetic pathway (Scheme 3) where the bipy molecule is chosen as the L ligand [86b].

The source of iron is the diamagnetic low-spin iron(II) complex $[Fe(bipy)_3]^{2+}$ which is treated with a large excess of cyanide (a 1:45 $[Fe(bipy)_3]^{2+}$:CN^- molar ratio was used in a typical experiment) under heating. The insoluble product of formula $[Fe(bipy)_2(CN)_2]\cdot 3H_2O$ separates as large violet needles in a high yield upon cooling. Its digestion in an hot aqueous solution

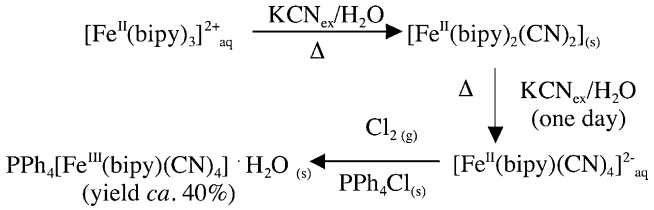

Scheme 3.

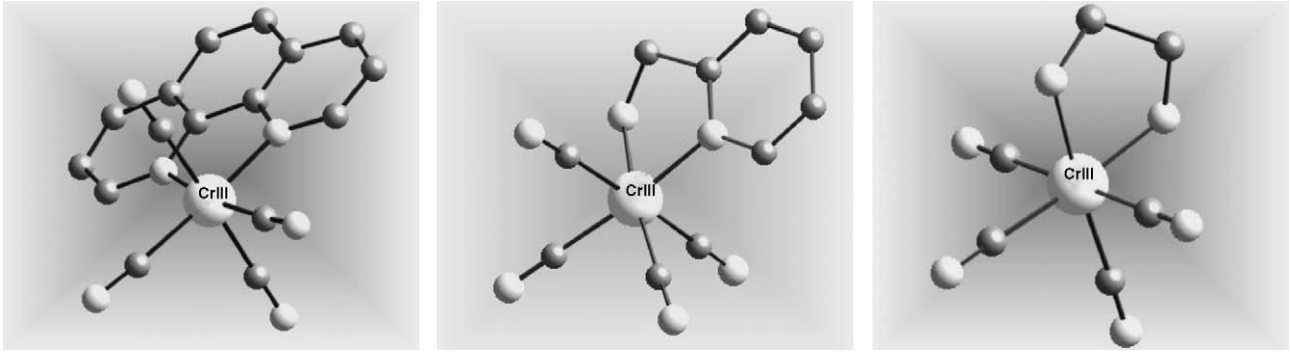

Fig. 3. Perspective views of $[Cr(phen)(CN_4)]^-$ (left), $[Cr(ampy)(CN_4)]^-$ (middle) and $[Cr(en)(CN_4)]^-$ (right). Adapted (left and middle) from Toma et al. [86g]. Copyright ©The Royal Society of Chemistry and the Centre Nationale de la Recherche Scientifique.

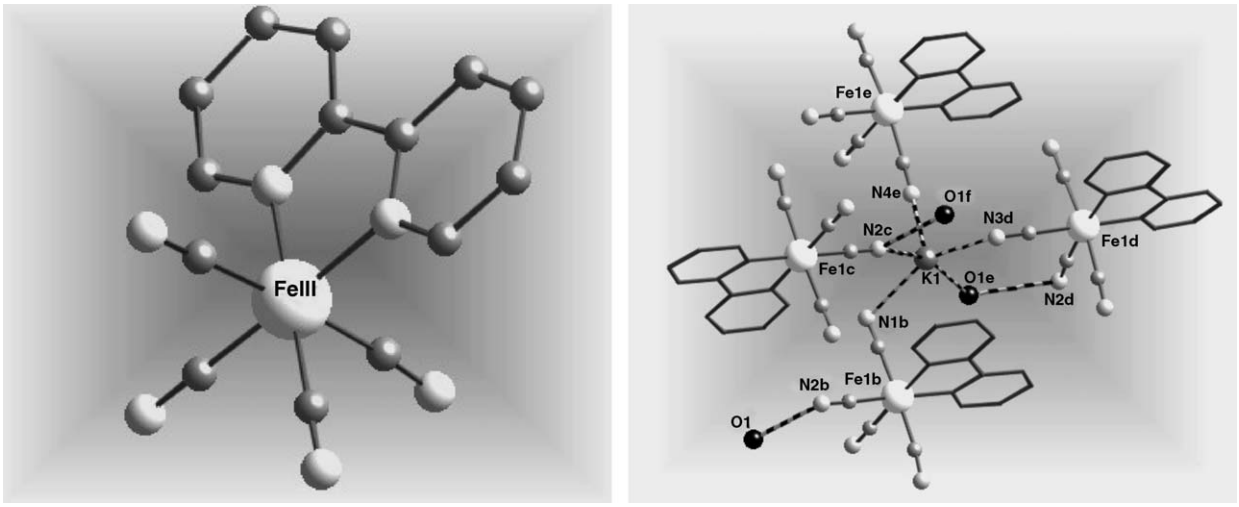

Fig. 4. Perspective view of the $[Fe(bipy)(CN)_4]^-$ anion (left). Molecular structure of $K[Fe(bipy)(CN)_4]\cdot H_2O$ showing the environment of K^+ cation (right). Adapted from Toma et al. [86c]. Copyright ©The Royal Society of Chemistry.

containing an excess of cyanide (a 1:360 iron to cyanide molar ratio) during one day yields the orange brown solid of formula $K_2[Fe(bipy)(CN)_4]\cdot 3H_2O$ in a practically quantitative yield. Oxidation by chlorine of this last compound in the presence of a suitable precipitating cation such as tetraphenylphosphonium affords the complex $PPh_4[Fe(bipy)(CN)_4]\cdot H_2O$ whose structure (Fig. 4, left) [86b] reveals the occurrence of a bidentate bipy ligand and four terminally bound cyanide groups. Its magnetic behaviour is as expected for a low-spin iron(III) complex, the value of μ_{eff} at room temperature being 2.38 BM. These anions are well separated from each other by the bulky organic PPh_4^+ cation. However, when the potassium cation is used as the precipitating agent, the compound of formula $K[Fe(bipy)(CN)_4]\cdot H_2O$ [86c] is obtained where the potassium atom is surrounded by four nitrogen-cyanide atoms from four $[Fe(bipy)(CN)_4]^-$ units and a water molecule taking a distorted square pyramidal environment (Fig. 4, right).

The structures of the related iron(III) complexes of formula $PPh_4[Fe(phen)(CN_4)]\cdot 2H_2O$ (Fig. 5, left) [86a], $PPh_4[Fe(ampy)(CN_4)]\cdot H_2O$ (Fig. 5, middle) [108], $PPh_4[Fe(bpym)(CN_4)]\cdot H_2O$ (Fig. 5, right) [109] and $PPh_4[Fe(dmbpy)(CN_4)]\cdot 3H_2O$ (Fig. 6) [110] have in common the bidentate nitrogen donor and the four terminally bound cyanide ligands building a distorted octahedron surrounding the iron atom. In the case of the dmbpy-containing complex, an unprecedented cyclic tetranuclear water ring with two dangling water molecules links two $[Fe(dmbpy)(CN_4)]^-$ anions. Focusing on the bpym-containing complex, the relevant aspect to be outlined is that it can act as a ligand through the two outer bpym-nitrogen atoms in addition to the four cyanide-nitrogen atoms, its complexing ability being thus higher to that of the other members of this family. The magnetic properties of these tetracyano-containing iron(III) complexes are as expected for magnetically isolated low-spin iron(III) complexes [86a,108–110].

2.1.2. With a tridentate end-cap ligand

Remarkable examples of tricyanide-bearing mononuclear species were prepared by Long and co-workers [74,81] to construct molecules consisting of just one of the fundamental cage units comprising the Prussian blue framework. Representative examples are: $[M(tacn)(CN)_3]$ ($M = Co^{3+}$, Cr^{3+}) [81a], $[M(Me_3tacn)(CN)_3]$ ($M = Cr^{3+}$, Mo^{3+}) [74,81b–e] and $[M(tach)(CN)_3]$ ($M = Cr^{3+}$, Fe^{3+}, Co^{3+}) [81g]. All these precursors have in common: the neutral character, the presence of a

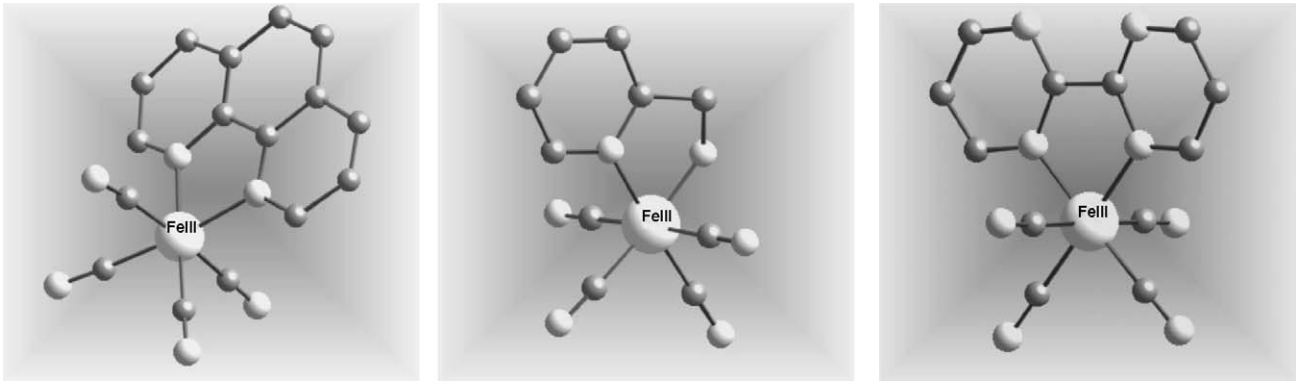

Fig. 5. Perspective views of the structures of $[Fe(phen)(CN_4)]^-$ (left), $[Fe(ampy)(CN_4)]^-$ (middle) and $[Fe(bpym)(CN_4)]^-$ (right). Adapted (left) from Lescouëzec et al. [86a]. Copyright ©American Chemical Society.

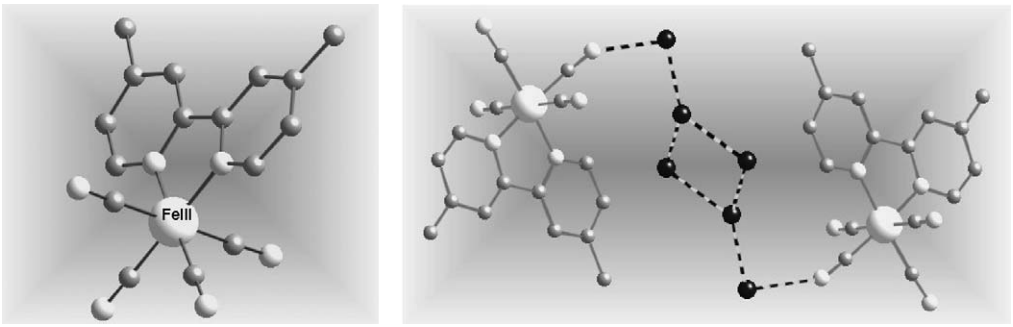

Fig. 6. Perspective view of the structure of $[Fe(dmbpy)(CN_4)]^-$ complex (left) and of the water cluster linking two complex units (right).

tridentate nitrogen donor in a *fac* arrangement and the occurrence of three cyanide ligands which also adopt a *fac* arrangement. This stereochemistry of the cyanide groups is very important because their arrangement is specially suited to build cage compounds of cubic symmetry, as already demonstrated. A typical synthesis of these precursors is exemplified by $[Cr(Me_3tacn)(CN)_3]$: the reaction of $[Cr(Me_3tacn)(CF_3SO_3)_3]$ [111,112] with KCN (7.5:180 chromium to cyanide molar ratio) in dimethyl sulfoxide at 120 °C during one day and under a dinitrogen atmosphere affords the species $[Cr(Me_3tacn)(CN)_3]$ in solution. It precipitates as a yellow solid by adding dichloromethane and cooling in an ice bath [81b].

Another relevant example of a cyanide-bearing precursor designed to build molecular cages and squares is the half-sandwich tricyanometallate of general formula $[M(C_5R_5)CN)_3]^-$ (R = H and CH_3; M = Co, Rh and Ir). In this case, the precursor is a monoanionic organometallic species whose versatility as a ligand toward partially blocked metal complexes has provided a large family of bimetallic cyanide-bridged boxes [80].

Our attempts in this framework have focused on the preparation of the low-spin iron(III) species $PPh_4\{Fe[HB(pz)_3](CN)_3\}\cdot H_2O$ [86d], $PPh_4\{Fe[B(pz)_4](CN)_3\}$ [113] and $PPh_4[Fe(bpca)(CN)_3]\cdot H_2O$ [86e] where the conformation of the tridentate blocking ligands, *fac* [$HB(pz)_3$ and $B(pz)_4$] and *mer* (bpca) determines that of the three cyanide groups, *fac* in the two former species and *mer* in the latter one. The preparative route used for the isolation of the pyrazolylborate-containing complexes is summarized hereunder (Scheme 4).

The hydrotris(1-pyrazolyl)borate ligand as a potassium salt was prepared by following Trofimenko's procedure [114]. The neutral and air-stable iron(II) compound $\{Fe[HB(pz)_3]_2\}$ precipitates as a purple solid by reaction between $K[HB(pz)_3]$ and $FeCl_2$ in a 2:1 molar ratio. A suspension of $\{Fe[HB(pz)_3]_2\}$ and KCN (1:3 iron to cyanide molar ratio) in 2-propanol is heated for 12 h at 80 °C in order to generate the compound $K_2\{Fe[HB(pz)_3](CN)_3\}$ as a yellow solid. Once dissolved in a minimum amount of water, it is oxidized to the corresponding iron(III) complex by 30% H_2O_2. The addition of tetraphenylphosphonium chloride allows its isolation. The substitution reaction of one $HB(pz)_3$ ligand of the $\{Fe[HB(pz)_3]_2\}$ species by three cyanide ligands is complete in one hour and a half when using Ph_4CN instead of KCN as the cyanide source. A similar synthetic pathway is used for the preparation of the tetrakis(1-pyrazolyl)borate-containing complex. The crystal structures of these two complexes (Fig. 7) show the *fac* arrangement of the three cyanide ligands, the symmetry of the coordination polyhedron of the iron atom being close to C_{3v} (Fig. 7, left) and C_s (Fig. 7, right).

The source of iron for the mononuclear complex PPh_4-*mer*-$[Fe(bpca)(CN)_3]\cdot H_2O$ is the compound $[Fe(bpca)Cl_2(EtOH)]$ [115] which is prepared by reaction between Hbpca [116]

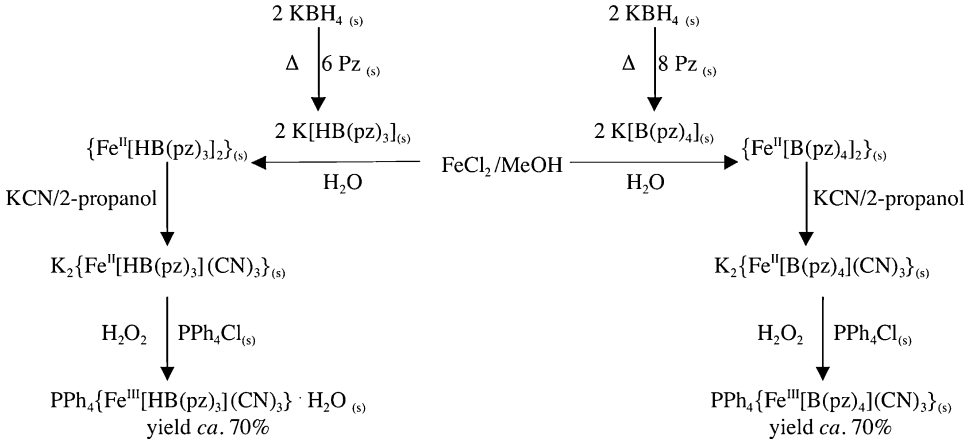

Scheme 4.

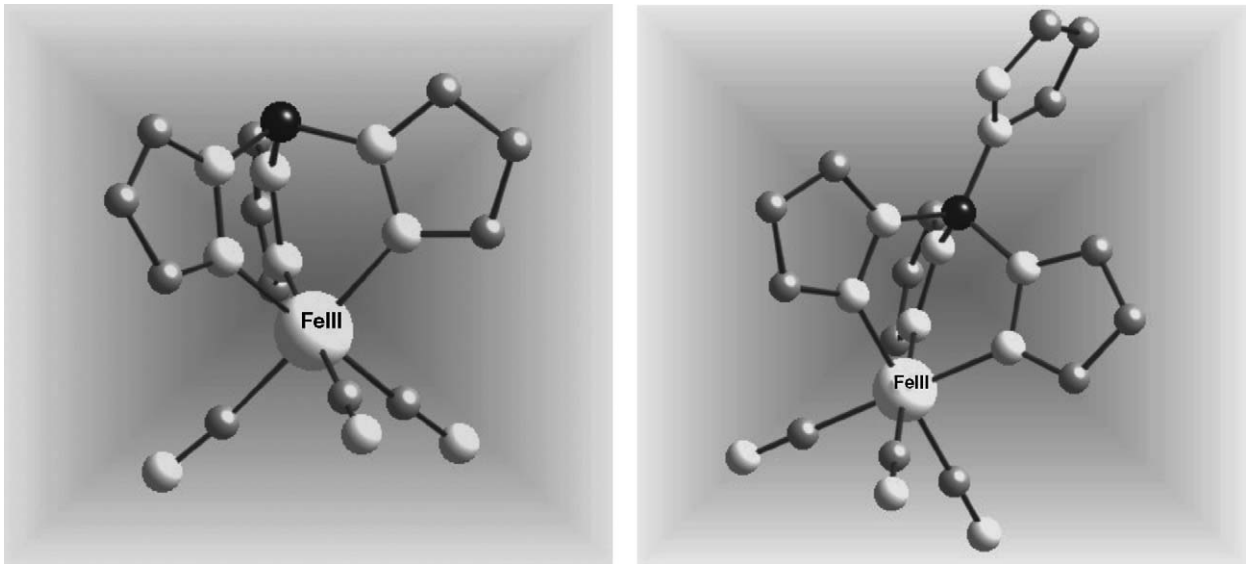

Fig. 7. Perspective views of the structures of the $\{Fe[HB(pz)_3](CN)_3\}^-$ (left) and $\{Fe[B(pz)_4](CN)_3\}^-$ (right). Adapted (left) from Lescouëzec et al. [86d]. Copyright ©American Chemical Society.

and anhydrous $FeCl_3$ in a 1:1 molar ratio. The addition of a concentrated and hot aqueous solution of KCN and PPh_4Cl to an aqueous solution of $[Fe(bpca)Cl_2(EtOH)]$ (3:1:1 cyanide:tetraphenylphosphonium:iron molar ratio) causes the precipitation of the compound $PPh_4[Fe(bpca)(CN)_3]\cdot H_2O$ which is purified by recrystallization from acetonitrile and methanol. Its X-ray crystal structure [86e] confirms the *mer* arrangement of the three cyanide ligands (Fig. 8, left) and the practically C_{2v} symmetry around the iron atom. The anionic entities are grouped by pairs through hydrogen bonds involving the crystallization water molecule, a carbonyl–oxygen atom and a cyanide–nitrogen atom (Fig. 8, right).

The magnetic moment at room temperature of these iron(III) complexes (μ_{eff} ca. 2.4 BM) demostrates that they are low-spin iron(III) complexes ($S_{Fe} = 1/2$). The values of the ν_{CN} stretching vibration at 2123, 2117 and 2126 cm^{-1} for the $HB(pz)_3^-$, $B(pz)_4^-$ and bpca-containing iron(III) complexes respectively, also support the doublet spin state for the iron(III) ion.

3. Cyanide-bridged low-dimensional bimetallic complexes with tetracyano-, tricyano- and dicyano-bearing building blocks

3.1. $[Cr^{III}(L)(CN)_4]^-$

The use of this building block with L = bipy as a ligand towards fully hydrated manganese(II) ions yielded the neutral trinuclear species $\{[Cr(bipy)(CN)_4]_2Mn(H_2O)_4\}\cdot 4H_2O$ and two one-dimensional compounds of formula $\{[Cr(bipy)(CN)_4]_2Mn(H_2O)_2\}$ and $\{[Cr(bipy)(CN)_4]_2Mn(H_2O)\}\cdot H_2O\cdot CH_3CN$

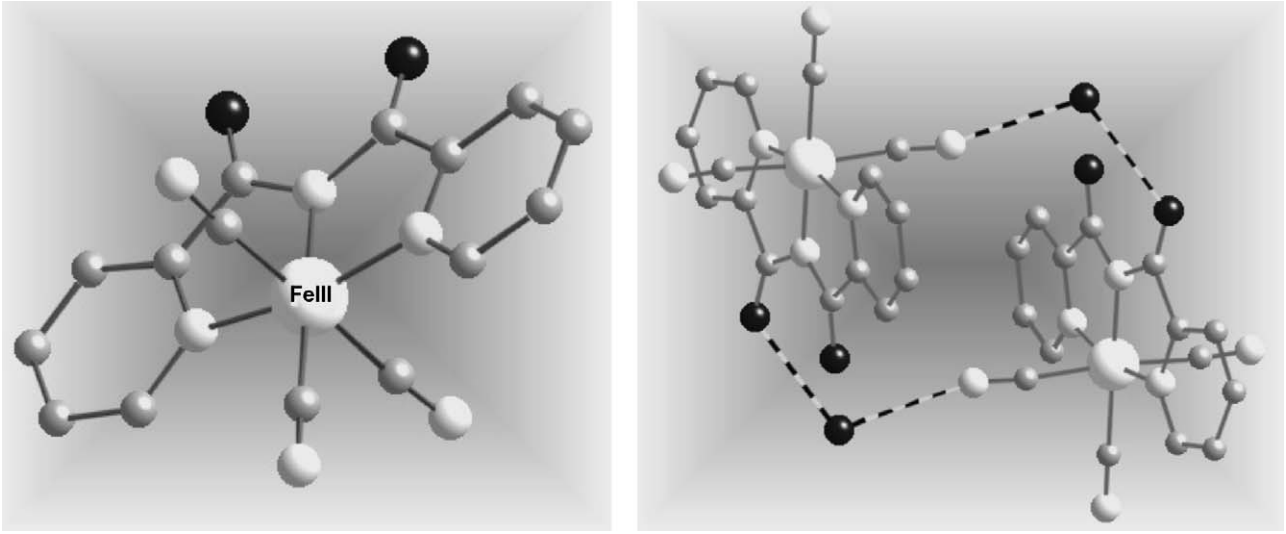

Fig. 8. Molecular structure of $PPh_4[Fe(bpca)(CN)_3]\cdot H_2O$: perspective view of the structure of the $[Fe(bpca)(CN)_3]^-$ anion (left) and of its pairing through hydrogen bonds (right). Adapted (left) from Lescouëzec et al. [86e]. Copyright ©American Chemical Society.

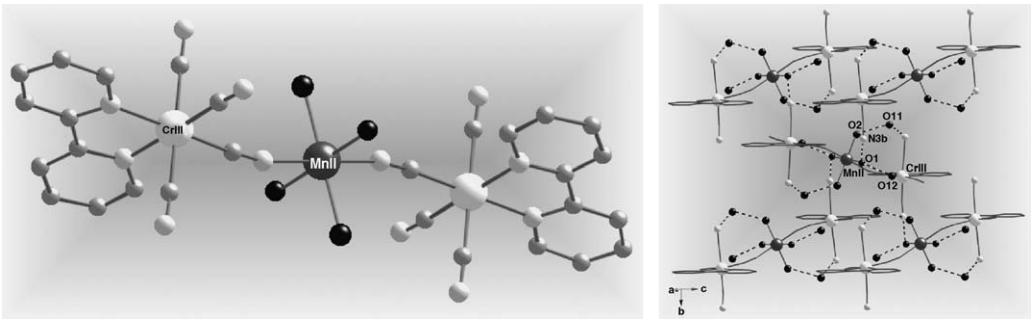

Fig. 9. Molecular structure of $\{[Cr(bipy)(CN)_4]_2Mn(H_2O)_4\}\cdot 4H_2O$: perspective view of the trinuclear motif (left) and a view of the hydrogen bonds linking the trinuclear motifs (right). Adapted from Toma et al. [86f]. Copyright ©Wiley-VCH.

[86f]. The $[Cr(bipy)(CN)_4]^-$ unit acts as a monodentate ligand towards a $[Mn^{II}(H_2O)_4]$ entity through one of its four cyanide ligands affording the neutral centrosymmetric trinuclear species which is shown in Fig. 9 (left). The Cr–C–N angles for the terminal cyanide groups are somewhat bent [177.9(6)–175.3(7)°] whereas those of the bridging cyanide depart significantly from strict linearity [170.7(7)° and 168.9(6)° for Cr–C–N and Mn–N–C, respectively]. The intramolecular $Cr(1)\cdots Mn(1)$ separation across the bridging cyanide is 5.364(1) Å. The trinuclear units are linked by hydrogen bonds involving the coordinated and crystallization water molecules and one of the three terminal cyanide ligands (Fig. 9, right). The magnetic properties of this compound in the form of $\chi_M T$ and χ_M versus T plots (Fig. 10) are consistent with the occurrence of a significant antiferromagnetic interaction between the peripheral spin quartets and the central spin sextuplet [$J = -6.2\ cm^{-1}$, the Hamiltonian being defined as $\hat{H} = -J(\hat{S}_{Cr(1)}\cdot\hat{S}_{Mn} + \hat{S}_{Cr(2)}\cdot\hat{S}_{Mn})$] leading to a ground spin doublet. This value of the magnetic coupling compares well with those reported for the Cr^{III}–CN–Mn^{II} unit in two heptanuclear complexes $[Cr^{III}\{CN\text{–}Mn^{II}(tetren)\}]^{9+}$ ($J = -10.8$ and $-7.2\ cm^{-1}$) [71]. Having in mind the electronic configurations of the interacting metal ions [$t_{2g}^3e_g^0$ and $t_{2g}^3e_g^2$ for octahedral Cr^{III} and Mn^{II} centers, respectively], both antiferromagnetic [$t_{2g}(Cr)$–$t_{2g}(Mn)$] and ferromagnetic [$t_{2g}(Cr)$–$e_g(Mn)$] contributions are involved. In the light of the magnetic coupling observed, the first are dominant [117].

The compound $\{[Cr(bipy)(CN)_4]_2Mn(H_2O)_2\}$ is a neutral 4,2-ribbon like bimetallic chain where the $[Cr(bipy)(CN)_4]^-$ unit acts as a bismonodentate bridging ligand toward two *trans*-

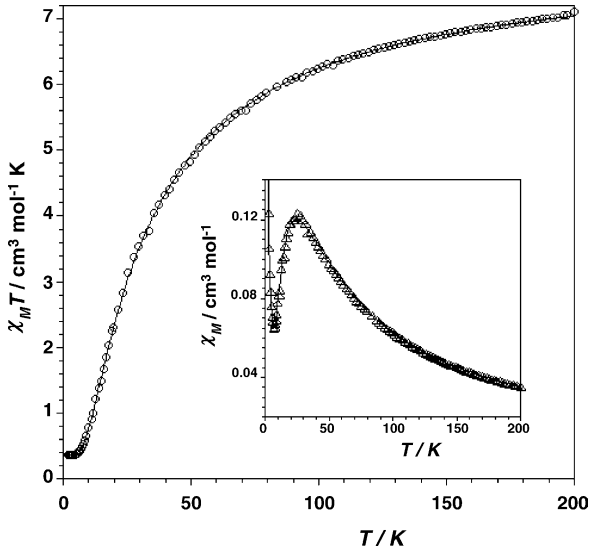

Fig. 10. $\chi_M T$ vs. T plot for $\{[Cr(bipy)(CN)_4]_2Mn(H_2O)_4\}\cdot 4H_2O$: (() experimental data; (—) best-fit curve. The inset shows the χ_M (△) vs. T plot in the low temperature region. Adapted from Toma et al. [86f]. Copyright ©Wiley-VCH.

diaquamanganese(II) entities through two of its four cyanide groups in *cis* positions (Fig. 11, left). Two types of chains running parallel to the *a*-axis occur in this compound (Fig. 11, right). As observed in the previous trinuclear complex, the Cr–C–N fragment for the bridging cyanide [169.6(5)°] is bent to a greater degree than those of the terminal cyanides [174.9(5)–172.3(5)°]. The departure from the strict linearity at the manganese side within the cyanide-bridged Cr–C–N–Mn fragment is very large

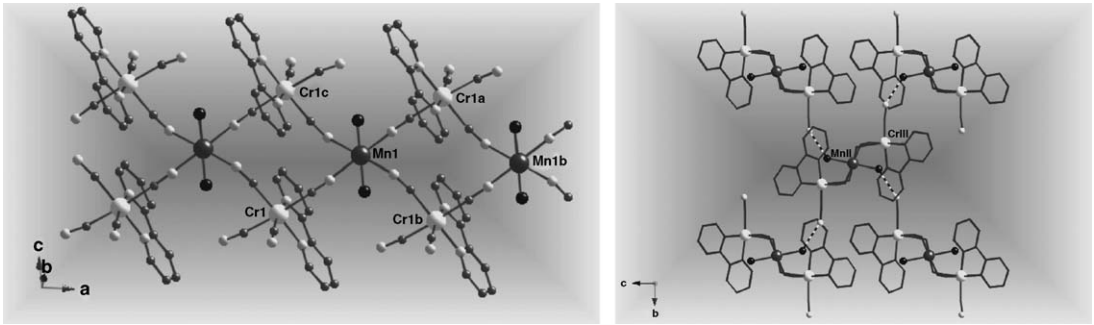

Fig. 11. Structure of the compound $\{[Cr(bipy)(CN)_4]_2Mn(H_2O)_2\}$: a view of a fragment of the chain running parallel to the *a* axis (left) and a projection along the along the *a* axis showing the arrangement of the neighbouring chains (right). Adapted (left) from Toma et al. [86f]. Copyright ©Wiley-VCH.

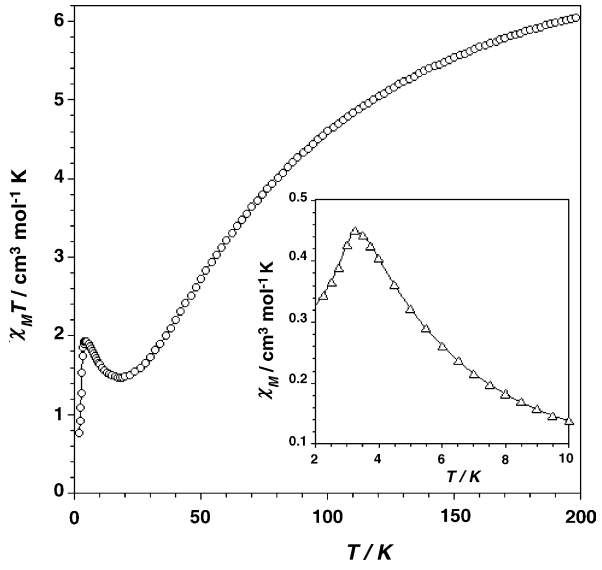

Fig. 12. $\chi_M T$ vs. T plot for $\{[Cr(bipy)(CN)_4]_2Mn(H_2O)_2\}$: (○) experimental data; (—) best-fit curve. The inset shows the χ_M (●) vs. T plot in the low temperature region. Adapted from Toma et al. [86f]. Copyright ©Wiley-VCH.

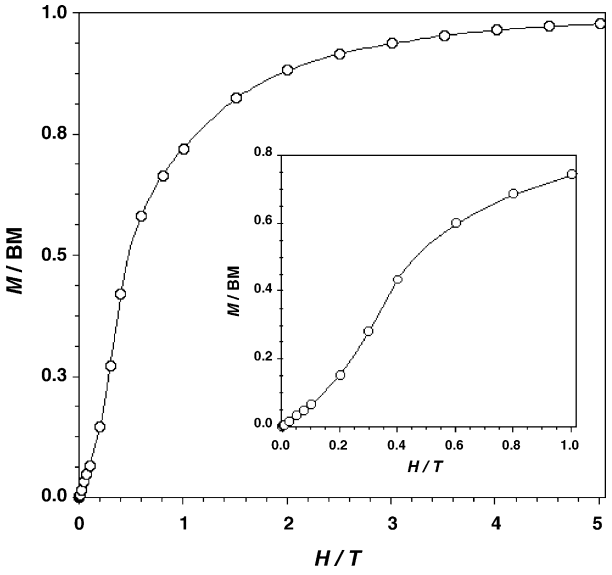

Fig. 13. Magnetization vs. H plot for $\{[Cr(bipy)(CN)_4]_2Mn(H_2O)_2\}$ at 2.0 K. The inset shows the low field region. The solid line is only an eye-guide. Reprinted from Toma et al. [86f]. Copyright ©Wiley-VCH.

[140.5(4) and 139.6(5)° for the Mn–N–C bond angle]. This causes a shortening of the intrachain Cr···Mn separation across the bridging cyanide [5.021(1) and 5.029(1) Å in the chain versus 5.364(1) Å in the trinuclear complex].

The magnetic properties of the bimetallic chain (Fig. 12) are as expected for a ferrimagnetic one-dimensional system [decrease of $\chi_M T$ in the high temperature range with a minimum of $\chi_M T$ at low temperatures] with weak interchain magnetic interactions (maximum of the magnetic susceptibility at 3.5 K under an applied magnetic field of $H = 50$ G, see inset of Fig. 12). The maximum of the magnetic susceptibility disappears for $H > 3000$ G and thus the magnetic behaviour of this compound corresponds to a metamagnet. This interpretation is supported by the magnetization versus H plot per $Cr^{III}_2Mn^{II}$ unit (Fig. 13): one can see there how the saturation value of the magnetization ($M_S = 0.98$ BM) is as expected for a low-lying spin doublet with $g = 1.98$ [$S = 2S_{Cr(III)} - S_{Mn(II)} = 6/2 - 5/2 = 1/2$] and the sigmoidal shape of the magnetization curve which is the signature of the metamagnetic behaviour [118]. A value for the interchain magnetic interaction of ca. 0.3 cm^{-1} is estimated from the value of the critical field $H_c = 3000$ G (inflexion point in the inset of Fig. 13). The lack of a theoretical model to analyze the magnetic data of this 4,2-ribbon like bimetallic chain precludes the determination of the two intrachain magnetic couplings. In an attempt to analyze the intrachain coupling and to evaluate the exchange coupling parameters, DFT type calculations and Quantum Monte Carlo simulations were carried out. DFT calculations demonstrate a correlation between the value of the magnetic coupling and the degree of bending of the C–N–Mn unit. The antiferromagnetic interaction is reinforced as the bending increases. This is well illustrated on a simple orbital picture which shows the most important contributions to the magnetic coupling in a dinuclear Cr^{III}–C–N–Mn^{II} unit (Fig. 14). Those involving the two t_{2g} orbitals (d_{xz} and d_{yz}) of the Cr^{III} are antiferromagnetic because of good overlap with the appropriate orbitals of the Mn^{II} (Fig. 14a and b, left). That involving one of the t_{2g} chomium orbitals (d_{xy}) and one of the e_g manganese orbitals ($d_{x^2-y^2}$) is ferromagnetic being a case of strict orthogonality between the two interacting magnetic orbitals (Fig. 14c, left). The effect of the bending of the C–N–Mn unit on the magnetic interaction (Fig. 14, right) consists of: (i) no modification of the antiferromagnetic contribution in the case of (a); (ii) a decrease of the antiferromagnetic contribution of the strict linearity in the case of (b); (iii) an increase of the antiferromagnetic contribution in the case of (c). The successful simulation of the $\chi_M T$ versus $T/|J|$ plot of the chain down to very low temperatures by the Quantum Monte Carlo methodology (QMC) provided an intrachain magnetic coupling of ca. -75 cm^{-1}.

The structure of the compound $\{[Cr(bipy)(CN)_4]_2Mn(H_2O)\}\cdot H_2O\cdot CH_3CN$ can be viewed as the condensation of two previous parallel 4,2-ribbon like chains shifted by $b/2$ after loss of one of the two coordinated water molecules of the manganese atom of each chain, its position being filled by a cyanide nitrogen of a terminal cyanide of the adjacent chain (Fig. 15, left). In a simplified manner, it can be described by a corrugated ladder-like chain with regular alternating chromium and manganese atoms along the edges [Mn(1) and Cr(1b) in Fig. 15, right], each rung being defined by a chromium–manganese pair [Mn(1) and Cr(1) in Fig. 15, right]; moreover, each pair of adjacent manganese atoms is connected through another chromium atom [Cr(2) in Fig. 15, right]. The $[Cr(bipy)(CN)_4]^-$ building block in this structure adopts two bridging coordination modes, bis- [Cr(2)] and tris-monodentate [Cr(1)] through two and three of its four cyanide ligands, respectively. Given that the synthesis of this compound is carried out in a H_2O/CH_3CN (10:90 v:v) mixture (to be compared with the preparation of the previous 4,2-ribbon like chain which was performed in water), the minimization of water as solvent in the preparative route seems

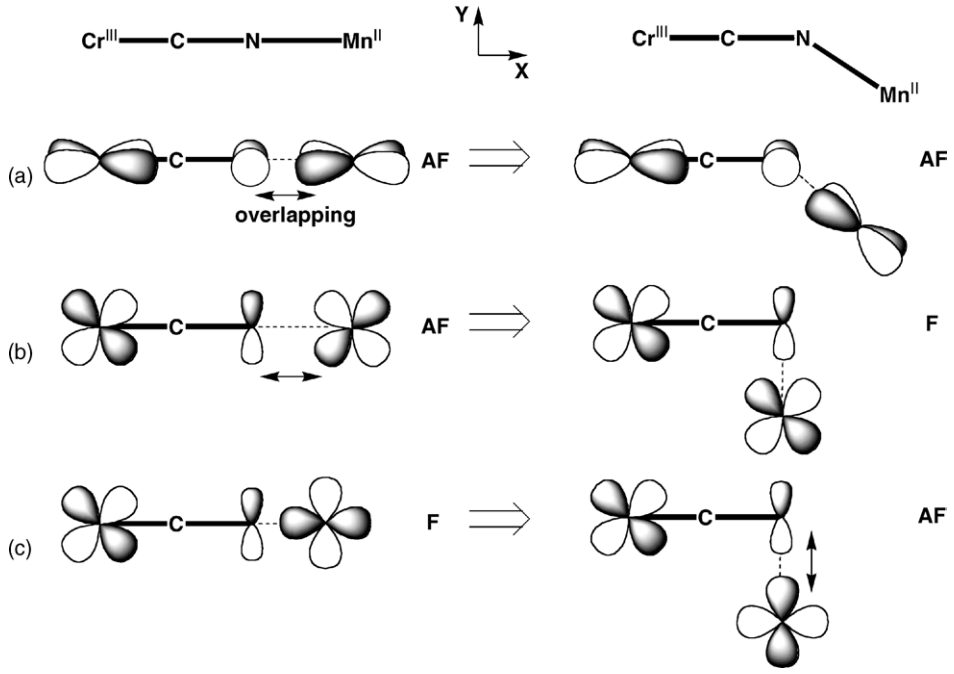

Fig. 14. Most relevant contributions to the magnetic coupling in $\{[Cr(bipy)(CN)_4]_2Mn(H_2O)_2\}$ showing the influence of the depart of the linearity of the Cr–C–N–Mn on them. Reprinted from Toma et al. [86f]. Copyright ©Wiley-VCH.

to favour the condensation of the chains. The magnetic properties of this double chain in the low temperature range are strongly dependent on the applied magnetic field (Fig. 16). When $H = 1$ T, its magnetic behaviour closely follows that of the previous chain: overall ferrimagnetic behaviour with a maximum of the magnetic susceptibility (inset of Fig. 16) at 9.5 K (3.5 K in the previous compound) which disappears for $H > 1.5$ T, indicating metamagnetism ($H_c = 1.5$ T). At lower fields, the minimum of $\chi_M T$ is shifted towards higher temperatures and a pronounced maximum of $\chi_M T$ appears at ca. 30 K. In addition, a further increase of $\chi_M T$ is observed at very low temperatures for $H = 50$ G. The susceptibility maximum observed at $H = 1$ T disappears when lowering the field (inset of Fig. 16) and magnetic ordering occurs (confirmed by the presence of a frequency-independent maximum of the imaginary component of the ac signal). This curious behavior was ascribed to the occurrence of a spin canting within the double chain whose origin could be the antisymmetric exchange [119–122]. High fields (1 T for instance) overcome the antisymmetric exchange and mask the effect of the spin canting [121,122]. The combined use of DFT and QMC calculations on this compound provided a good match of the $\chi_M T$ versus T plot, the estimated values for the intra-chain magnetic couplings being -5.6 (linear Cr–CN–Mn) and $-10.4\ cm^{-1}$ (non-linear Cr–CN–Mn).

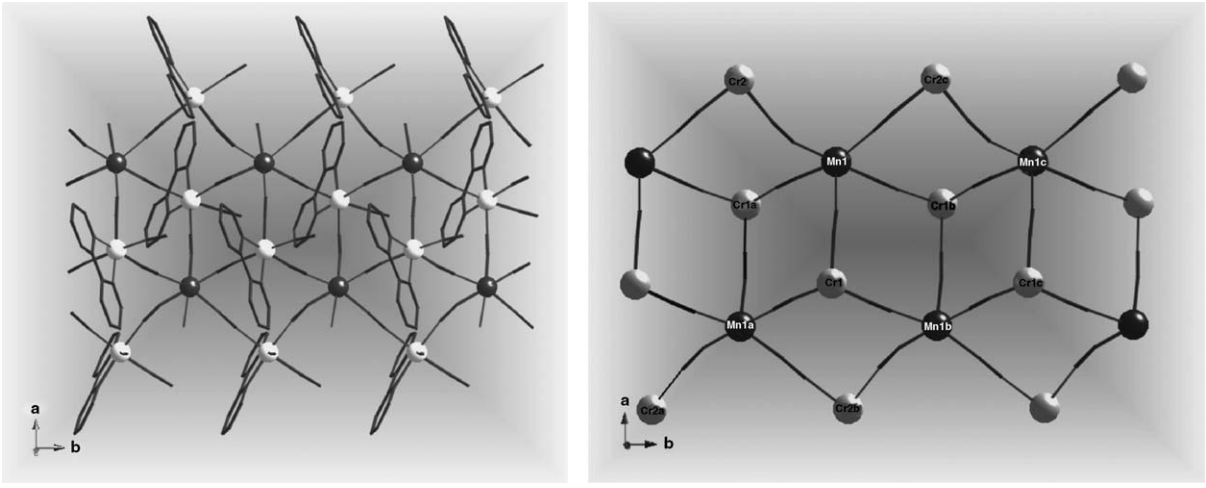

Fig. 15. Structure of $\{[Cr(bipy)(CN)_4]_2Mn(H_2O)\}\cdot H_2O\cdot CH_3CN$: perspective view of a fragment of the two condensed 4,2-ribbon like chains running parallel to the *b* axis (left) and a schematic view of the same motif where only the metal atoms and the cyanide bridges are drawn (right). Adapted from Toma et al. [86f]. Copyright ©Wiley-VCH.

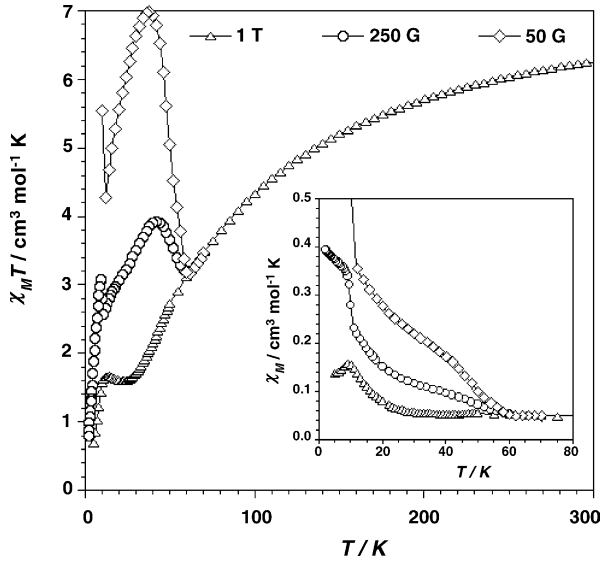

Fig. 16. $\chi_M T$ vs. T plot for $\{[Cr(bipy)(CN)_4]_2Mn(H_2O)\}\cdot H_2O\cdot CH_3CN$ under applied magnetic fields of 1 T (△), 250 G (◯) and 50 G (◊). The inset shows the thermal dependence of χ_M at $T \leq 80$ K. Reprinted from Toma et al. [86f]. Copyright ©Wiley-VCH.

Very recently, in our attempts to extend the use of the $[Cr(bipy)(CN)_4]^-$ unit as a ligand towards partially blocked metal complexes, we obtained the heterodinuclear complex $\{[Cr(bipy)(CN)_4][Cu(bpca)(H_2O)]\}$ (Fig. 17, left) where only one of the four cyanide ligands of the chromium precursor occupying an equatorial position around the copper atom acts as bridge between the Cr^{III} and Cu^{II} metal ions (5.049 Å for the intramolecular metal-metal separation) [123]. Its magnetic properties (Fig. 17, right) are typical of a ferromagnetically coupled Cr^{III}–Cu^{II} pair with a $S = 2$ low-lying level ($J = +33.3\,cm^{-1}$, $\hat{H} = -J\hat{S}_{Cr}\cdot\hat{S}_{Cu}$) which is confirmed by the the magnetisation versus H plot (inset of Fig. 17, right) with a quasi saturation value of 4 BM. This ferromagnetic coupling is due to the strict orthogonality between the interacting magnetic orbitals of the Cr^{III} (t_{2g}) and Cu^{II} (e_g) ions.

The use of the $[Cr(ampy)(CN)_4]^-$ and $[Cr(phen)(CN)_4]^-$ units as ligands towards the fully hydrated manganese(II) ions afforded the crossed double chains $\{[Cr(ampy)(CN)_4]_2Mn(H_2O)_2\}\cdot 6H_2O$ [86g] (Fig. 18, left) and $\{[Cr(phen)(CN)_4]_2Mn(H_2O)_2\}\cdot 4H_2O$ [85b,86g] (Fig. 18, right). Their structures are made of neutral 4,2-ribbon like bimetallic chains where the chromium precursor acts as a bismonodentate bridging ligand. Both compounds behave as ferrimagnetic $Cr_2^{III}Mn^{II}$ chains which exhibit a metamagnetic behaviour with values of the critical field of 1 T and 5000 G, respectively. Below 4 K, the phen-containing chain shows a spin-canted structure with a quite narrow hysteresis loop, the value of the coercive field being 50 G.

Interestingly, the combined use of $[Cr(phen)(CN)_4]^-$ and azide as ligands towards $[Mn(H_2O)_6]^{2+}$ yielded the compound $\{[Cr(phen)(CN)_4]_2Mn(N_3)(CH_3OH)\}\cdot CH_3OH$ [85b] which is the first example of a cyano/azide-bridged species. The $[Cr(phen)(CN)_4]^-$ unit in this compound is linked to three manganese atoms through three of its four cyanide ligands to form a 3,3-ladder like chain [4], the adjacent ladders being further connected by two μ-1,1-azido bridges on the closest manganese atoms resulting in a layered structure. This shows ferrimagnetic behavior and metamagnetism (a maximum of the magnetic susceptibility occurs at 21.8 K which disappears for $H > 5000$ G).

Recent examples of the rational preparation of discrete heterobimetallic species through the reaction of $[Cr(ampy)(CN)_4]^-$ and $[Cr(phen(CN)_4]^-$ with partially blocked metal complexes are the heterodinuclear complex $\{[Cr(ampy)(CN)_4][Mn(MeOsalen)(H_2O)]\}\cdot 4H_2O$ (Fig. 19, left) [124] and the bimetallic tetranuclear species $\{[Cr(phen)(CN)_4]_2[Ni_2L^1(H_2O)_2]\}\cdot 2CH_3CN$ (Fig. 19, right) [125]. The chromium precursor acts as a monodentate ligand in both complexes through one of its four cyanide ligands toward the Mn^{III} and Ni^{II} ions, respectively. The magnetic coupling between the Cr^{III} and Ni^{II} ions in the tetranuclear species is ferromagnetic ($J = +11.8\,cm^{-1}$), as expected due to the strict orthogonality between the interacting magnetic orbitals (t_{2g} at the Cr^{III} versus e_g at the Ni^{II}).

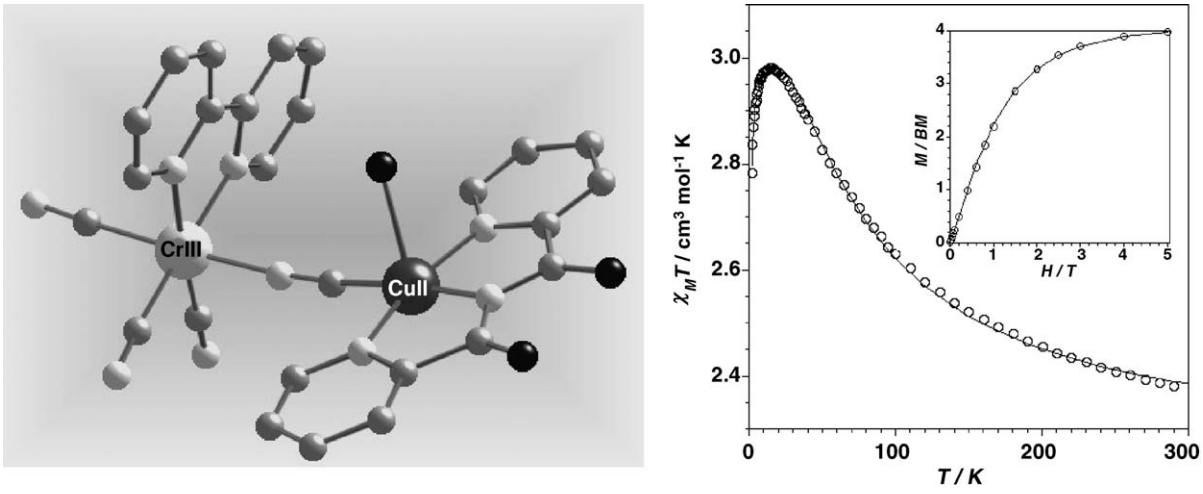

Fig. 17. Molecular structure of $\{[Cr(bipy)(CN)_4][Cu(bpca)(H_2O)]\}$ (left) and its magnetic properties under the form of $\chi_M T$ vs. T plot (right). The inset shows the magnetization plot at 2.0 K.

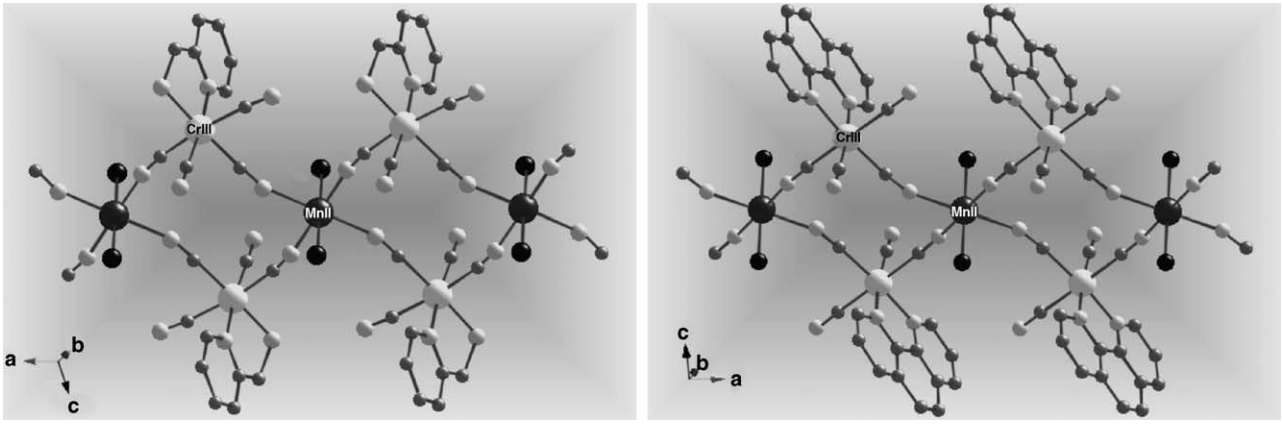

Fig. 18. Perspective views of fragments of the crossed double chains $\{[Cr(ampy)(CN)_4]_2Mn(H_2O)_2\}\cdot 6H_2O$ (left) and $\{[Cr(phen)(CN)_4]_2Mn(H_2O)_2\}\cdot 4H_2O$ (right). Adapted from Toma et al. [86g]. Copyright ©The Royal Society of Chemistry and the Centre Nationale de la Recherche Scientifique.

3.2. $[Fe^{III}(L)(CN)_4]^-$

The use of the building block $[Fe^{III}(bipy)(CN)_4]^-$ as a ligand toward the fully hydrated species $[M(H_2O)_6]^{2+}$ (M = Mn, Fe, Co and Zn) yielded a wide variety of topologies of polynuclear species: the trinuclear neutral complexes $\{[Fe^{III}(bipy)(CN)_4]_2M^{II}(H_2O)_4\}\cdot 4H_2O$ (M = Mn and Zn) [86b], the corrugated ladder-like compounds $\{[Fe^{III}(bipy)(CN)_4]M^{II}\}\cdot 2H_2O$ (M = Cu and Zn [86b,126], the 4,2-ribbon like chains $\{[Fe^{III}(bipy)(CN)_4]_2M^{II}(H_2O)_2\}\cdot 4H_2O$ (M = Co and Cu) [126,127] and the bis double zigzag chains $\{[Fe^{III}(bipy)(CN)_4]_2M^{II}(H_2O)\}\cdot 1/2H_2O\cdot CH_3CN$ (M = Co and Mn) [128].

In the structure of the centrosymmetric trinuclear species (Fig. 20), the $[Fe^{III}(bipy)(CN)_4]^-$ unit acts as a monodentate ligand toward $M^{II}(H_2O)_4$ (M = Mn and Zn) through one cyanide group, the other three ones remaining terminal. The intramolecular Fe-M distances are 5.126(1) (M = Mn) and 5.018(1) Å (M = Zn). The analysis of the magnetic properties of the manganese derivative show the occurrence of very weak antiferromagnetic interactions between the adjacent low-spin iron(III) and high-spin manganese(II) ions through the bridging cyanide ($J = -0.9\,cm^{-1}$) and between the peripheral low-spin iron(III) ions through the –CN–Mn–CN– bridging framework ($J' = -1.3\,cm^{-1}$). This last value is equal to that found in the zinc-containing trimer. A net overlap of the magnetic orbitals through the π t_{2g}–t_{2g} pathway [$t_{2g}^5e_g^0$ and $t_{2g}^3e_g^2$ electronic configurations for Fe(III) and Mn(II), respectively] accounts for the antiferromagnetic interaction between the low-spin iron(III) and the high-spin manganese(II) ions. It seems surprising that J' is larger than J given that the separation between the interacting spins is double in the former than in the latter. However, when

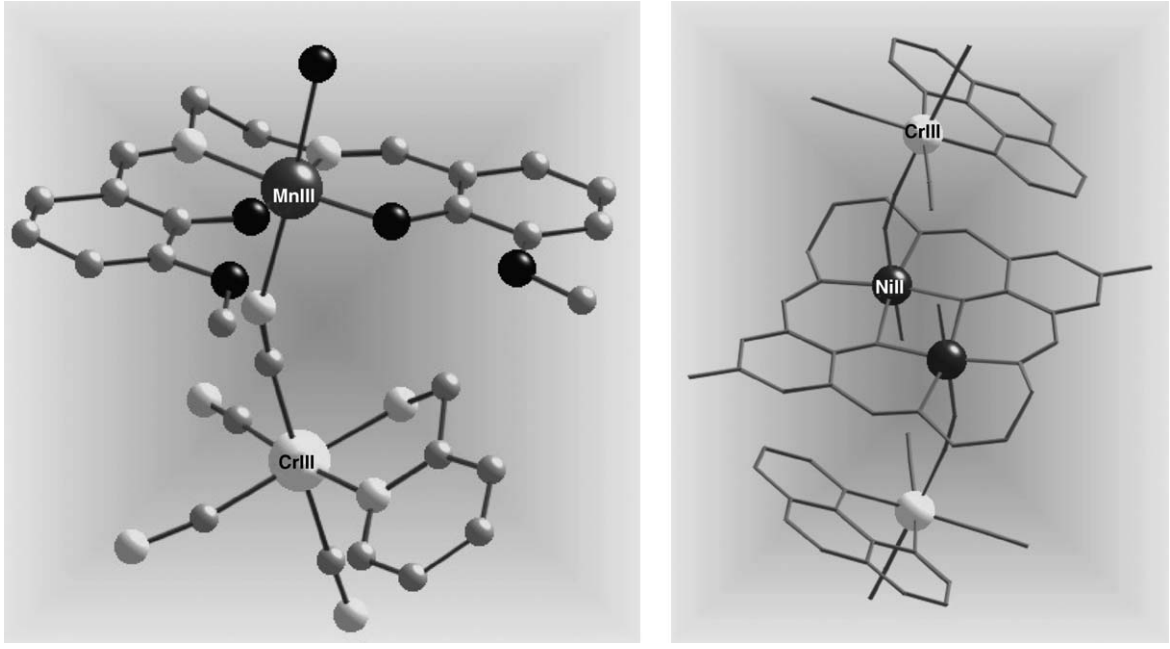

Fig. 19. Molecular structures of $\{[Cr(ampy)(CN)_4][Mn(MeOsalen)(H_2O)]\}\cdot 4H_2O$ (left) and $\{[Cr(phen)(CN)_4]_2[Ni_2L^1(H_2O)_2]\}\cdot 2CH_3CN$ (right). Adapted (right) from Toma et al. [125]. Copyright ©The Royal Society of Chemistry.

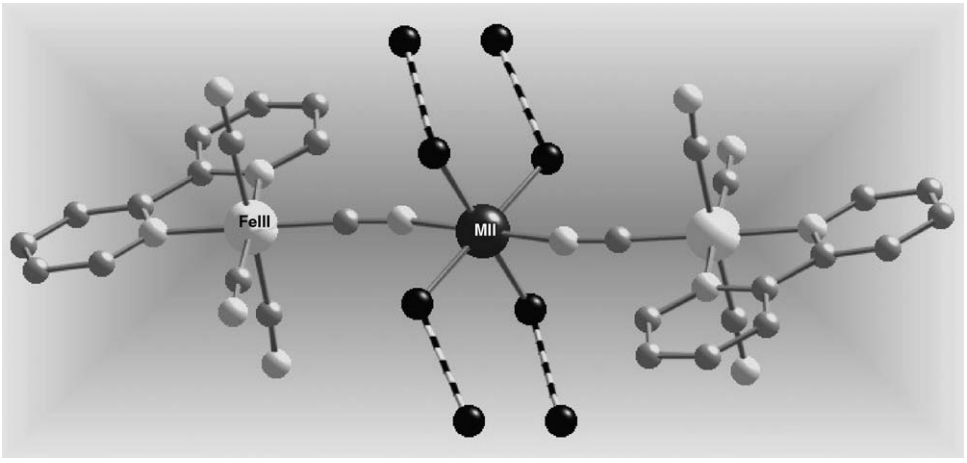

Fig. 20. Molecular structure of the trinuclear complex $\{[Fe^{III}(bipy)(CN)_4]_2M^{II}(H_2O)_4\}\cdot 4H_2O$ (M = Mn and Zn). The hydrogen bonds involving the water molecules are drawn as broken lines. Adapted from Lescouëzec et al. [86b]. Copyright ©American Chemical Society.

the number of the unpaired electrons (n_M) of the interacting centres is considered (one versus one in J' and five versus one in J), the situation becomes clearer given that the coupling energies to be compared [129] $n_{Fe}n_{Fe}J'$ ($-1.3\,cm^{-1}$) versus $n_{Fe}n_{Mn}J$ ($-4.5\,cm^{-1}$).

The structure of the isostructural corrugated ladder-like compounds $\{[Fe^{III}(bipy)(CN)_4]M^{II}\}\cdot 2H_2O$ with M = Cu and Zn (Fig. 21) resembles that of the two condensed chains of the compound $\{[Cr(bipy)(CN)_4]_2Mn(H_2O)\}\cdot H_2O\cdot CH_3CN$ (see Fig. 15), the main difference being that M is five-coordinate (five cyanide nitrogen atoms form a highly distorted MN_5 square pyramid) whereas the manganese atom in the chromium compound is six-coordinate (two *trans* coordinated water molecules and four cyanide nitrogen atoms form a somewhat distorted MnN_4O_2 octahedron).

The structure of the 4,2-ribbon like chain $\{[Fe^{III}(bipy)(CN)_4]_2Co^{II}(H_2O)_2\}\cdot 4H_2O$ (Fig. 22, left) is like the preceding ones observed in the chromium family but in the present case, there are two orientations of the chains in the unit cell (Fig. 22, right). This compound exhibits intrachain ferromagnetic coupling, slow magnetic relaxation and hysteresis effects being thus a single chain magnet (SCM). The analysis and discussion of this interesting behavior will be performed later (see Section 4.2). The poor diffraction pattern of the crystals of the related compound with copper(II) precluded an accurate structural determination but showed unambiguously that it is also a 4,2-ribbon like chain, the elongation axis at the six-coordinate copper atom being defined by two *trans*-coordinated water molecules. The magnetic behaviour of this compound corresponds to that of a ferromagnetically coupled chain of low-spin iron(III) and copper(II) ions with frequency dependence of the out-of-phase ac susceptibility signal at $T < 3.0$ K.

The isostructural bis double zigzag chains $\{[Fe^{III}(bipy)(CN)_4]_2M^{II}(H_2O)\}\cdot 1/2H_2O\cdot CH_3CN$ (M = Co and Mn) (Fig. 23) can be viewed as derived from the condensation of two parallel 4,2-ribbon like chains, one of the axially coordinated water molecule to the metal atom M of one chain being replaced by a cyanide nitrogen from the other chain. Each M atom in these condensed chains is thus six-coordinate MN_5O. Tris- and bis-monodenate bridging modes of the $[Fe^{III}(bipy)(CN)_4]^-$ precursor occur in these chains. The synthesis is carried out by the reaction of the precursor $[Fe^{III}(bipy)(CN)_4]^-$ precursor with the

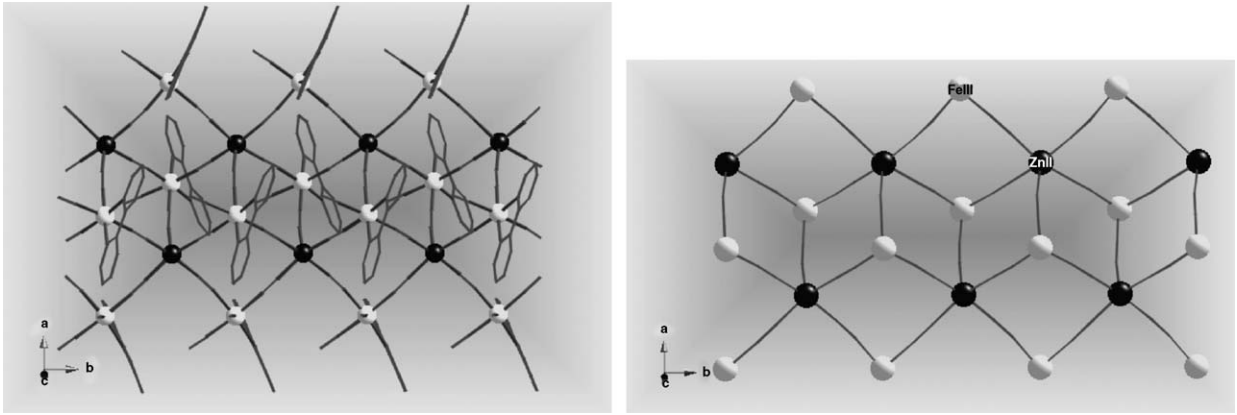

Fig. 21. Structure of $\{[Fe^{III}(bipy)(CN)_4]Zn^{II}\}\cdot 2H_2O$: perspective view of a fragment of the two condensed 4,2-ribbon like chains running parallel to the *b* axis (left) and a schematic view of the same motif where only the metal atoms and the cyanide bridges are drawn (right). Adapted from Lescouëzec et al. [86b]. Copyright ©American Chemical Society.

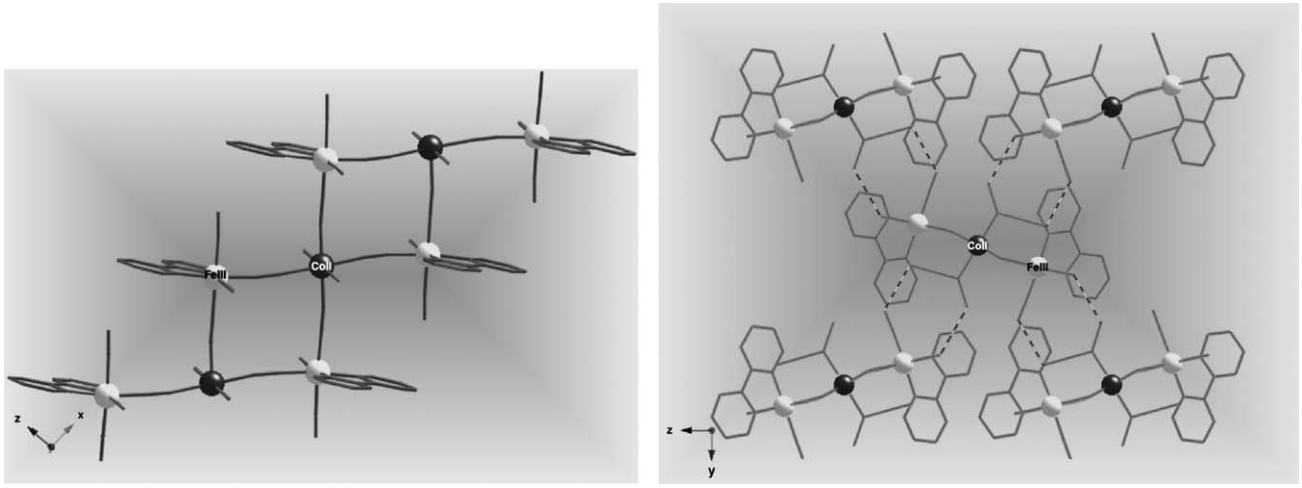

Fig. 22. Crystal structure of $\{[Fe^{III}(bipy)(CN)_4]_2Co^{II}(H_2O)_2\}\cdot 4H_2O$: perspective view of a fragment of the 4,2-ribbon like chain running parallel to the *a* axis (left) and a projection down the *a* axis showing the two orientations of the chains in the unit cell (right). Adapted (left) from Lescouëzec et al. [127]. Copyright ©Wiley-VCH.

fully solvated M^{II} ion in a CH_3CN:H_2O 90:10 (v/v) mixture. The magnetic behaviour of the manganese derivative corresponds to two ferrimagnetic $Fe^{III}_2Mn^{II}$ chains coupled by a weak antiferromagnetic interaction. Interestingly, the cobalt derivative exhibits intrachain ferromagnetic coupling and interchain antiferromagnetic coupling (this last interaction being overcome by an applied magnetic field $H > 600$ G), slow magnetic relaxation and hysteresis effects constituting thereby a new example of a chain magnet (a thorough discussion of the magnetic properties of this compound is done in Section 4.2).

As done with the previous cyanide-bearing chromium(III) precursors, the use of the $[Fe^{III}(bipy)(CN)_4]^-$ unit as a ligand toward partially blocked metal complexes such as $[Cu^{II}(bpca)]^+$, $[Mn^{III}(MeOsalen)]^+$ and $[Mn^{II}_2(bpym)(H_2O)_8]^{4+}$ has produced the neutral heterodinuclear species $\{[Fe^{III}(bipy)(CN)_4][Cu^{II}(bpca)(H_2O)]\}$ [130] (Fig. 24, left) and $\{[Fe^{III}(bipy)(CN)_4][Mn^{III}(MeOsalen)(H_2O)]\}$ [131] (Fig. 24, right) and the tetranuclear compound $(\mu\text{-bpym})[Mn(H_2O)_3\{Fe(bipy)(CN)_4\}]_2[Fe(bipy)(CN)_4]_2\cdot 12H_2O$ [86c] (Fig. 25). The cyanide-bearing precursor in the three compounds acts as a monodentate ligand through one of its four cyanide groups and also acts as a counterion in the last compound. Analysis of the magnetic properties of the tetranucear species shows the occurrence of significant antiferromagnetic interactions between the two high-spin manganese(II) ions through bridging bpym ($J = -1.2\ cm^{-1}$) and between the low-spin iron(III) and the high-spin manganese(II) ions across the single cyanide bridge ($J' = -3.0\ cm^{-1}$). The value of the antiferromagnetic interaction through bridging bpym is in the range of those previously reported for bpym-bridged manganese(II) compounds [$-J$ values yarying in the range 0.93–1.2 cm^{-1}] [132]. The value of magnetic coupling within the Fe^{III}–C–N–Mn^{II} unit ($J' = -3.0\ cm^{-1}$) in this tetranuclear complex is somewhat larger than that reported for the trinuclear compound $\{[Fe^{III}(bipy)(CN)_4]_2Mn^{II}(H_2O)_4\}\cdot 4H_2O$ ($-0.9\ cm^{-1}$) [86b]. The somewhat larger iron-manganese separation [5.092(4) Å (tetranuclear) versus 5.126(1) Å (trinuclear)] and the different chromophore around the manganese atom [MnN_3O_3 (tetranuclear) versus MnN_2O_4 (trinuclear)] [133] favour a larger antiferromagnetic interaction in the tetranuclear compound.

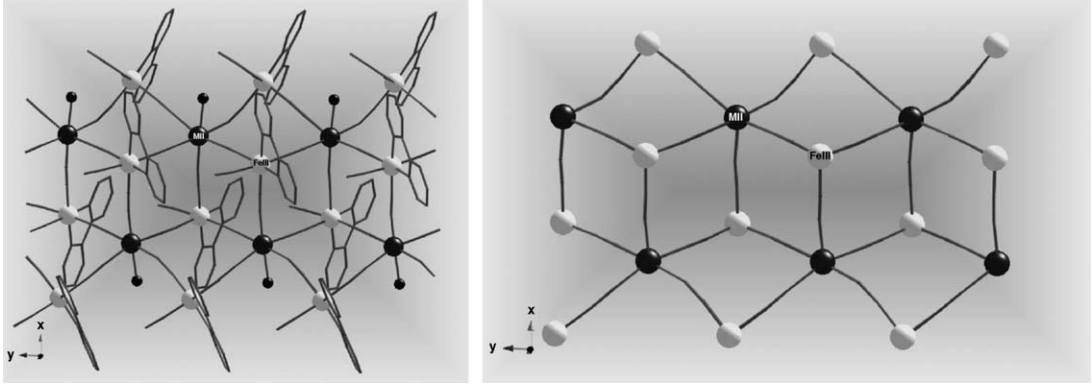

Fig. 23. Crystal structure of $\{[Fe^{III}(bipy)(CN)_4]_2M^{II}(H_2O)\}\cdot 1/2H_2O\cdot CH_3CN$: the two condensed 4,2-ribbon like chains running parallel to the *b* axis, the solvent molecules being omitted (left) and a schematic view of the same motif where only the metal atoms and the cyanide bridges are drawn (right). Adapted from Toma et al. [128]. Copyright ©The Royal Society of Chemistry.

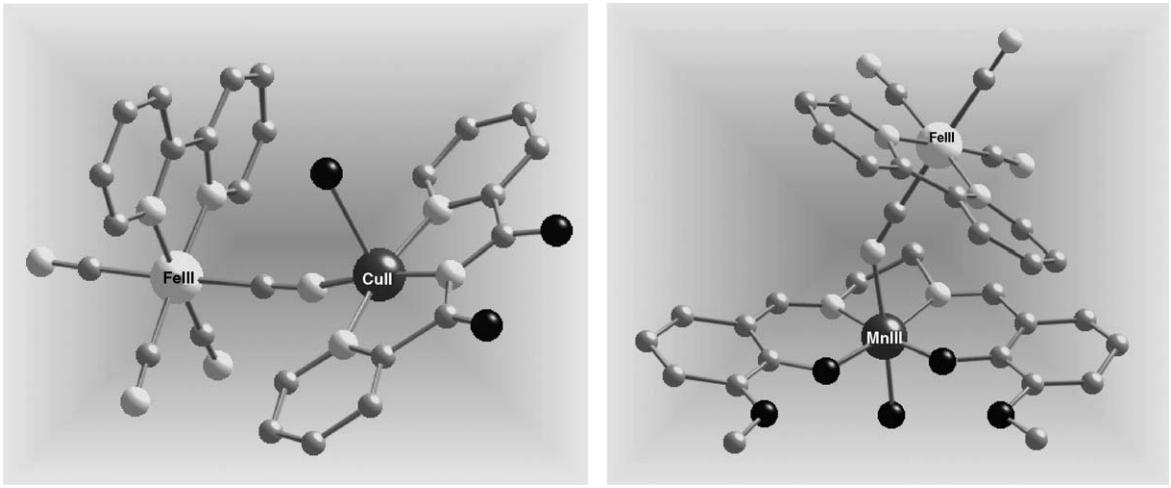

Fig. 24. Molecular structures of $\{[Fe^{III}(bipy)(CN)_4][Cu^{II}(bpca)(H_2O)]\}$ (left) and $\{[Fe^{III}(bipy)(CN)_4][Mn^{III}(MeOsalen)(H_2O)]\}$ (right).

Other parameters to be taken into account when analyzing the magnetic coupling in cyano-bridged species are the departure from the linearity of the Fe–C–N–Mn entity and the tilting at the cyanide bridge, as shown by theoretical calculations on homodinuclear cyano-bridged copper(II) and nickel(II) complexes [134].

The use of the building block $[Fe^{III}(phen)(CN)_4]^-$ as a ligand towards the fully hydrated species $[M(H_2O)_6]^{2+}$ (M = Mn, Co and Zn) yielded the 4,2-ribbon like bimetallic chains of formula $\{[Fe^{III}(phen)(CN)_4]_2M^{II}(H_2O)_2\}\cdot 4H_2O$ (M = Mn, Co and Zn) [86a,127] where the $[Fe(phen)(CN)_4]^-$ unit acts as a bismonodentate bridging ligand and the M atom is six-coordinate with four nitrogen-cyanide atoms in equatorial positions and two water molecules in the axial ones (Fig. 26). This structural motif has been previously observed when $[Fe^{III}(bipy)(CN)_4]^-$ and $[Cr(L)(CN)_4]^-$ (L = bidentate nitrogen donor) are used as ligands (see above). The compound $\{[Fe^{III}(phen)(CN)_4]_2Mn^{II}(H_2O)_2\}\cdot 4H_2O$ exhibits one-dimensional ferrimagnetic behaviour due to the non-compensation of the local interacting spins ($S_{Mn} = 5/2$ and $S_{Fe} = 1/2$) which interact antiferromagnetically through the bridging cyano groups. No magnetic ordering is observed for this compound above 1.9 K according to ac and zero field cooled magnetization measurements. The t_{2g}–t_{2g} pathways ensure the antiferromagnetic coupling between the high-spin Mn^{II} ($t_{2g}^3e_g^2$) and the low-spin Fe^{III} ($t_{2g}^5e_g^0$) of this $Fe_2^{III}Mn^{II}$ double zigzag chain. The magnetic properties of the $Fe_2^{III}Zn^{II}$ chain correspond to the sum of two magnetically isolated spin triplets, the magnetic coupling between the low-spin iron(III) centers through the –CN–Zn–CN– bridging skeleton (iron-iron separation larger than 10.2 Å) being negligible. The magnetic properties of the $Fe_2^{III}Co^{II}$ chain correspond to those of a single chain magnet and will be discussed in detail below (see Section 4.2).

As done with the previous cyanide-bearing iron(III) and chromium(III) precursors, the $[Fe^{III}(phen)(CN)_4]^-$ unit is also able to form heterometallic species when reacting with partially blocked metal complexes. So, its reaction with the $[Ni_2L^1(H_2O)_4]^{2+}$ dinuclear nickel(II) complex and the $[Cu(bpca)]^+$ mononuclear copper(II) species yielded the neutral tetranuclear complex $\{[Fe(phen)(CN)_4]_2[Ni_2L^1(H_2O)_2]\}\cdot 2CH_3CN$ [125] (Fig. 27) and the chain $\{[Fe(phen)(CN)_4][Cu(bpca)]\}\cdot CH_3OH\cdot H_2O$ [135] (Fig. 28). Curiously, the hexanuclear compound of formula $\{[Fe^{III}(phen)(CN)_4]_4Nd^{III}(NO_3)(H_2O)_3\}\cdot 2H_2O$ (Fig. 29)

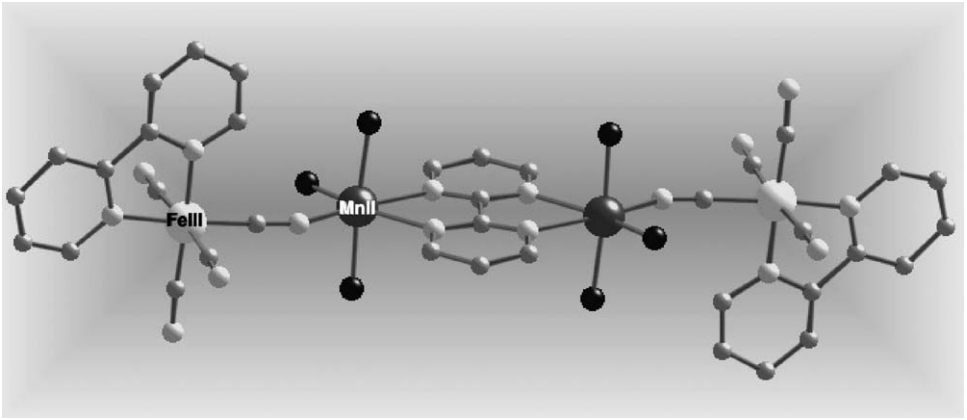

Fig. 25. Perspective view of the structure of the tetranuclear fragment $(\mu\text{-bpym})[Mn(H_2O)_3\{Fe(bipy)(CN)_4\}]_2^{2+}$. Adapted from Toma et al. [86c]. Copyright ©The Royal Society of Chemistry.

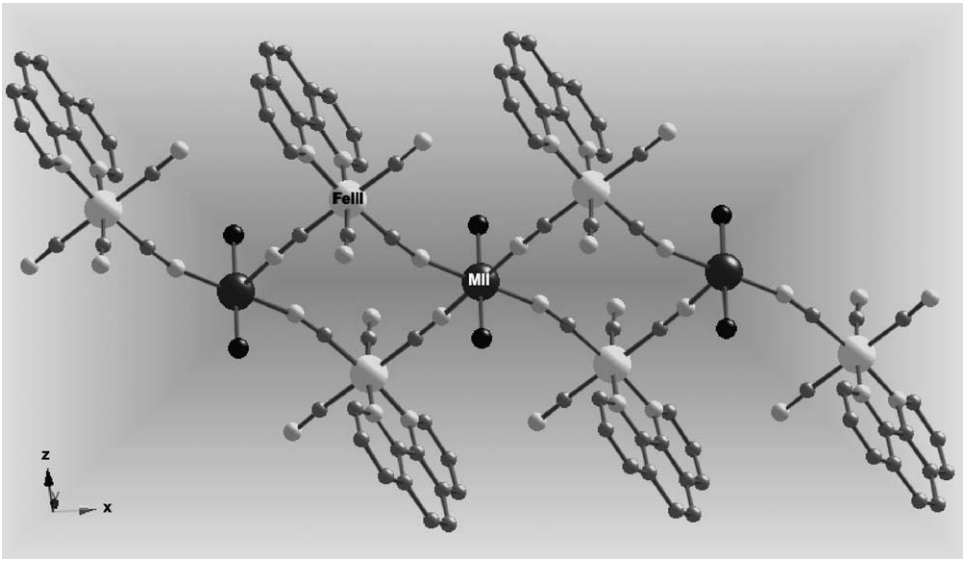

Fig. 26. Perspective view of a fragment of the 4,2-ribbon like chain formula $\{[Fe^{III}(phen)(CN)_4]_2M^{II}(H_2O)_2\}\cdot 4H_2O$ (M = Mn, Co and Zn). Adapted from Lescouëzec et al. [86a]. Copyright ©American Chemical Society.

was obtained when the $[Fe^{III}(phen)(CN)_4]^-$ unit reacts with neodymium(III) nitrate in aqueous aqueous solution [136]. The coordination of the nitrate as a bidentate ligand to the trivalent lanthanide ion leads to the divalent cation $[Nd(NO_3)]^{2+}$ which plays the role of a divalent metal ion, the electroneutrality motif being ensured under the hexameric topology of the $Fe^{III}_4Nd^{III}_2$ entity.

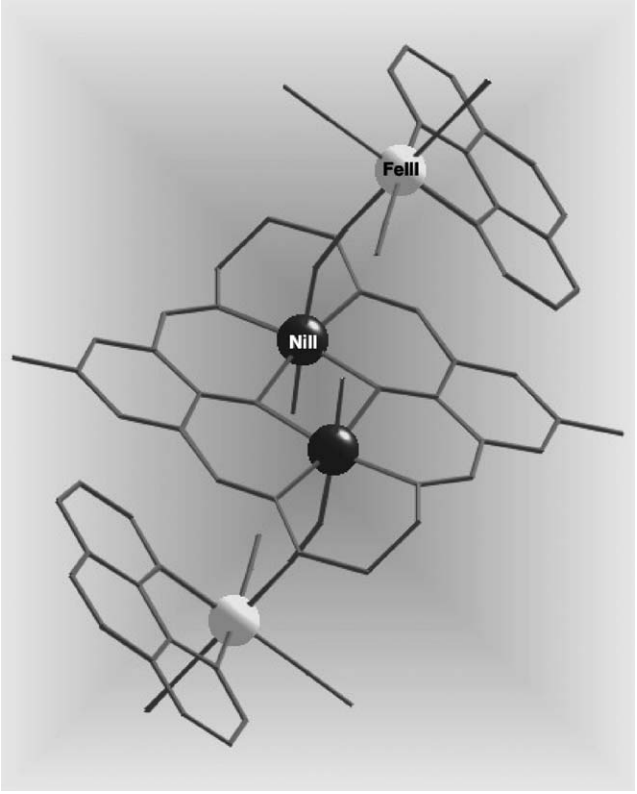

Fig. 27. Molecular structure of the compound $\{[Fe(phen)(CN)_4]_2[Ni_2L^1(H_2O)_2]\}\cdot 2CH_3CN$. The acetonitrile molecules are omitted. Adapted from Toma et al. [125]. Copyright ©The Royal Society of Chemistry.

Our first attempts to use the $[Fe^{III}(bpym)(CN)_4]^-$ complex as a ligand toward divalent first-row transition metal ions yielded the isostructural 4,2-ribbon like bimetallic chains of formula $\{[Fe^{III}(bpym)(CN)_4]_2M^{II}(H_2O)_2\}\cdot 6H_2O$ (M = Co and Cu) where water hexamer clusters (M = Co) (Fig. 30) and regular alternating fused six- and four-membered water rings (M = Cu) (Fig. 31) with two dangling waters are trapped between the ferromagnetically coupled cyanide-bridged low-spin Fe^{III} and M^{II} ions [137].

The cobalt derivative shows magnetic relaxation and hysteresis effects being another example of a single chain magnet (see Section 4.2) whereas the copper-containing chain exhibits metamagnetic behaviour with a value of the critical field of 400 G. The different cyclic motifs which interlink the two chains seem to be at the origin of this different magnetic behaviour: metamagnetism in the copper derivative and negligible interchain magnetic interactions in the cobalt one. The strict orthogonality between the magnetic orbital of the low-spin iron(III) ion and that of the copper(II) ion (t_{2g} and e_g type orbitals, respectively) accounts for the ferromagnetic coupling in the copper derivative whereas ferro- and antiferromagnetic contributions coexist in the case of the cobalt one [electronic configurations $t^5_{2g}e^0_g$ (Fe(III)) and ($t^5_{2g}e^2_g$) (Co(II))], but the ferromagnetic ones are predominant.

3.3. $[Fe^{III}(L)(CN)_3]^-$

The use of the mononuclear complex $[Fe^{III}(bpca)(CN)_3]^-$ as a ligand toward the fully hydrated manganese(II) ion yielded the ladder-like bimetallic chain $\{[Fe^{III}(bpca)(CN)_3Mn^{II}(H_2O)_3][Fe(bpca)(CN)_3]\}\cdot 3H_2O$ (Fig. 32, left) where the bpca-containing precursor plays two structural roles: it acts as a trismonodenate bridging ligand and also as a counterion [86e]. The *mer*-arrangement of the three cyanide groups of the mononuclear precursor seem to be specially suited to design ladder-like arrangements of metal ions. The environment of the

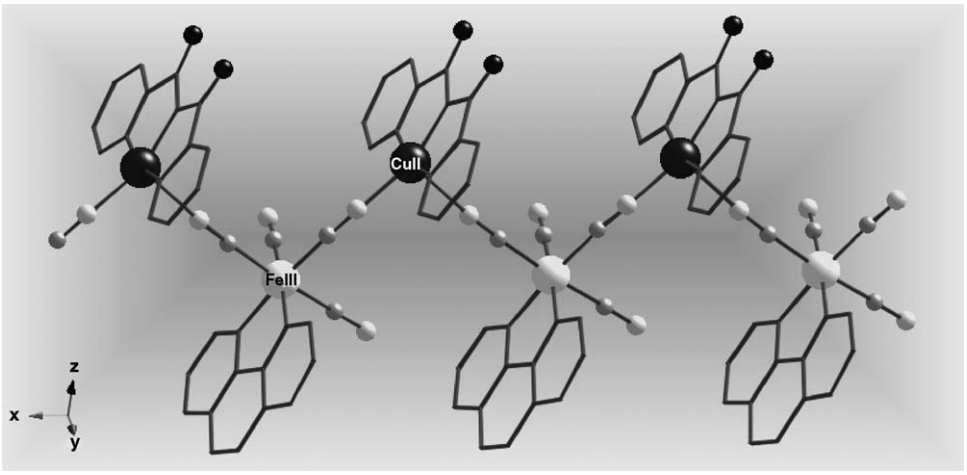

Fig. 28. Perspective view of a fragment of the chain $\{[Fe(phen)(CN)_4][Cu(bpca)]\}\cdot CH_3OH\cdot H_2O$. The solvent molecules are omitted.

manganese atom is six-coordinate with three water molecules in a *mer* arrangement and three cyanide-nitrogen atoms from three $[Fe^{III}(bpca)(CN)_3]^-$ units building a distorted octahedral MnN_3O_3 environment. The magnetic properties of this compound correspond to a ferrimagnetic chain (Fig. 32, right) with significant intrachain antiferromagnetic coupling between the low-spin iron(III) centres and the high-spin manganese(II) cations. The antiferromagnetic interaction is supported by the fact that the value of $\chi_M T$ in the minimum (4.0 $cm^3\,mol^{-1}\,K$) is well below that expected for two low-spin Fe(III) and one magnetically isolated high-spin Mn(II) ion. This is also confirmed by the saturation value of the magnetisation (5.0 BM) (inset of Fig. 32, right) which is as expected for a spin $S = 2$ arising from an antiferromagnetically coupled Mn(II)–Fe(III) pair [$S_{Mn} - S_{Fe} = 5/2 - 1/2 = 2$] plus an isolated low-spin Fe(III) ($S_{Fe} = 1/2$).

DFT type calculations on the $[Fe(bpca)(CN)_3]^-$ precursor show that its magnetic orbital is defined by a d_{xy} type orbital lying in the plane formed by the three cyanide ligands [the *x* and *y* axes being roughly defined by the iron to imide–nitrogen bond and the vector comprising the iron and the two *trans* cyanide ligands, respectively]. As shown in Fig. 33, a large spin density is located on the metal ion (+1.033) which is accompanied by a small delocalization on a *p* magnetic orbital centered on the nitrogen atom of the cyanide groups (+0.036). So, although ferro- and anitiferromagnetic contributions are involved in the magnetic coupling between a high-spin Mn(II) (electronic configuration $t_{2g}^3e_g^2$) and a low-spin Fe(III) ($t_{2g}^5e_g^0$), the magnetic properties of $\{[Fe^{III}(bpca)(CN)_3Mn^{II}(H_2O)_3][Fe(bpca)(CN)_3]\}\cdot 3H_2O$ show that the antiferromagnetic ones [t_{2g} (at the Mn) versus t_{2g} (at the iron)] are dominant. The lack of a theoretical model to analyze the magnetic properties of this bimetallic ladder-like chain

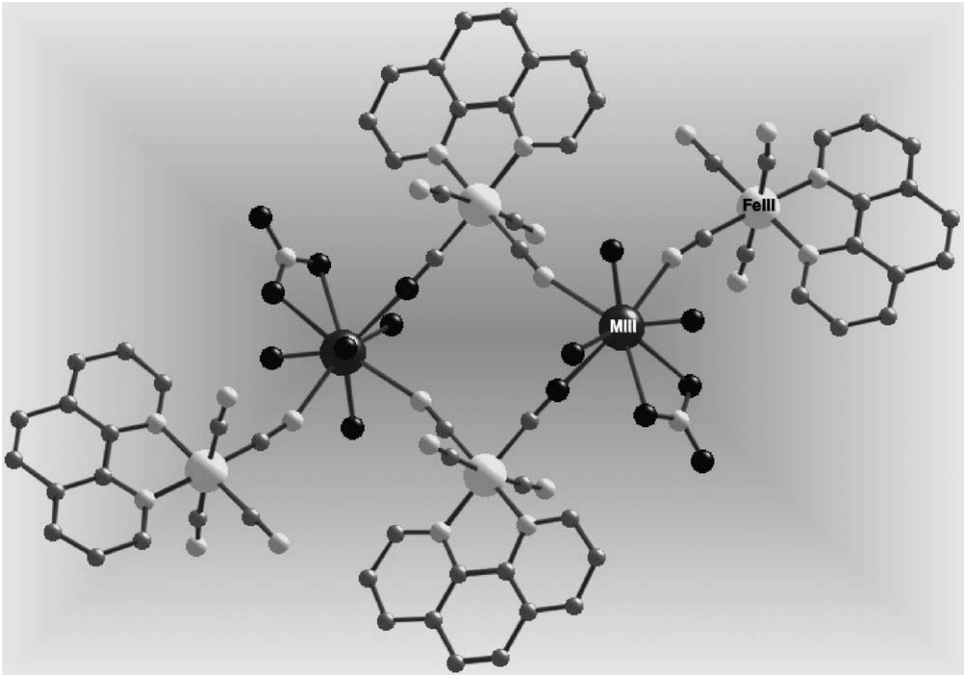

Fig. 29. Molecular structure of the hexameric complex $\{[Fe^{III}(phen)(CN)_4]_4[Nd^{III}(NO_3)(H_2O)_3]_2\}\cdot 2H_2O$. The crystallization water molecules are omitted.

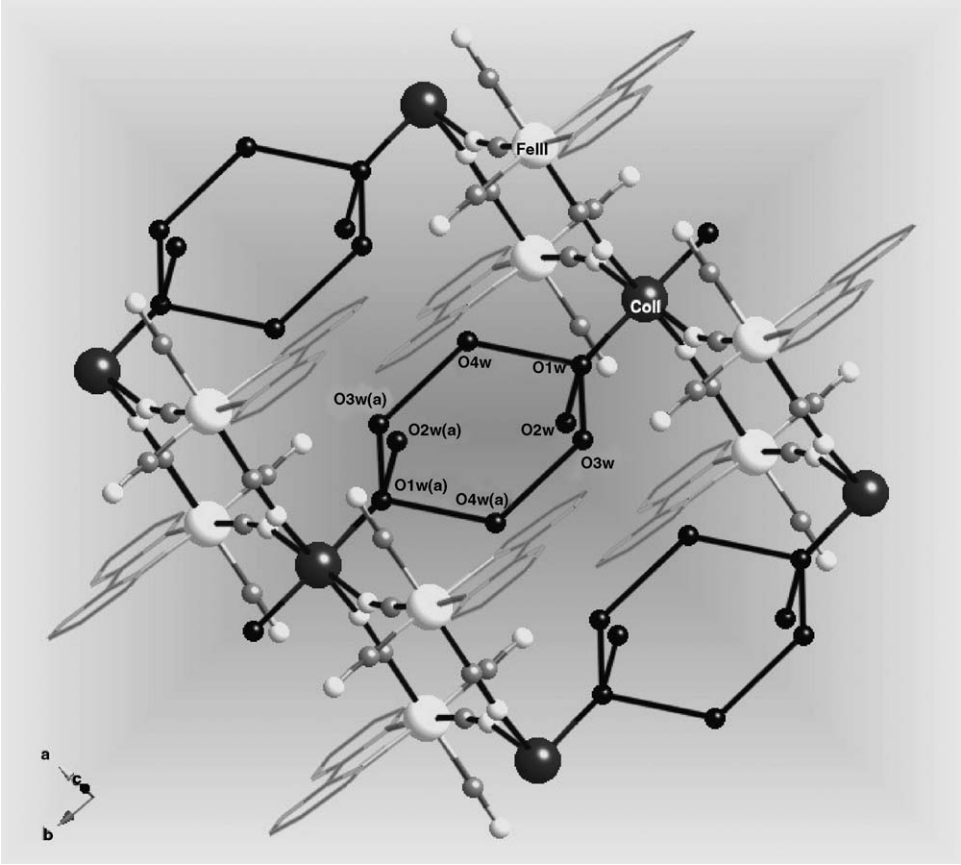

Fig. 30. Perspective view of the stacking of two fragments of adjacent chains of $\{[Fe^{III}(bpym)(CN)_4]_2Co^{II}(H_2O)_2\}\cdot 6H_2O$ showing the interchain linking through hydrogen bonds.

precludes the determination of the antiferromagnetic coupling involved.

The structure of the heterobimetallic compound $[Fe^{III}(bpca)(CN)_3Mn^{III}(MeOsalen)H_2O)]\cdot CH_3CN\cdot H_2O$ [138] (Fig. 34) is an illustrative example of the potential of the $[Fe^{III}(bpca)(CN)_3]^-$ building block in the design of cyanide-bridged metal assemblies where the nuclearity is strongly dependent on the denticity and charge of the blocking ligand on the outer metal ion (a tetradentate dianion in the present case).

The reaction between the *fac*-$\{Fe[HB(pz)_3](CN)_3\}^-$ unit and iron(III) chloride in aqueous solution yielded the tetranuclear complex *fac*-$\{[Fe^{III}\{HB(pz)_3\}(CN)_2(\mu\text{-}CN)]_3Fe^{III}(H_2O)_3\}\cdot 6H_2O$ [86d] (Fig. 35, left) where three low-spin iron(III) $[Fe[HB(pz)_3](CN)_3]^-$ units are bound to a central high-spin iron(III) through single cyanide bridges. The central iron atom is six-coordinate with three water molecules in *fac* positions and three cyanide–nitrogen atoms building a distorted octahedral motif. The facial stereochemistry in both the peripheral and central units in the resulting tetranuclear species suggests stereochemical control exerted by the *fac* precursor. The magnetic properties of this compound (Fig. 35, right) reveal the occurrence of ferromagnetic coupling between the central high-spin iron(III) ion and the three peripheral low-spin iron(III) ions leading to a nonet low-lying spin state as demonstrated by the magnetization plot at 1.9 K (inset of Fig. 35, right). This is an original example of molecular compound with ferromagnetic interaction between iron(III) ions exhibiting different spin states. Also, this compound opens new vistas in the design of high-spin heterometallic assemblies.

The structure and magnetic properties of the trinuclear species $\{[Fe^{III}\{HB(pz)_3\}(CN)_3]_2Mn(MeOH)_4\}\cdot 2MeOH$, the tetranuclear square compound $\{[Fe^{III}\{HB(pz)_3\}(CN)_3]_2[Mn(bipy)_2]_2\}(ClO_4)_2\cdot 4CH_3CN$, the 4,2-ribbon like bimetallic chain $\{[Fe^{III}\{HB(pz)_3\}(CN)_3]_2Cu(MeOH)\}\cdot 2MeOH$ and the face-centered cubic cluster $\{[Fe^{III}\{HB(pz)_3\}(CN)_3]_8[Cu(H_2O)]_6\}(ClO_4)_4\cdot 12H_2O\cdot 2Et_2O$ have been published very recently [77,85c,87]. In the trinuclear species, two peripheral $[Fe[HB(pz)_3](CN)_3]^-$ units are coordinated to a central manganese(II) ion as monodentate ligands in *trans* geometry, resulting in a linear trinuclear structure. In the tetranuclear species, the $[Fe[HB(pz)_3](CN)_3]^-$ unit acts as a bismonodenate bridging ligand through two of its three cyanide groups toward two $[Mn(bipy)]^{2+}$ entities to form a cyclic tetranuclear structure. This bridging mode of the $[Fe[HB(pz)_3](CN)_3]^-$ entity also occurs in the chain compound whose basic structural unit is a $Cu^{II}{}_2(CN)_4Fe^{III}{}_2$ square with each copper atom shared by two squares. The copper environment is distorted square pyramidal with four cyanide-nitrogen atoms occupying the equatorial positions and a methanol molecule in the axial one. Finally, the $[Fe[HB(pz)_3](CN)_3]^-$ entity in the cluster compound acts as a bridging trismonodentate ligand through its three cyanide groups toward three copper atoms, the eight iron-capped

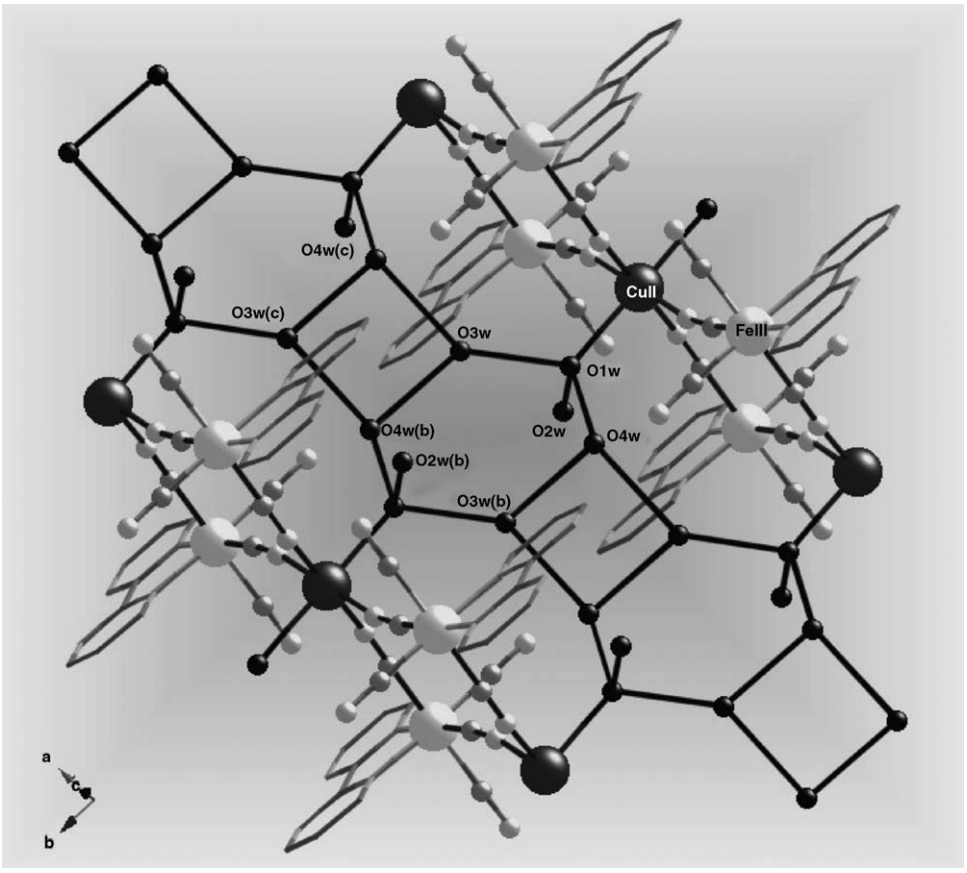

Fig. 31. Perspective view of the stacking of two fragments of adjacent chains of $\{[Fe^{III}(bpym)(CN)_4]_2Cu^{II}(H_2O)_2\}\cdot 6H_2O$ showing the interchain linking through hydrogen bonds.

units being arranged in a cube and the copper atoms located above the center of each cube face. The copper environment is distorted square pyramidal with four cyanide-nitrogen atoms in the equatorial positions and a water molecule in the apical one. Overall antiferromagnetic (trinuclear and tetranuclear) and ferromagnetic (chain and cluster) behavior was observed, the two last compounds being a SCM (chain) (see below, Section 4.2) [85c] and a SMM (cluster) [77].

The reaction of the $[Fe[HB(pz)_3](CN)_3]^-$ unit with the partially blocked species $[M(bpym)(H_2O)_4]^{2+}$ afforded a family

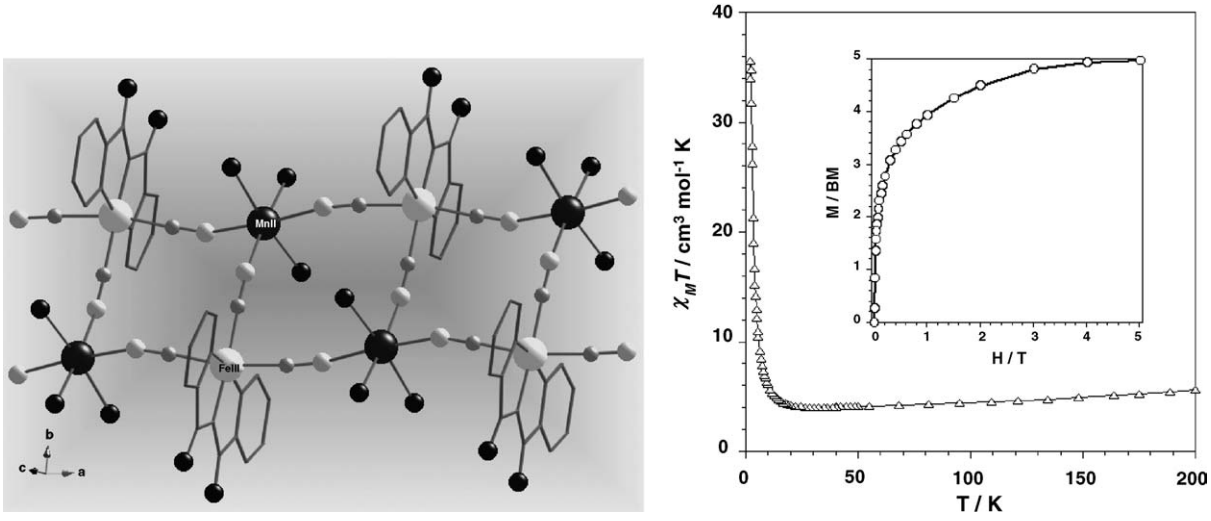

Fig. 32. Pespective view of a fragment of the ladder-like cationic chain $[Fe^{III}(bpca)(CN)_3Mn^{II}(H_2O)_3]^+$ (left) from compound $\{[Fe^{III}(bpca)(CN)_3Mn^{II}(H_2O)_3][Fe(bpca)(CN)_3]\}\cdot 3H_2O$. Temperature dependence of the $\chi_M T$ product for $\{[Fe^{III}(bpca)(CN)_3Mn^{II}(H_2O)_3][Fe(bpca)(CN)_3]\}\cdot 3H_2O$ [$H = 0.1$ T ($T > 50$ K) and 50 G ($T < 50$ K)] (right). The inset shows the M against H plot at 1.9 K [(△, ◯) experimental data; (—) eye guide lines]. Adapted (left) and reprinted (right) from Lescouëzec et al. [86e]. Copyright ©American Chemical Society.

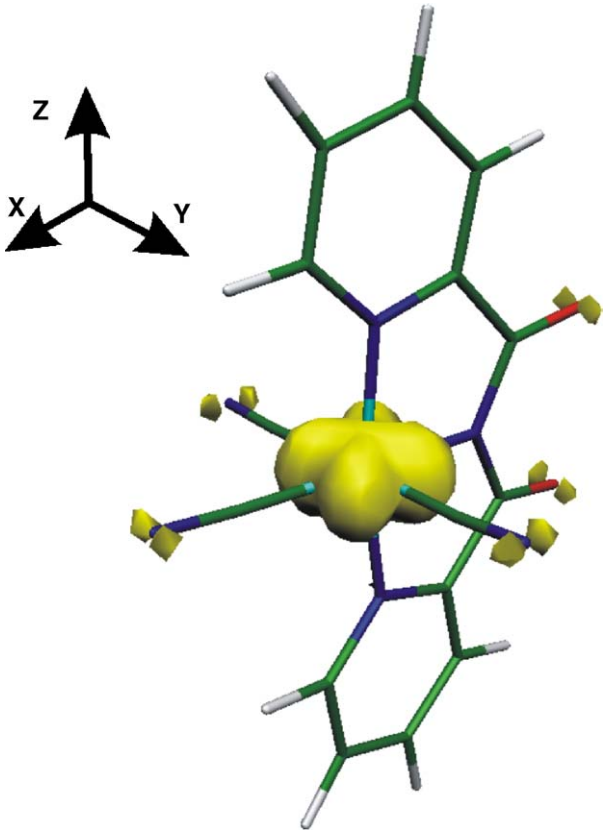

Fig. 33. Spin density map for the mononuclear precursor $[Fe(bpca)(CN)_3]^-$. The values of the atomic spin density in electron units are: +1.033 (Fe), −0.015 ($N_{bpca\text{-}pyridyl}$), −0.002 ($N_{bpca\text{-}imido}$), −0.043 (C_{cyano}) and +0.036 (N_{cyano}). Average values are given for the atoms other than iron and nitrogen-imido of bpca. Reprinted from Lescouëzec et al. [86e]. Copyright© American Chemical Society.

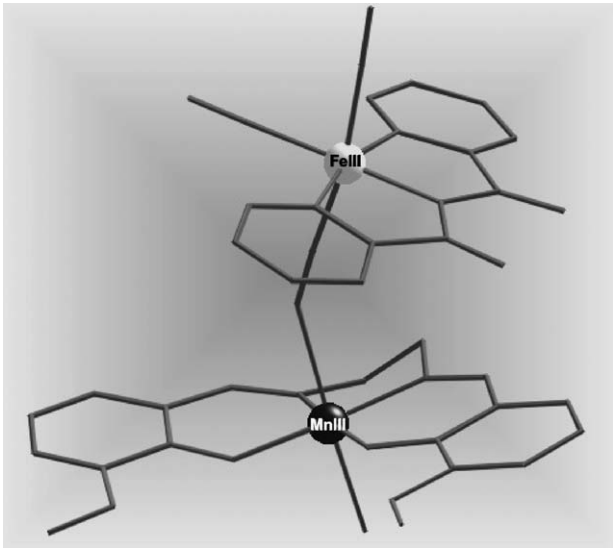

Fig. 34. Molecular structure of the heterobimetallic species $[Fe^{III}(bpca)(CN)_3Mn^{III}(MeOsalen)H_2O)]\cdot CH_3CN\cdot H_2O$. The solvent molecules are omitted.

of isostructural and centrosymmetric hexanuclear complexes of formula $\{[Fe^{III}\{HB(pz)_3\}(CN)_3]_4[M_n{}^{II}(bpym)(H_2O)]_2\}$ (M = Fe, Mn, Co and Zn) (Fig. 36) where the cyano-bearing mononuclear precursor acts as a monodentate [Fe(3)] and bismonodentate [Fe(1)] ligand toward the $[M(bpym)(H_2O)]^{2+}$ entity [139]. The M atom is six-coordinate with two bpym-nitrogen atoms, three cyanide-nitrogen atoms and a water molecule building a distorted octahedral structure. Preliminar variable-temperature magnetic susceptibility measurements on these compounds show several interesting features: (i) first, Mn(II), Fe(II) and Co(II) are high-spin ions; (ii) second, the magnetic behaviour of the zinc derivative practically correspond to that of four magnetically isolated low-spin iron(III) ions;

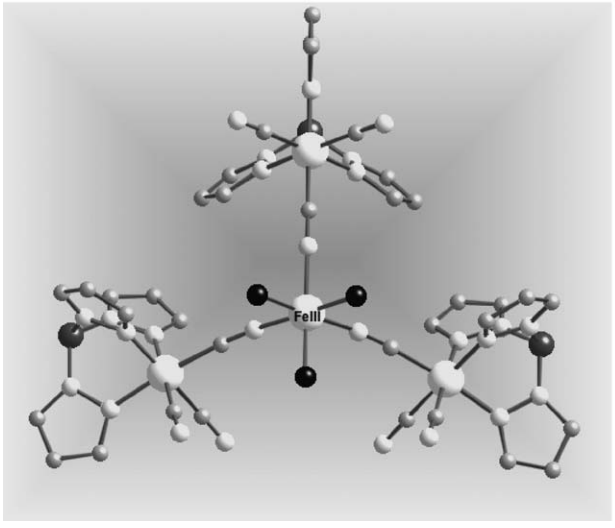

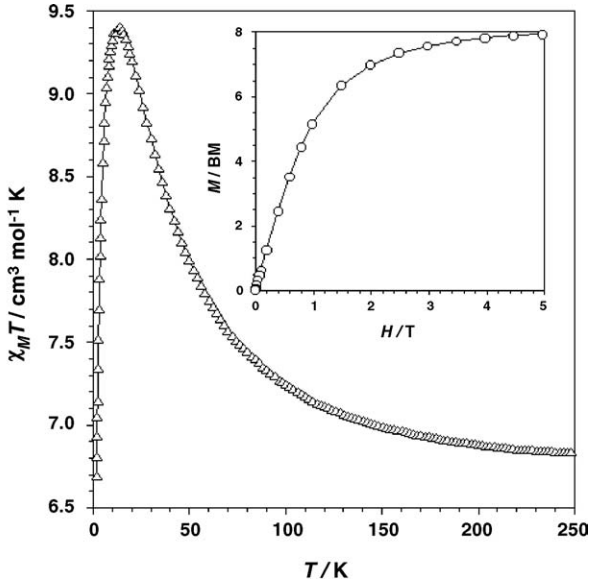

Fig. 35. Molecular structure of the tetranuclear compound *fac*-$\{[Fe^{III}\{HB(pz)_3\}(CN)_2(\mu\text{-}CN)]_3Fe^{III}(H_2O)_3\}\cdot 6H_2O$ (left) and temperature dependence of its $\chi_M T$ product (right). The inset shows the *M* vs. *H* plot at 1.9 K [(△, ◯) experimental data; (—) eye-guide lines]. Adapted (left) and reprinted (right) from Lescouëzec et al. [86d]. Copyright ©American Chemical Society.

(iii) third, overall antiferromagnetic coupling is observed for the manganese derivative, whereas ferromagnetic interactions occur in the iron- and cobalt-containing compounds.

Bimetallic zigzag chains of formula $\{[Fe^{III}\{HB(pz)_3\}(CN)_3][Co^{II}(dmphen)(NO_3)]\}$ (Fig. 37) and $\{[Fe^{III}\{HB(pz)_3\}(CN)_3][Cu^{II}_2(apox)(NO_3)]\} \cdot 3H_2O$ (Fig. 38) are obtained when using the mononuclear precursor $\{Fe[HB(pz)_3](CN)_3\}^-$ as a ligand toward the preformed species $[Co(dmphen)]^{2+}$ and $[Cu_2(apox)]^{2+}$, respectively [140]. $\{Fe[HB(pz)_3](CN)_3\}^-$ acts a bismonodentate bridging ligand in both compounds and in the latter one it acts also as a terminal monodentate ligand. The bisterdentate bridging mode of the apox ligand in the iron-copper chain was previously observed in other structurally characterized oxamidato-containing complexes [141]. The cobalt(II) ion has a highly distorted octahedral structure because of the coordination of a nitrate group as a bidentate ligand. The copper(II) ion exhibits square planar and square pyramidal stereochemistries, with the amine and amidate nitrogen atoms and the carbonyl–oxygen of the apox ligand and one cyanide–nitrogen atom occupying the equatorial positions and another cyanide–nitrogen atom filling the axial position.

3.4. $[M^{III}(L)_2(CN)_2]^{(2l-1)-}$ (M = Fe and Ru)

The preparation and structural characterization of the stable low-spin *cis*-dicyanobis(2,2′-bipyridyl)iron(III) species as a perchlorate salt [104,107] made possible its use as a ligand to design cyanide-bridged heterometallic assemblies. The reaction of this precursor with the preformed complex $[Cu(bipy)]^{2+}$ in methanol yielded the cyclic tetranuclear complex $\{[Fe^{III}(bipy)_2(CN)_2]_2[Cu^{II}(bipy)]_2\}(PF_6)_6 \cdot 4CH_3CN \cdot 2CHCl_3$ [82a] where iron(III) and copper(II) ions alternate in the vertexes of a square with single cyanide bridges defining the edges. The copper environment is square planar with four nitrogen atoms (from the bidentate bipy and two cyanide groups). The magnetic coupling between the adjacent spin doublets [low-spin iron(III) and copper(II)] is ferromagnetic ($J = +12.6\,cm^{-1}$) leading to a low-lying quintet spin state [107]. The strict orthogonality between the interacting magnetic orbitals (t_{2g} at the iron versus e_g at the copper) accounts for this ferromagnetic interaction. More interestingly, when the bipy ligands in the previous example are replaced by the bidentate dmbpy group (at the iron) and imino nitroxyl radical impy (at the copper), the square complex of formula $\{[Fe^{III}(dmbpy)_2(CN)_2]_2[Cu^{II}(impy)]_2\}(ClO_4)_6 \cdot 4CH_3OH \cdot 4H_2O$ was obtained ([82c] where the strong ferromagnetic coupling between the spin doublets of the copper(II) ion and the radical [d_σ (at the copper) versus p_π (at the radical)] allows consideration of the copper(II)–radical pair as a triplet spin state at room temperature. So, alternating spin doublets and triplets occur in the square core of this compound and given that the ferromagnetic coupling through the single cyanide bridge is ensured (case of strict orthogonality as commented above), a heptuplet ground spin state is achieved in this compound. This is a nice example of how the spin of the ground spin state of a given topology ($Fe^{III}_2Cu^{II}_2$ square planar) can be increased by playing on the nature of the outer ligands.

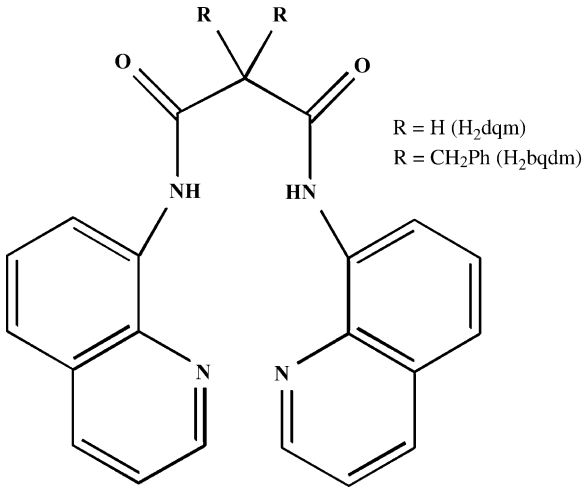

Scheme 5.

The replacement of the two bidentate ligands in the low-spin dicyano-iron(III) precursor by a tetradentate ligand makes possible the isolation of the *cis*- and *trans*- dicyano derivatives, as shown very recently by the structural determination of two low-spin iron(III) dicyano–dicarboxamido complexes which have been prepared from *N*,*N*′-bis(8-quinolyl)malonamide derivatives (see Scheme 5) [142]. The crystal structures of the complexes $NEt_4[Fe(bqm)(CN)_2]$ and $NEt_4[Fe(bqbm)(CN)_2] \cdot CH_3CN$ show that the four nitrogen atoms from the tetradentate ligand are arranged in the equatorial plane of the iron with the two cyanides *trans* to each other in the axial positions when the malonyl fragment is disubstituted (bqbm). However, the unsubstituted malonyl results in only three nitrogen atoms from the tetradentate ligand binding in the equatorial plane with the fourth in the apical position and the two cyanides occupying the *cis* sites, one equatorial and the other axial. Here, the substituents on the multidentate ligand allow the stereochemical control of the cyanide ligands. The use of these precursors as ligands to prepare heterometallic assemblies appears very promising but much work remains to be done.

The trivalent ruthenium ion represents an extension to 4d metal ions of the impressive number of magneto-structural studies which have been carried out with the paramagnetic hexacyanometallate species $[M^{III}(CN)_6]^{3-}$, M being a 3d metal ion such as Cr, Mn or Fe. Enhanced magnetic interactions are expected for heavier transition metal ions due to the greater diffuseness of the 4d and 5d orbitals when compared to the 3d ones. This is at the origin of the recent attempts to prepare cyanide-bearing ruthenium(III) complexes to be used as ligands [85a,102a]. Although the existence of $[Ru(CN)_6]^{3-}$ has been known more than fifty years, its molecular structure as a salt of formula $(AsPh_4)_3[Ru(CN)_6] \cdot 2H_2O$ was determined only in 2003 [102a]. The great instability of the low-spin $[Ru(CN)_6]^{3-}$ species ($S_{Ru} = 1/2$), in particular in solvents such as water and alcohols [143], (a feature which contrasts with the robustness and availability of the corresponding low-spin $[Fe(CN)_6]^{3-}$ complex), accounts for the poor knowledge of its chemistry. Oxidation of aqueous solutions of $[Ru(CN)_6]^{4-}$ by Ce(IV) in the presence of $AsPh_4^+$ affords the $(AsPh_4)_3[Ru(CN)_6] \cdot 2H_2O$

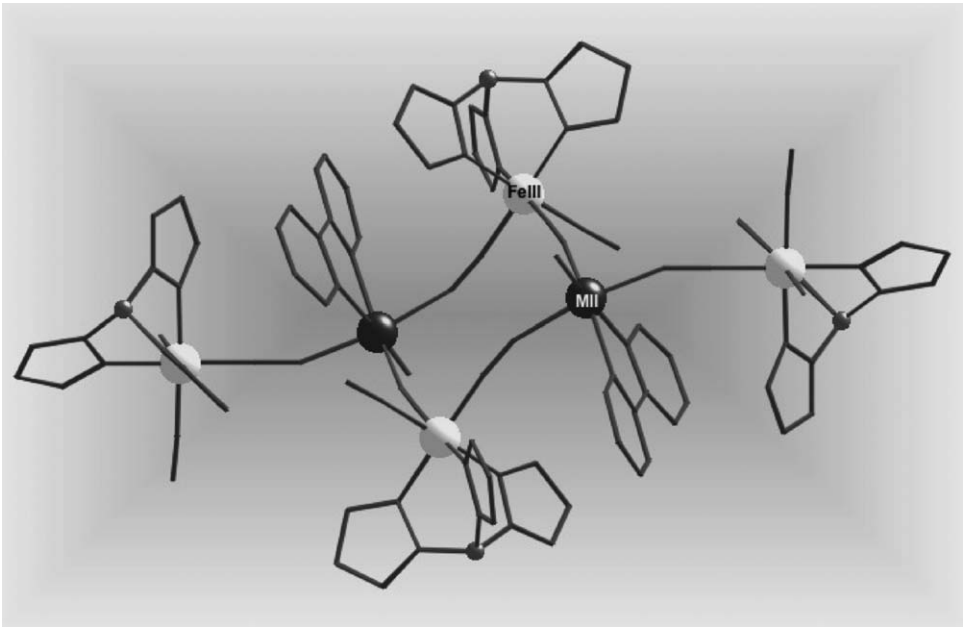

Fig. 36. Molecular structure of $\{[Fe^{III}\{HB(pz)_3\}(CN)_3]_4[Fe^{II}(bpym)(H_2O)]_2\}$.

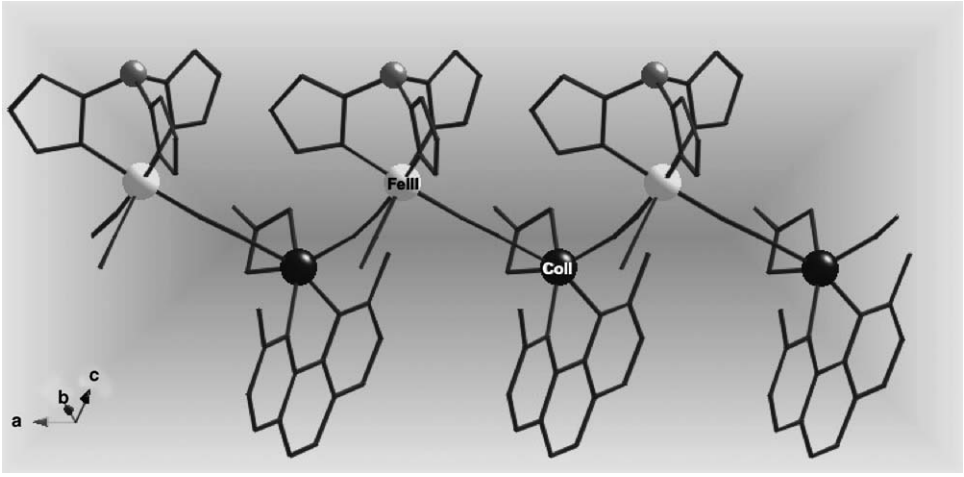

Fig. 37. Perspective view of a fragment of the zigzag chain $\{[Fe^{III}\{HB(pz)_3\}(CN)_3][Co^{II}(dmphen)(NO_3)]\}$.

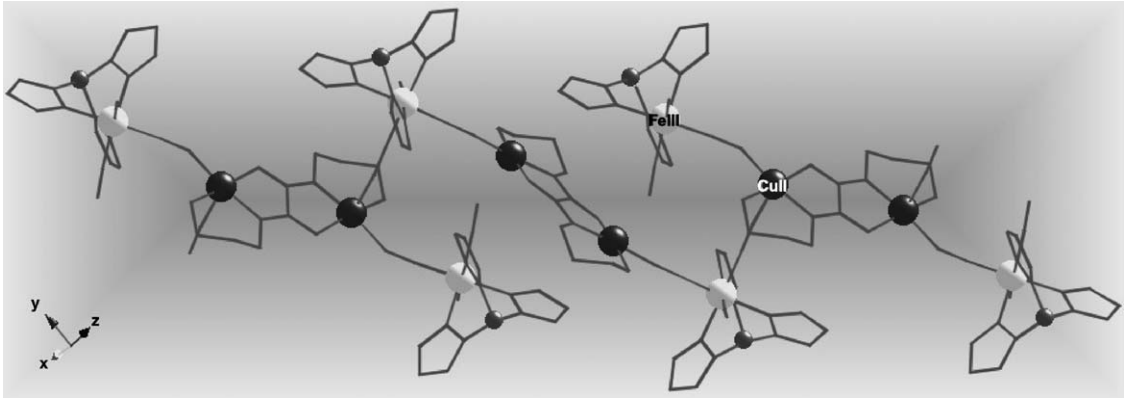

Fig. 38. Perspective view of a fragment of the chain $\{[Fe^{III}\{HB(pz)_3\}(CN)_3][Cu^{II}_2(apox)(NO_3)]\} \cdot 3H_2O$.

salt as yellow needles [102a]. The solid is quite stable at room temperature but it is photosensitive and its aqueous solutions decompose over a period of hours, the rate depending on the concentration and pH. These features make its use as a building block to prepare cyanide-bridged metal assemblies much more difficult than the above mentioned cyanide-containing precursors. DFT calculations on the $[Ru(CN)_6]^{3-}$ species have shown that it has a significantly higher spin density on the cyanide ligands than its iron congener [for instance, the spin densities on the terminal nitrogen atoms are approximately twice as large in the ruthenium as in the hexacyanoferrate(III) complex] [102a]. Very recently, the values of the spin densities on the cyanide ligands of $[Fe(CN)_6]^{3-}$ and $[Mn(CN)_6]^{3-}$ were determined by solid-state ^{13}C and ^{15}N NMR spectra [144], these types of studies being very important for the analysis and interpretation of the exchange pathways in cyanide-bridged metal complexes.

The instability of the $[Ru(CN)_6]^{3-}$ precursor directed the efforts of interested researchers toward alternative stable cyano complexes of ruthenium(III). So, the mononuclear complex of formula *trans*-$PPh_4[Ru(acac)_2(CN)_2]$ [85a] was prepared by reaction of *trans*-$PPh_4[Ru(acac)_2Cl_2]$ [145] with KCN in methanol. The ruthenium atom is six coordinate: four oxygen atoms from two bidentate acac ligands and two carbon atoms from two cyanide ligands in *trans* configuration build a somewhat distorted octahedral structure around the metal atom. Electrochemical data in acetonitrile as solvent reveal that $[Ru(acac)_2(CN)_2]^-$ is very stable with respect to both oxidation and reduction. In addition, electrospray mass spectrometry on methanolic solutions of this species indicates that it remains stable in this medium. At room temperature, the value of the μ_{eff} for this mononuclear compound is 1.91 BM, as expected for a low-spin configuration (t_{2g}^5) with $S = 1/2$. Consequently, this species fills the requirements to be used as a building block to design magnetic cyanide-bridged metal assemblies.

In fact, the use of $[Ru(acac)_2(CN)_2]^-$ as a ligand toward the manganese(II) ion in methanol yielded the three-dimensional cyano-bridged Ru^{III}-Mn^{II} bimetallic compound of formula $\{Mn[Ru(acac)_2(CN)_2]_2\}$ [85a]. Each manganese atom has a tetrahedral environment which is built by four nitrogen-cyanide atoms from four $[Ru(acac)_2(CN)_2]^-$ units leading to a three-dimensional network with a diamond-like structure. Its IR spectrum shows a cyanide stretching peak at 2125 cm^{-1} (to be compared with the corresponding stretching band at 2099 cm^{-1} of the terminal cyanide in the IR spectrum of the mononuclear precursor). Interestingly, it exhibits overall ferromagnetic behavior and magnetic ordering below 4 K ($T_c = 3.6$ K, this value being determined by ac magnetic susceptibility measurements). A characteristic hysteresis loop is observed at 1.85 K with very small values of the remnant magnetization and coercive field. The magnetic interaction between the Ru^{III} and Mn^{II} ions, through the oxalato bridge in the two-dimensional compound $NBut_4[Mn^{II}Ru^{III}(ox)_3]$, was also ferromagnetic but no magnetic ordering was detected down to 2.0 K [95].

In our efforts to extend the coordination chemistry of the $[Ru(acac)_2(CN)_2]^-$ unit to other metal ions, we explore its coordinating ability toward the cobalt(II) ion and the preformed complexes $[Ni_2L^1(H_2O)_4]^{2+}$, $[Co(dmphen)]^{2+}$ and $[Ni(dmphen)]^{2+}$. Four new compounds of formula $\{Co[Ru(acac)_2(CN)_2]_2\}$, $\{[Ru(acac)_2(CN)_2][Ni_2L^1(H_2O)_2]\}[Ru(acac)_2(CN)_2]_2 \cdot 2H_2O$ and $\{[Ru(acac)_2(CN)_2][M(dmphen)(NO_3]\} \cdot H_2O$ (M = Co and Ni) were isolated and structurally characterized [146]. The structure of the first complex is three-dimensional and consists of two interpenetrated (6,4) nets with twelve-gon cycles showing regular alternating $Co(NC)_4$ (cyano) tetrahedra and $Ru(acac)_2(CN)_2$ octahedra (Fig. 39).

In the first compound, the ruthenium precursor acts as a bismodentate bridging ligand toward two cobalt atoms and each cobalt atom is tetrahedrally coordinated by four cyanide-nitrogen atoms from four ruthenium units. The structure of the second compound consists of cationic chains of regular alternating $[Ru(acac)_2]$ and $[Ni_2L^1(H_2O)_2]$ units linked by single cyanide bridges (Fig. 40), the electroneutrality being achieved by uncoordinated $[Ru(acac)_2(CN)_2]^-$ anions.

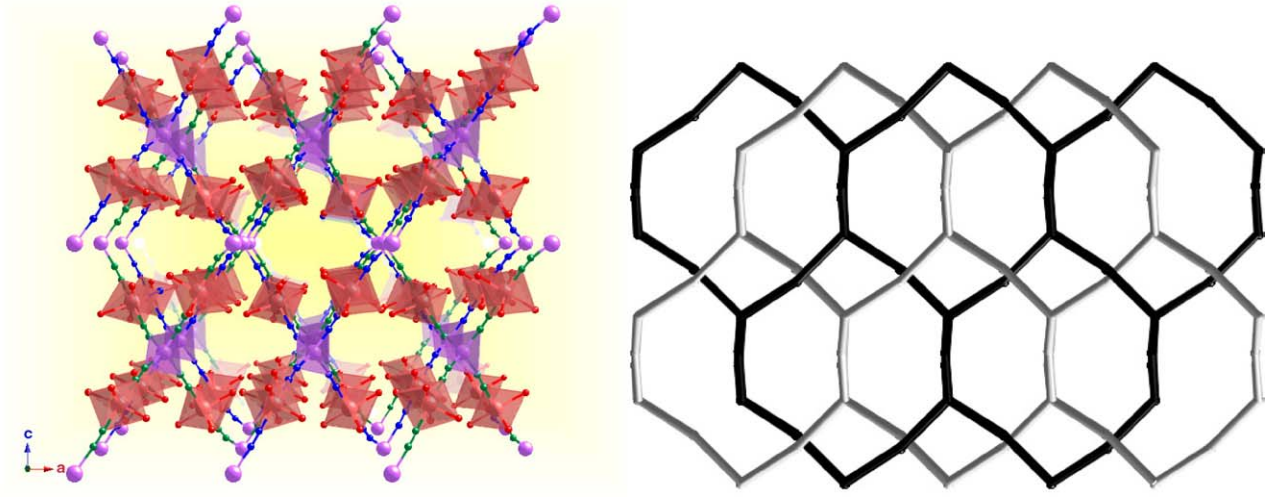

Fig. 39. Projection down the *b* axis showing two interpenetrated networks of $\{Co[Ru(acac)_2(CN)_2]_2\}$ (left); a schematic view along the [1 0 1] direction showing the interpenetration of two (6,4) nets (right).

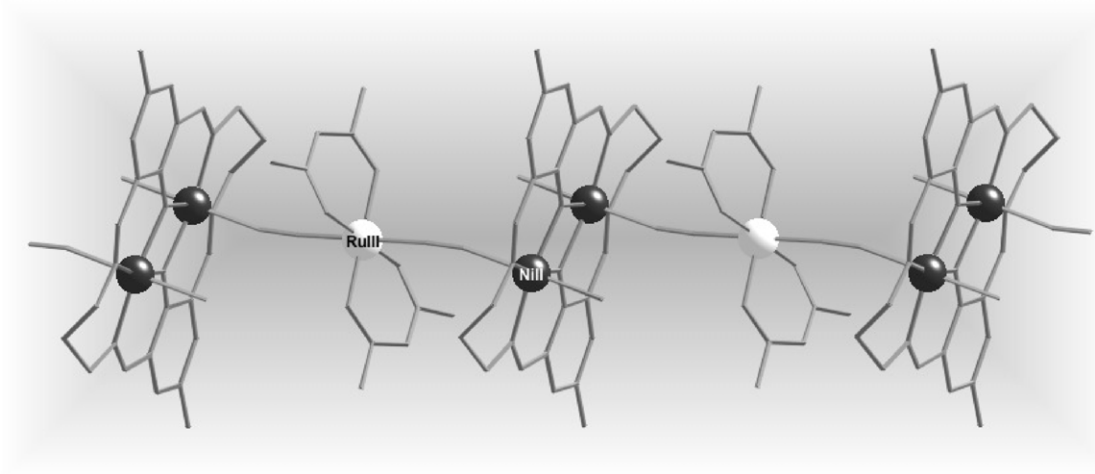

Fig. 40. Perspective view of a fragment of the cationic chain $\{[Ru(acac)_2(CN)_2][Ni_2L^1(H_2O)_2]\}^+$.

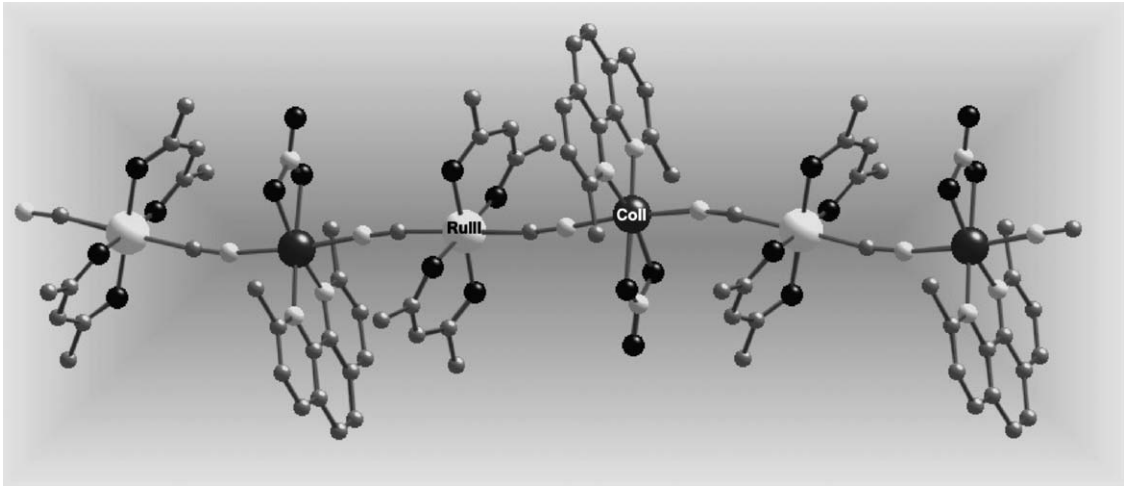

Fig. 41. Perspective view of a fragment of the bimetallic chain $\{[Ru(acac)_2(CN)_2][Co(dmphen)(NO_3]\}\cdot H_2O$.

A bimetallic chain is also observed in the third compound with regular alternating $[Ru(acac)_2]$ and $[Co(dmphen(NO_3)]$ units linked by single cyanide bridges in *trans* positions (Fig. 41). The same motif is observed in the last compound. These structures demonstrate that the use of the $[Ru(acac)_2(CN)_2]-$ unit as a ligand is an open field of research that will provide a plethora of new extended magnetic systems in a very near future.

4. Single chain magnet (SCM) behavior

4.1. A new type of magnet

Nowadays, single molecule magnets (SMMs) and single chain magnets (SCMs) (also referred to as magnetic nanowires) are two hot topics in molecular magnetism. The choice of the building block is very important in both topics where the so-called bottom-up synthetic approach is used. SMMs are molecules that exhibit slow magnetic relaxation below a blocking temperature (T_B) [78,147]. A ground state with both high spin (S) and large negative axial magnetic anisotropy (D) together with negligible intermolecular interactions are the conditions to be fullfillled to avoid three-dimensional ordering and to observe the properties of a nano-scale object. These properties are strongly dependent on the nuclearity and topology of the cluster as well as on the interacting metal centres and the bridging and blocking ligands [103,148]. The number of systems responding to these criteria is growing continuously and an exhaustive review is out of the scope of the present contribution Interested readers are referred to the excellent reviews by Gatteschi and Sessoli [78] and Winpenny [147]. Recent new examples which demonstrate that the SMM field is rapidly expanding are a Mn_{12} complex with carboxylate-sulfonate ligation [149], a Mn_{21} cluster with an unusual and low symmetry structure [150], a Mn_{22} wheel-like cluster [151], a citrate-containing Ni_{21} species [152], a polycationic Mn_{12} cluster bearing sixteen quaternary ammonium substituents in the periphery [153], a high-spin octanuclear nickel(II) complex [154] and the 3d/4f heterometallic systems Cu_2Tb_2 [155], Dy_6Mn_6 [156] and Ln_4Mn_{11} (M = Nd, Gd, Dy, Ho and Eu) [157]. Surprisingly, the simple out-of-plane dimer of Mn^{III} of formula $[Mn_2(saltmen)_2(ReO_4)_2]$

($S = 4$ ground spin sate) behaves as a SMM, being to date the smallest magnetic unit to show this behaviour [158]. Bridging oxygen atoms link the metal ions of the cluster in the known SMMs providing in general homometallic compounds. However, very recently, the cyanide ligand has proven to be a suitable bridging ligand to design SMMs with the added value of its asymmetric character. This last feature makes easier the preparation of heterometallic SMMs [74–77].

We focus on SCM behaviour which is at the heart of the present contribution. Magnetic chain compounds have been the subject of thorough investigation in the recent years in the area of molecular magnetism aimed at preparing molecule-based magnets because of their possibility to achieve long-range magnetic order through interchain interactions [35,90,159]. The key point was to control the stacking of the ferrimagnetic chains in such a way as to induce interchain ferromagnetic interactions at the lattice level and so, magnetic ordering in the bulk.

A new strategy to create magnets with one-dimensional magnetic compounds arose from Glauber's theoretical work as early as 1964 [160]. He suggested that the conditions to be fullfilled to observe slow magnetic relaxation in a one-dimensional compound were: (i) it must behave as an Ising ferro- or ferrimagnetic chain and (ii) the ratio J/J' has to be larger than 10^4 (J and J' being the intrachain and interchain magnetic interactions, respectively). This prediction has opened exciting new perspectives to store information in low-dimensional materials. However, more than three decades were needed to observe this behavior for the first time because strong intrachain and very weak interchain magnetic interactions are required in addition to the Ising anisotropy.

The first example of this type of system was reported in 2001 and concerned the compound [Co(hfac)$_2$(NITPhOMe] where alternating high-spin [Co(hfac)$_2$] units and bismonodentate NITPhOMe radicals build a helical chain with a trigonal axis [161–164]. This chain behaves as a one-dimensional ferrimagnet [antiferromagnetic coupling between the high-spin cobalt(II) and the radical] because of the non-compensation of the interacting magnetic moments. The alternating current (ac) magnetic susceptibility of this compound is strongly frequency-dependent below 17 K with maxima of the in-phase (χ'_M) and out-of-phase (χ''_M) susceptibility components. The χ'_M versus the χ''_M plot (Cole–Cole plot) almost describe a semicircle [165,166] supporting only one relaxation process and discarding spin glass behaviour for this compound. The relaxation time (τ) follows the Arrhenius law [$\tau = \tau_0 \exp(E_a/k_B T)$] which is characteristic of a thermally activated mechanism with an energy barrier (E_a) to reverse the magnetization direction, of 107 cm^{-1}, and a pre-exponential factor of 3.0×10^{-11} s. The height of the energy barrier is very close to the absolute value of the nearest-neighbor coupling constant J estimated from the analysis of the magnetic susceptibilty using the Ising model. The isothermal magnetization has a hysteretic behaviour when the external magnetic field is applied parallel to the trigonal axis but no hysteresis was observed when the magnetic field is applied in the trigonal plane. The related manganese(II) derivative orders ferrimagnetically at 4.6 K [167], this different behavior being due to the negiglible anisotropy of the manganese(II) centers. It is clear that the anisotropy of the high-spin cobalt/radical exchange interaction produces a barrier for the orientation of the magnetization.

The first heterometallic SCMs were also reported in 2002 by R. Clérac et al. and they involve a large family of general formula [Mn^{III}_2(saltmen)$_2$$Ni^{II}(pao)_2L_2$]A$_2$ where L a is a nitrogen donor heterocyclic ligand and A is a univalent anion [168,169]. The synthetic strategy consists of reacting the out-of-plane [Mn^{III}_2(saltmen)$_2$(H$_2$O)$_2$]A$_2$ dimer with the [Ni^{II}(pao)$_2$L$_2$] monomer in a methanol/water medium. Bimetallic chains with regular alternating single oximato bridges between Ni^{II} and Mn^{III} and double phenolate-oxo bridges between pairs of Mn^{III} ions occur. The terminal L ligand and the A anion have been used to modulate the interchain separation and thus to minimize the interchain interactions. The whole family of compounds exhibits a quasi-identical magnetic behavior: antiferromagnetically coupled Mn^{III}–Ni^{II}–Mn^{III} trimers (across oximate bridges) connected through Mn^{III}–Mn^{III} ferromagnetic interaction (across the phenolate bridge) leading to a ferromagnetic chain with $S = 3$ units. Coercivity and slow relaxation of the magnetization below 3.5 K are observed with values for the pre-exponential factor (τ_0) and energy barrier (E_a) of ca. 1.0×10^{-10} s and 48.7 cm^{-1}, respectively.

In 2003, Gao et al. reported the first example of a homospin SCM which corresponds to the helical chain compound of formula [Co(bt)(N$_3$)$_2$] where high-spin cobalt(II) ions are bridged by double end-on azido groups, bt acting as a bidentate ligand [170]. Intrachain ferromagnetic couping [J values of 12.4(1) and 10 cm^{-1} were estimated through a Fisher chain model ($S = 3/2$) and mean-field expresion for the Curie–Weiss temperature, respectively] was observed, as expected for this type of bridging mode of the azide ligand [171]. Slow magnetic relaxation and hysteresis effects occur in this chain compound. The blocking temperature is below ca. 5 K with a strong frequency dependence of the real and imaginary parts of linear ac susceptibility. The Arrhenius law is also obeyed with values of τ_0 and E_a of ca. 3.4×10^{-12} s and 65.5 cm^{-1}. Again the magnetic anisotropy of the high-spin cobalt(II) ion is a key point for this behavior.

In 2004, some of us observed SCM behaviour in the oxamato-bridged heterobimetallic chain compound of formula [$Co^{II}Cu^{II}$(2,4,6-tmpa)$_2$(H$_2$O)$_2$]·4H$_2$O [93e] (Fig. 42) which is obtained by reaction of the oxamatocopper(II) precursor [Cu(2,4,6-tmpa)]$^{2-}$ with cobalt(II) ions in aqueous solution by slow difusion in an H-shaped tube. Its structure is made up of neutral ribbon-like oxamato-bridged $Co^{II}Cu^{II}$ chains where the bis(oxamato)copper(II) entity acts as a bisbidentate ligand through the *cis*-carbonyl oxygen atoms toward *trans*-diaquacobalt(II) units (Fig. 42, left). The phenyl ring which is quasi perpendicular to the oxamate skeleton provides an effective isolation between adjacent chains in the *ab* plane (Fig. 42, right). The magnetic properties of this chain are characteristic of a one-dimensional ferrimagnetic compound. The lack of a dc susceptibility maximum in the χ_M versus T plot together with the absence of a λ-peak in the heat capacity measurements of polycrystalline samples of this compound discard the occurrence of a 3D long-range magnetic order, showing that the chains are

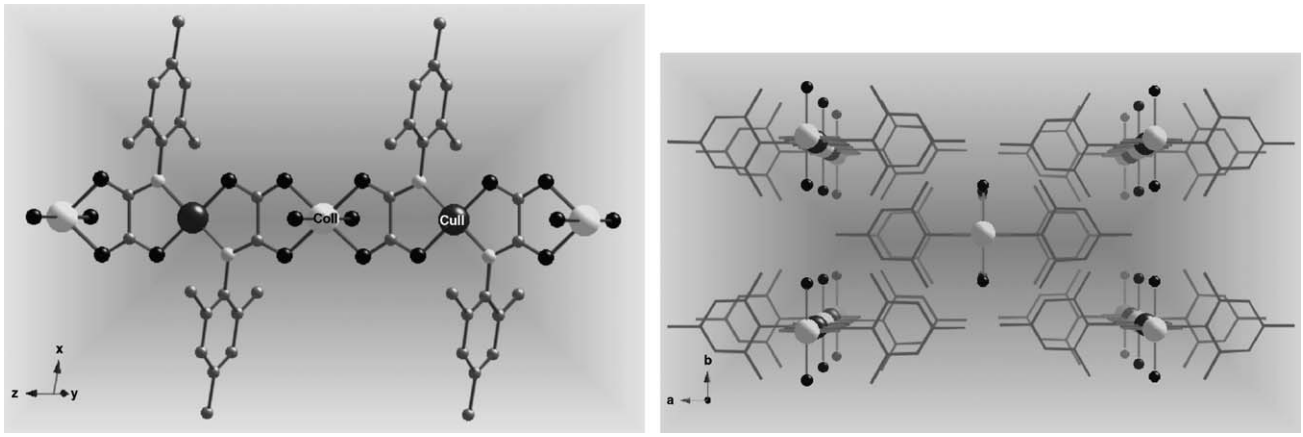

Fig. 42. Perspective views of a fragment of the bimetallic chain $[Co^{II}Cu^{II}(2,4,6\text{-tmpa})_2(H_2O)_2]\cdot 4H_2O$ (left) and of the crystal packing along the *c* axis (right). Adapted from Pardo et al. [93e]. Copyright ©Wiley-VCH.

well isolated from each other. The magnetization versus *H* plot at 2.0 K per CoCu pair exhibits fast saturation with about 80% of the maximum magnetization value reached within a field of 2000 G. This supports the antiparallel alignment of the spins of the Cu^{II} and Co^{II} ions in the chain. The antiferromagnetic coupling between Co^{II} and Cu^{II} across the oxamato bridge is $J = -26.6\,cm^{-1}$, a value which is significantly stronger than that found in the related chain $[CoCu(pbaOH)(H_2O)_3]\cdot 2H_2O$ ($J = -18.0\,cm^{-1}$) [172]. This difference in the magnetic coupling is due to the fact that the copper atom lies in the oxamato plane in the former compound (CuN_2O_2 chromophore with square planar surrounding), whereas it is out of the plane in the latter one (CuN_2O_3 chromophore in a square pyramidal environment), a better overlap between the magnetic orbitals through the σ in-plane exchange pathway occurring in the former and thus, a larger antiferromagnetic coupling.

In-phase and out-of-phase ac signals which are frequency dependent occur at very low temperatures (Fig. 43, left). The Cole–Cole plot at 2.0 K in the frequency range 1.0–1400 Hz gives an almost perfect semicircle supporting only one relaxation process and ruling out spin glass behavior (Fig. 43, right). The relaxation time follows the Arrhenius law (inset of Fig. 43, left) with values of τ_0 and E_a of 4.0×10^{-9} s and 16.3 cm^{-1}, respectively. These values are obtained by treating the experimental data in a very narrow temperature range and consequently, they have to be regarded with caution.

Finally, the first examples of SCMs comprising Mn_7 clusters were reported in 2004. They correspond to compounds of formula $[Mn_7O_8(O_2SePh)_8(O_2CMe)(H_2O)]$ and $[Mn_7O_8(O_2SePh)_9(H_2O)]$ which were prepared by reacting $HPhSeO_2$ with $[Mn_{12}O_{12}(O_2CMe)_{16}(H_2O)_4]$ in acetonitrile [173]. Both compounds contain an unprecedented $[Mn_7O_8]^{9+}$ core with a central $[Mn_3^{III}(\mu_3\text{-}O)_4]^{+}$ entity linked to $[Mn_2^{IV}(\mu\text{-}O)_2]^{4+}$ and $[Mn_2^{IV}(\mu\text{-}O)(\mu_3\text{-}O)]^{4+}$ units on either side. Magnetic studies suggest a low ground-state spin value of $S = 2$ and the appearance in the ac susceptibility of out-of-

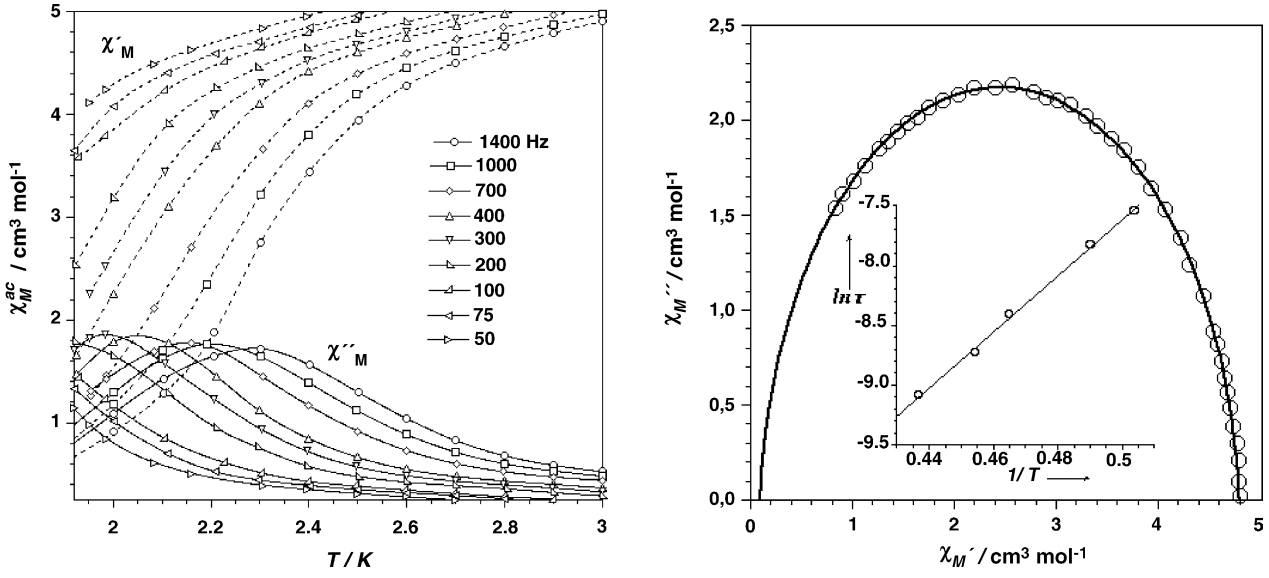

Fig. 43. Temperature dependence of χ'_M and χ''_M for $[Co^{II}Cu^{II}(2,4,6\text{-tmpa})_2(H_2O)_2]\cdot 4H_2O$ in zero applied static field and under 1 G oscillating field at different frequencies of the oscillating field (left). Cole–Cole plot at 2.0 K (the inset shows the Arrhenius plot) (right). Adapted from Pardo et al. [93e]. Copyright ©Wiley-VCH.

phase signals characteristic of slow magnetization relaxation. The authors pointed out that the slow relaxation is caused by SCM behavior with the relaxation barrier ($E_a = 9.87\,cm^{-1}$) arising from a combination of the molecular anisotropy and the exchange interaction between the individual Mn_7 molecules.

4.2. Cyanide-bridged bimetallic one-dimensional magnets

As commented previously, SCM behaviour has also be observed in cyanide-bridged heterometallic species [76,85c,126–128,137]. Keeping in mind that the elongated octahedral geometry for the high-spin Mn^{III} complex is known to result in a $^5B_{1g}$ ground state with a negative axial zero field splitting [174], Schiff-base complexes of Mn^{III} were allowed to react with the well known hexacyanometallate ions to afford a plethora of cyanide-bridged networks from which we would like to outline two of them, namely the linear trinuclear compound $K[(5\text{-Brsalen})_2(H_2O)_2Mn^{III}_2Fe^{III}(CN)_6]\cdot 2H_2O$ [76] and the alternating chain $Et_4N[Mn^{III}_2(5\text{-MeOsalen})Fe(CN)_6]$ [175]. Magnetic data of the former compound reveal the occurrence of weak exchange interactions within the clusters leading to a ground spin state $S = 5/2$ with significant zero field splitting, frequency-dependence of the out-of-phase signals and a reversal energy barrier of $16\,cm^{-1}$, the overall picture corresponding to a SMM. For the latter compound, the magnetic properties reveal the occurrence of interchain ferromagnetic interactions (between the Fe^{III} and Mn^{III} ions through the single cyanide bridge and between a pair of Mn^{III} ions across the double phenolato bridge) and slow relaxation of the magnetization, being a new example of SCM obtained by coupling ferromagnetically single-molecule magnets (the Mn^{III} dimer and the Mn^{III}–Fe^{III}–Mn^{III} trimer) in one dimension. Below, we finish the present contribution with a summary of the SCMs obtained by using the tricyano- and tetracyano-containing low-spin iron(III) units, which are specified above, as cyanide precursors.

4.2.1. Single 4,2-ribbon like chains

The reaction of the building blocks $[Fe^{III}L(CN)_4]^-$ (L = bipy and phen) with the fully hydrated cobalt(II) ions afforded the isostructural 4,2-ribbon like bimetallic chains of formula $\{[FeL(CN)_4]_2Co^{II}(H_2O)_2\}\cdot 4H_2O$ which run pararell to the *a* axis (Fig. 22, L = bipy). In these chains, the low-spin $[FeL(CN)_4]^-$ entity acts as a bismonodentate bridge through two of its four cyanide groups in *cis* positions toward *trans*-diaquacobalt(II) units. Each cobalt atom is six-coordinate with two water molecules and four cyanide-nitrogen atoms providing a somewhat distorted CoN_4O_2 motif. The values of the Co–O_w bond distances [2.103(2) (L = bipy) and 2.0886(4) Å (L = phen)] are in agreement with those observed in aqua complexes of high-spin cobalt(II) [176] and those of the Co–$N_{cyanide}$ [2.125(2) and 2.104(2) Å (L = bipy) and 2.147(2) and 2.113(2) Å (L = phen)] are longer than those observed in the Co^{III} (diamagnetic)–N–C–Fe^{III} (low-spin) unit of the single cyanide-bridged complexes $[L^2Co^{III}NCFe^{III}(CN)_5]\cdot 4H_2O$ [1.941(8) Å] and $[L^3Co^{III}NCFe^{III}(CN)_5]\cdot 4H_2O$ [1.897(14) Å] [177]. The $\{[FeL(CN)_4]_2Co^{II}(H_2O)_2\}\cdot 4H_2O$ chains have two orientations in the unit cell, their mean Fe_2Co_2 planes forming a dihedral angle of ±70° with the *b* axis. Their Co–O_w bonds make an angle of ±31° with the *b* axis. The magnetic properties of these one-dimensional compounds (we focus here on the magnetic behaviour of the bipy-containing chain, those of the phen derivative being practically identical) on polycrystalline powder samples correspond to ferromagnetic coupled chains of high-spin Co^{II} and and low-spin Fe^{III} ions with significant orbital contributions (Fig. 44). Below 8 K, hysteresis loops as well as maxima of the in-phase and out-of-phase signals, which are strongly frequency dependent, are observed for both chains indicating that they are examples of SCMs. Magnetization measurements on oriented single crystals of the bipy-containing chain were performed to characterize its anisotropy. The chains in the unit cell run parallel to the *a* axis but there are two chains in the unit cell with different orientations, the Co–O_w bonds of which make an angle of ±31° with the *b* axis. The Co–O_w bond defines the easy magnetization axis, the orientation of the resulting vectors in the *bc* plane being depicted in Fig. 45 (left). According to this picture, the magnetization along any direction ($M\alpha$) in the *bc* plane obeys the equation $M\alpha = m_1 \cos\alpha + m_2 \cos(\alpha + 62)$. This equation nicely reproduces the experimental magnetization data in the *bc* plane (Fig. 45, right). The magnetization minima occur when the applied magnetic field is perpendicular to one of the two vectors (that is ±59° with respect to the *b* axis). The thermal dependence of the magnetization along the crystallographic axes (Fig. 46) reveals that the magnetization along *a* is very weak, as expected due to the fact that the m_1 and m_2 vectors are perpendicular to this axis. All these features demonstrate the anisotropic Ising-type behavior of each of the two chains.

The value of the coercive field (H_c) and the hysteresis loop for a single crystal of $\{[Fe^{III}(bipy)(CN)_4]_2Co^{II}(H_2O)_2\}\cdot 4H_2O$

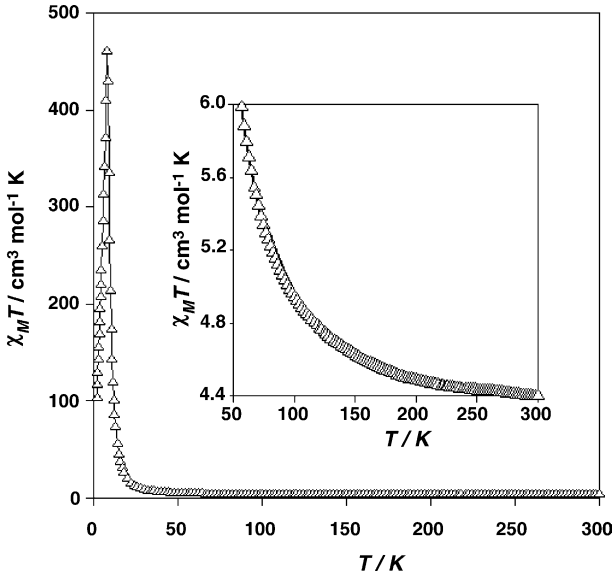

Fig. 44. Temperature dependence of the $\chi_M T$ product (χ_M is the magnetic susceptibility per Fe_2Co unit) for $\{[Fe^{III}(bipy)(CN)_4]_2Co^{II}(H_2O)_2\}\cdot 4H_2O$ under an applied magnetic field of 100 G. The inset shows a detail of the high temperature range.

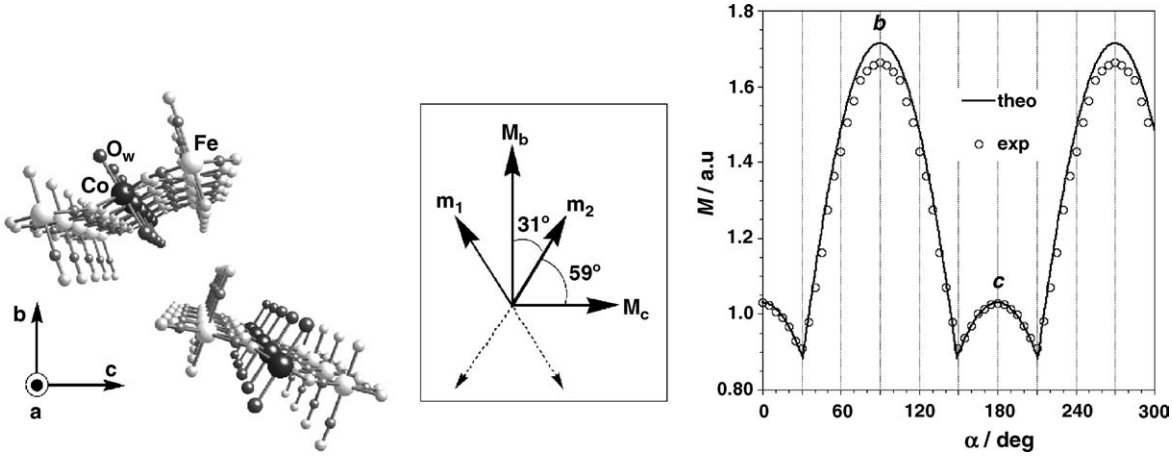

Fig. 45. Orientation of the magnetization vectors of $\{[Fe^{III}(bipy)(CN)_4]_2Co^{II}(H_2O)_2\}\cdot 4H_2O$ (left). Dependence of the magnetization (M) (a.u. units) of a single crystal of $\{[Fe^{III}(bipy)(CN)_4]_2Co^{II}(H_2O)_2\}\cdot 4H_2O$ vs. the rotation angle α in the bc plane under an applied magnetic field of 0.5 T at 5 K. The values of 0 and 90° correspond to $H//c$ and $H//b$, respectively: (○) experimental data; (—) theoretical data obtained from the equation above (right). Reprinted (left and middle) and reprinted (right) from Lescouëzec et al. [127]. Copyright ©Wiley-VCH.

are strongly dependent on the temperature and the sweep rate as demonstrated by using micro-SQUID and Hall probe techniques. So, for $H//b$, H_c increases from 1000 to 12000 G when going from 2 to 1.1 K at 0.002 T s^{-1} (Fig. 47, left) whereas it decreases when increasing the sweep rate (5000 and 750 G when going from 0.07 to 0.001 T s^{-1} at 2 K) (Fig. 47, right). The observed rapid saturation of the magnetization and hysteresis effects are the signature of a 'magnet type' behavior.

Finally, ac measurements on a single crystal of $\{[Fe^{III}(bipy)(CN)_4]_2Co^{II}(H_2O)_2\}\cdot 4H_2O$ along the b axis show frequency dependence of the in-phase and out-of-phase signals below 10 K, the relaxation time following an Arrhenius plot with $\tau_0 = 9.4 \times 10^{-12}$ s and $E_a = 98.7$ cm^{-1}. Similar behavior occurs

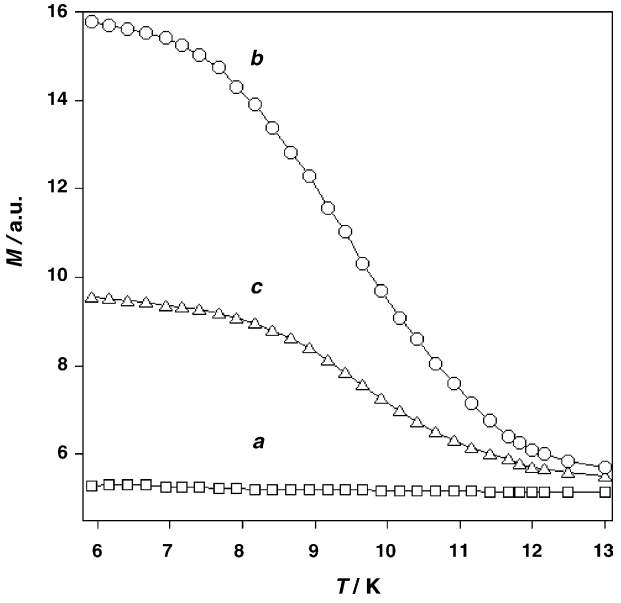

Fig. 46. Field-cooled magnetization (FCM) of a single crystal of $\{[Fe^{III}(bipy)(CN)_4]_2Co^{II}(H_2O)_2\}\cdot 4H_2O$ along the crystallographic a, b and c axes, under an external field of 1000 G. Reprinted from Lescouëzec et al. [127]. Copyright ©Wiley-VCH.

in the phen derivative. In summary, these 4,2-ribbon like $Fe^{III}_2Co^{II}$ ferromagnetic chains are Ising-like systems which fulfill the conditions required to observe slow relaxation of the magnetization.

The ferromagnetic coupling between the low-spin iron(III) and the high-spin cobalt(II) ions could be qualitatively understood on the basis of DFT type calculations which provided an orbital picture of the magnetic interaction. These calculations, show that in a local octahedral geometry, the three unpaired electrons on the cobalt atom are described by d_{z^2}, $d_{x^2-y^2}$ and d_{xy} orbitals [the z axis being defined by the Co–O_w bond and the x and y axes by the Co–C–N(cyanide) bonds]. As far as the low-spin iron(III) unit $[Fe(bipy)(CN)_4]^-$ is concerned, its spin density map (Fig. 48) shows that its unpaired electron is described by a t_{2g} type orbital. The spin density is mostly localized at the iron atom, the carbon and nitrogen atoms of the cyanide ligands presenting small spin densities whose sign is determined by the spin polarization mechanism. Having in mind the definition of the axes given in Fig. 48 [x and y axes being roughly defined by the Fe–N(bipy) bonds], this magnetic orbital corresponds to the combination $d_{xz} - d_{yz}$. As easily inferred on a symmetry basis, two ferromagnetic terms [strict orthogonality between the t_{2g} (at the Fe^{III}) and the d_{z^2} and $d_{x^2-y^2}$ (at the Co^{II}) orbitals] and an antiferromagnetic one [weak overlap between the t_{2g} (at the Fe^{III}) and the d_{xy} (at the Co^{II}) orbitals] contribute to the magnetic coupling in the $\{[Fe^{III}(bipy)(CN)_4]_2Co^{II}(H_2O)_2\}\cdot 4H_2O$ chain. The former ones are predominant and lead to a net ferromagnetic coupling.

Our attempts to extend this work to other anisotropic cations such as copper(II), afforded compounds of formula $\{[Fe^{III}(phen)(CN)_4]_2Cu^{II}(H_2O)_2\}\cdot 4H_2O$ and $\{[Fe^{III}(bipy)(CN)_4]_2Cu^{II}(H_2O)_2\}\cdot 4H_2O$ [126]. The structure of the former compound is made up of neutral cyanide-bridged 4,2-ribbon like $Fe^{III}_2Cu^{II}$ chains (Fig. 49) where each $[Fe(phen)(CN)_4]^-$ unit adopts as a bismonodentate bridging mode toward a *trans*-diaquacopper(II) entity through two of its four cyanide groups in *cis* positions.

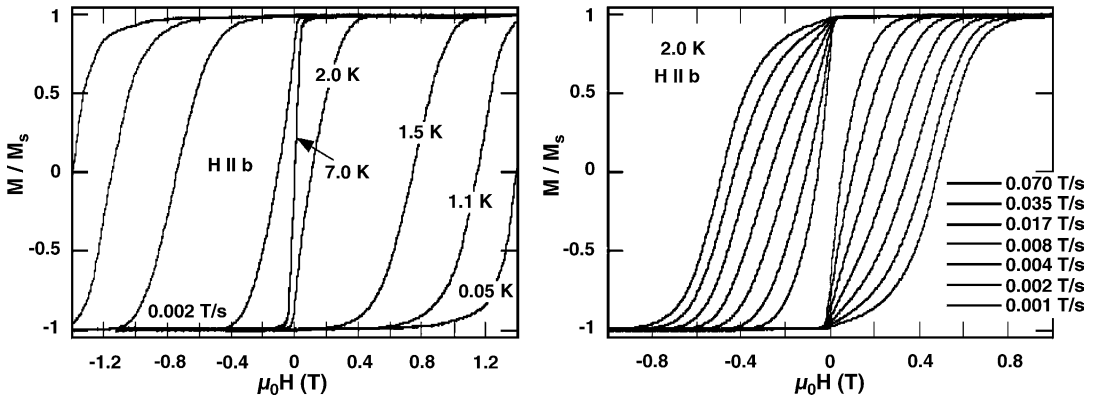

Fig. 47. Field dependence of the normalized magnetization (M/M_S) measured on a single crystal of $\{[Fe^{III}(bipy)(CN)_4]_2Co^{II}(H_2O)_2\}\cdot 4H_2O$ along the *b* axis: hysteresis loops measured at various temperatures with 0.002 T s^{-1} field sweep rate (left) and at 2.0 K under different field sweep rates (right).

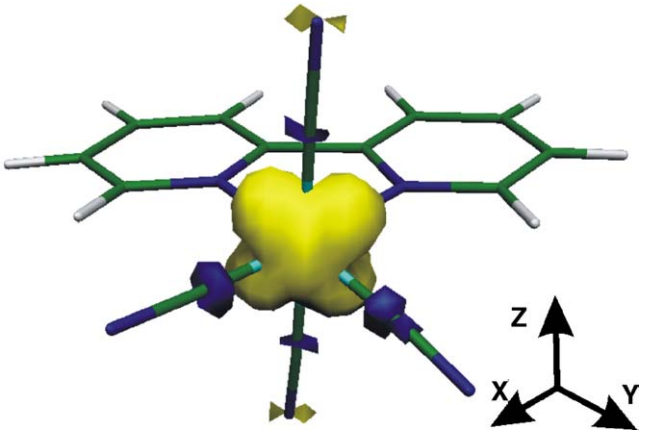

Fig. 48. Spin density map for $[Fe(bipy)(CN)_4]^-$. The values of the atomic spin densities in electron units are: +1.131 (Fe), −0.018 (N_{bipy}), −0.059 (C_{cyano}) and +0.038 (N_{cyano}). Mean values are given for the atoms other than iron. Spin density is plotted with cutoff at 0.005 e.

Each copper atom lies on an inversion center and has a distorted elongated octahedral geometry: two water molecules in *trans* positions [O(1) and O(1a)] and two cyanide nitrogen atoms [N(3) and N(3a] form the equatorial plane whereas two other cyanide nitrogen atoms [N(1c) and N(1d)] occupy the axial positions. The magnetic properties of this chain compound correspond to a ferromagnetically coupled $Fe^{III}_2Cu^{II}$ trimer ($J_{FeCu} = +5.0\,cm^{-1}$). Because of the long axial Cu–N (cyanide) bonds (ca. 2.56 Å), the axial cyanide-to-copper exchange pathway is discarded and the Fe(1)–C(3)–N(3)–Cu(1)–N(3a)–C(3a)–Fe(1a) trinuclear unit is the appropriate model to analyze the magnetic data of the compound. The strict orthogonality between the interacting magnetic orbitals [t_{2g} (at the iron) versus e_g (at the copper) type orbitals] accounts for the ferromagnetic nature of the magnetic interaction. A somewhat stronger ferromagnetic coupling ($J_{FeCu} = +12\,cm^{-1}$) was observed in the related quasi-square complex $[Fe^{III}_2Cu^{II}_2(\mu\text{-}CN)_4(bipy)_6](PF_6)_6 \cdot 4CH_3CN \cdot 2CHCl_3$ where single cyanide bridges link alternatively low-spin iron(III) and copper(II) ions [82a]. The greater linearity of the cyanide bridges at the C–N–Cu fragment in this last compound [171.9(3) and 176.3(3)° versus 164.6(6)° in the phen-containing complex] is responsible for its larger magnetic coupling.

The poor difraction pattern of the crystals of the related bipy-containing $Fe^{III}_2Cu^{II}$ compound precluded a detailed structural determination. However, analysis of the available data revealed the occurrence of a neutral 4,2-ribbon like chain

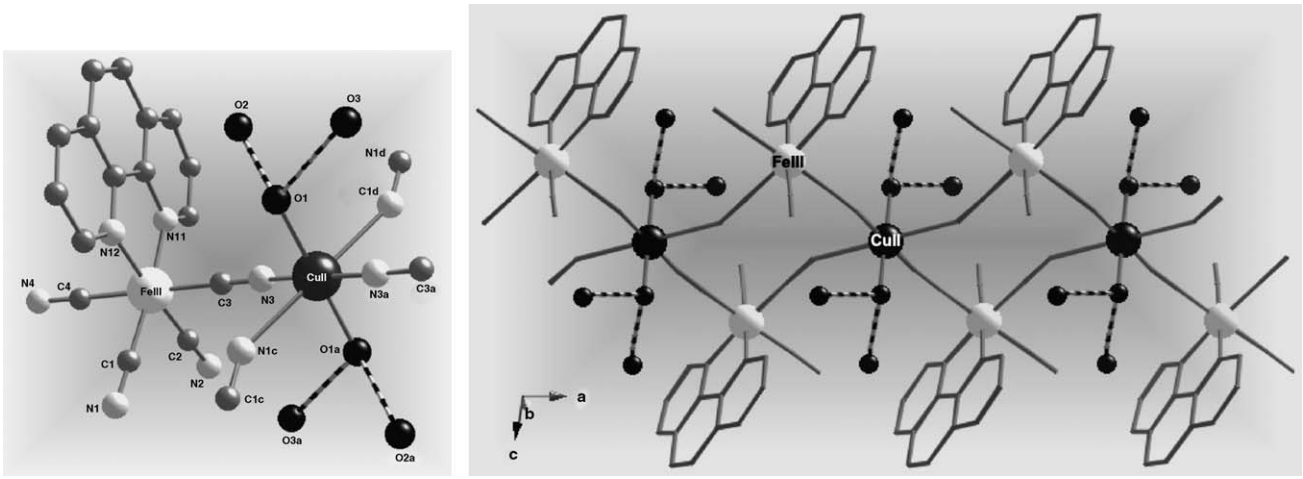

Fig. 49. Perspective views of the asymmetric unit of $\{[Fe^{III}(phen)(CN)_4]_2Cu^{II}(H_2O)_2\}\cdot 4H_2O$ with the atom numbering (left) and of a fragment of the chain structure showing the intrachain hydrogen bonds (right). Adapted from Toma et al. [126]. Copyright ©The Royal Society of Chemistry.

$\{[Fe^{III}(phen)(CN)_4]_2Cu^{II}(H_2O)_2\}$ similar to the previous one with phen but having a different orientation of the elongation axis at the copper atom: the two *trans* coordinated water molecules are now in *axial* positions and consequently, the four cyanide bridges fill the equatorial positions at the copper atom. This structural modification has a strong influence on the magnetic properties because the number of ferromagnetic intrachain exchange pathways in this compound is twice that of the related phen-containing chain. So, the $\chi_M T$ versus T plot of $\{[Fe^{III}(bipy)(CN)_4]_2Cu^{II}(H_2O)_2\}\cdot 4H_2O$ increases faster with cooling than that of $\{[Fe^{III}(phen)(CN)_4]_2Cu^{II}(H_2O)_2\}\cdot 4H_2O$. Indeed, values of $\chi_M T$ (per $Fe^{III}_2Co^{II}$ unit) of 1.78 and 83 $cm^3\,mol^{-1}\,K$ for $\{[Fe^{III}(phen)(CN)_4]_2Cu^{II}(H_2O)_2\}\cdot 4H_2O$ and $\{[Fe^{III}(bipy)(CN)_4]_2Cu^{II}(H_2O)_2\}\cdot 4H_2O$, respectively, at 3.5 K (under an applied field of 250 G) are observed. A sharp decrease of $\chi_M T$ is observed at very low temperatures, the value of $\chi_M T$ at 1.9 K being 61 $cm^3\,mol^{-1}\,K$. The magnetization plot of the $\{[Fe^{III}(bipy)(CN)_4]_2Cu^{II}(H_2O)_2\}\cdot 4H_2O$ compound (Fig. 50, left) unambiguously shows the occurrrence of ferromagnetic coupling: M increases very rapidly when H increases and it tends to a saturation value close to 3.2 BM at 5 T. This saturation value is as expected for a spin state $S = 3/2$ arising from the parallel alignment of three spin doublets ($S = S_{Cu} + 2S_{Fe}$ with $S_{Fe} = S_{Cu} = 1/2$ and $g_{Fe} = g_{Cu} = 2.0$). The occurrence of a plateau in the magnetic susceptibility plot at $T < 3$ K under low magnetic fields (inset of Fig. 50, left) indicates a saturation effect. The ac magnetic susceptibility measurements (Fig. 50, right) show the occurrence of a maximum of the real component at ca. 3.0 K and non-zero values for the imaginary component below 3 K which are frequency dependent. These features rule out the three-dimensional magnetic ordering of this compound and support its behaviour as a SCM. The evaluation of the energy barrier is precluded in the present case due to the very low temperatures ($T < 1.8$ K) where the maxima of χ''_M occur. Most likely, the lower anisotropy of the copper(II) when compared to the high-spin cobalt(II) is at the origin of this shift toward the lower temperatures of the maxima of the out-of-phase signals in these ferromagnetically coupled 4,2-ribbon-like bimetallic chains.

Compounds of formula $\{[Fe^{III}(bpym)(CN)_4]_2M^{II}(H_2O)_2\}\cdot 6H_2O$ [M = Co (Fig. 30) and Cu (Fig. 31)] are also examples of ferromagnetically coupled 4,2-ribbon like bimetallic chains [137]. The cobalt derivative exhibits slow magnetic relaxation and hysteresis effects behaving as a SCM. The values of the coercive field (H_c) and remnant magnetization (M_r) for this compound (Fig. 51, left) are 250 G and 2.0 BM, respectively. The ac signals are frequency dependent at low temperatures (Fig. 51, right) and the relaxation times follow an Arrhenius law with $E_a = 18\,cm^{-1}$ and $\tau_0 = 1.2 \times 10^{-9}$ s.

The isostructural copper derivative exhibits metamagnetism. The thermal dependence of $\chi_M T$ for this compound (Fig. 52) reveals the occurrence of a significant intrachain ferromagnetic coupling, the decrease of $\chi_M T$ at low temperatures being due to interchain magnetic interactions. The maximum of the magnetic susceptibility which occurs at 2.2 K under an applied field of 100 G moves toward lower temperatures when increasing the applied field and it disappears for $H \geq 400$ G (inset of Fig. 52). This suggests a field-induced transition from an antiferromagnetic to a ferromagnetic ground state. Such magnetic behaviour is consistent with the structure: two parallel $Fe^{III}_2Cu^{II}$ ferromagnetic chains with weak interchain antiferromagnetic interactions through the alternating four- and six-membered water rings (Fig. 31). In the case of the cobalt derivative, the six-membered rings which connect the parallel $Fe^{III}Co^{II}$ ferromagnetic chains seem not to be able to mediate any significant interchain magnetic coupling down to 1.9 K and the SCM behavior is observed.

The 4,2-ribbon like chain compound $\{[Fe^{III}\{HB(pz)_3\}(CN)_3]_2Cu(MeOH)\}\cdot 2MeOH$ where the *fac*-$\{[Fe^{III}\{HB(pz)_3\}(CN)_3]^-$ unit acts as a bismonodentate bridging ligand is also

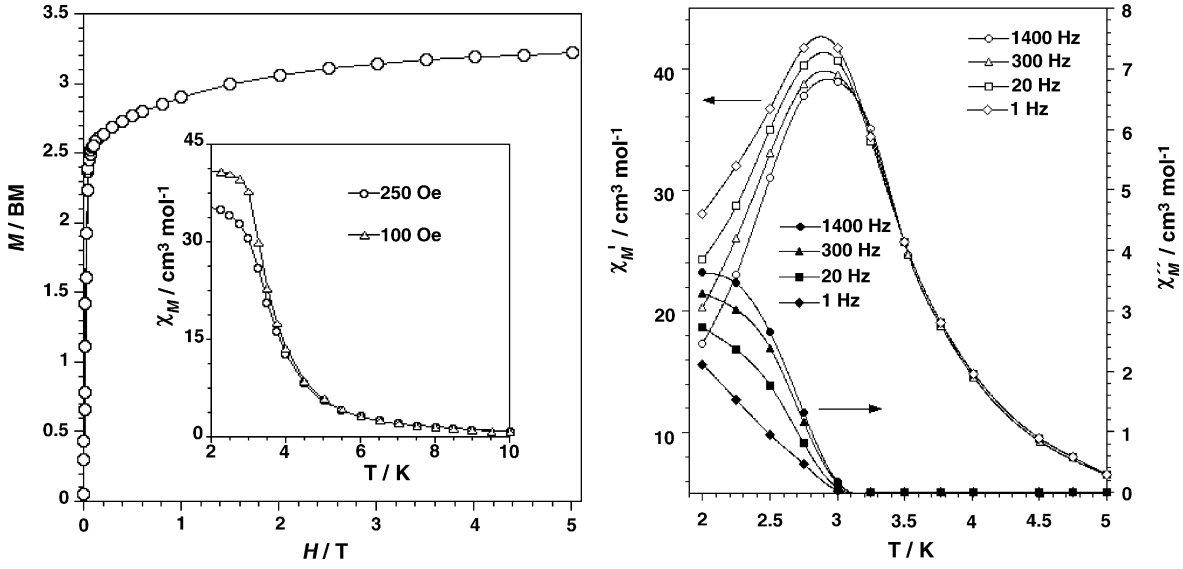

Fig. 50. Magnetization plot of $\{[Fe^{III}(bipy)(CN)_4]_2Cu^{II}(H_2O)_2\}\cdot 4H_2O$ at 2.0 K: (◯) experimental data; (—) eye-guide line. The inset shows the field dependence of the magnetic susceptibility at very low temperatures (left). Real (χ'_M) and imaginary (χ''_M) components of ac susceptibility in a 1 G field oscillating at different frequencies (1–1400 Hz) without dc magnetic field (left). Reprinted from Toma et al. [126]. Copyright ©The Royal Society of Chemistry.

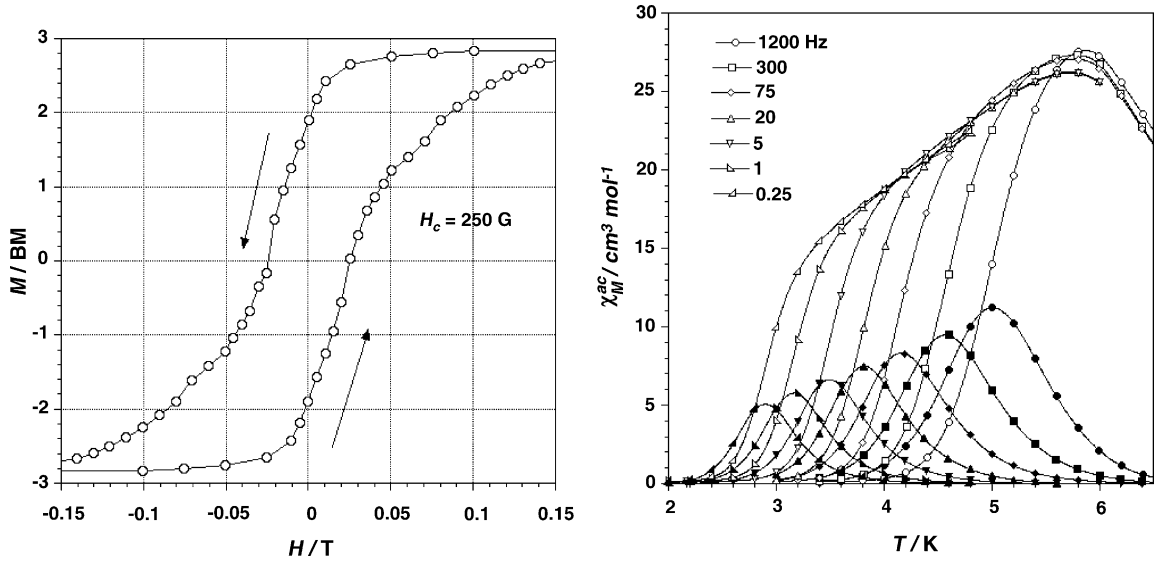

Fig. 51. Hysteresis loop of $\{[Fe^{III}(bpym)(CN)_4]_2Co^{II}(H_2O)_2\}\cdot 6H_2O$ at 2.0 K: (○) experimental data; (—) eye-guide line (left). In-phase (open symbols) and out-of-phase (full symbols) components of the ac susceptibility at $T \leq 6.4$ K in a 1 G field oscillating at different frequencies (0.25–1200 Hz) without dc magnetic field (right).

a very recent example of SCM [85c]. Again, the intrachain magnetic interaction between the low-spin iron(III) ion and the copper(II) ion is ferromagnetic and interchain magnetic interactions were not observed down to 1.8 K. Ac signals are frequency dependent below 6 K and the value of E_a and τ_0 obtained by fit to an Arrhenius plot are 78.0 cm^{-1} and 2.8×10^{-13} s. Although this tailored cyano precursor is already well adapted to prepare magnetically isolated chains, the geometric constraints caused by replacement of its boron-hydrogen by bulky organic groups will provide researchers in the near future with a straightforward synthetic route to obtain well isolated low-dimensional heterometallic magnetic species.

4.2.2. Double 4,2-ribbon like chains

As commented in Section 3.2, isostructural bis double zigzag chains $\{[Fe^{III}(bipy)(CN)_4]_2M^{II}(H_2O)\}\cdot 1/2H_2O\cdot CH_3CN$ (M = Co and Mn) (Fig. 23) result from the the condensation of two parallel 4,2-ribbon like chains, one of the axially coordinated water molecule to the metal atom M of one chain being replaced by a cyanide nitrogen from the other chain [128]. The magnetic behaviour of the manganese derivative for $Fe_2^{III}Mn^{II}$ unit (Fig. 53) corresponds to an overall antiferromagnetic interaction. Upon cooling, $\chi_M T$ continuously decreases from 5.20 $cm^3\ mol^{-1}$ K at 300 K to 1.10 $cm^3\ mol^{-1}$ K at 1.9 K.

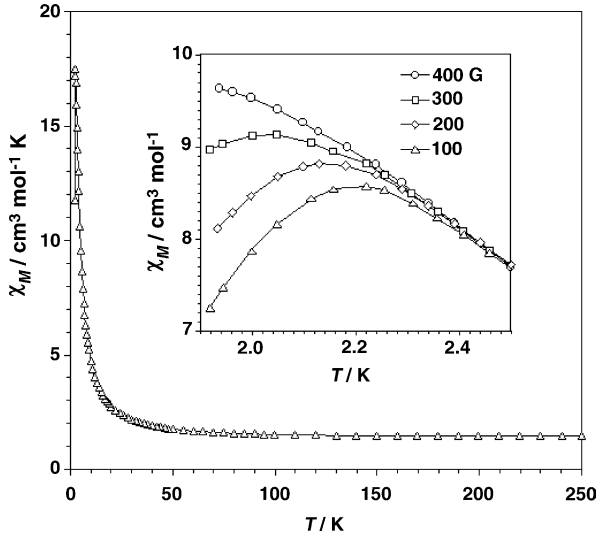

Fig. 52. Thermal dependence of the $\chi_M T$ product for $\{[Fe^{III}(bpym)(CN)_4]_2Cu^{II}(H_2O)_2\}\cdot 6H_2O$ under an applied magnetic field of 100 G: (△) experimental data; (—) eye-guide line. The inset shows the field dependence of the magnetic susceptibility at very low temperatures (H varying in the range 100–400 G).

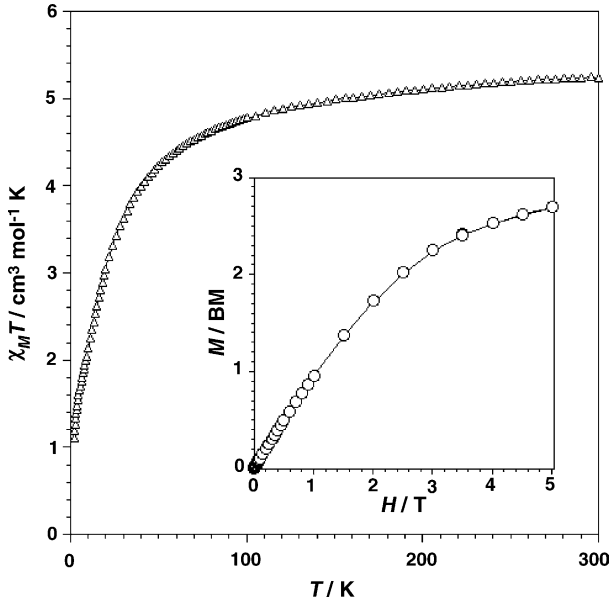

Fig. 53. Thermal dependence of the $\chi_M T$ product for $\{[Fe^{III}(bipy)(CN)_4]_2Mn^{II}(H_2O)\}\cdot 1/2H_2O\cdot CH_3CN$ under an applied field of 100 G: (△) experimental data; (—) eye-guide line. The inset shows the magnetization versus H plot at 2.0 K.

The magnetization plot (inset of Fig. 53) confirms the antiferromagnetic coupling between the low-spin iron(III) and the high-spin manganese(II) with a magnetization value at 5 T of ca. 2.8 BM which is close to that expected for $S = 3/2 = S_{Mn} - 2S_{Fe}$ (3.0 BM with $g_{Mn} = g_{Fe} = 2.0$). In the light of the electronic configurations of the high-spin Mn(II) ($t_{2g}^3 e_g^2$) and low-spin Fe(III) ($t_{2g}^5 e_g^0$) ions, dominant antiferromagnetic contributions will occur and consequently, the intrachain antiferromagnetic coupling is anticipated, as observed.

Interestingly, the $\chi_M T$ versus T plot of the cobalt derivative on polycrystalline samples increases monotonically from room temperature upon cooling to reach a maximum of ca. 94 $cm^3\,mol^{-1}\,K$ at 10 K and then decreases to 5 $cm^3\,mol^{-1}\,K$ at 1.9 K (Fig. 54, left). A susceptibility maximum is observed at 7 K under applied magnetic fields lower than 600 G (inset of Fig. 54, left). This maximum disappears for $H > 600$ G, suggesting a field-induced transition from an antiferromagnetic to a ferromagnetic ground state. These magnetic features are consistent with the crystal structure: presence of two parallel $Fe_2^{III}Co^{II}$ chains with intrachain ferromagnetic coupling which interact antiferromagnetically. The metamagnetic behavior of this compound is evident from the sigmoidal shape of the M versus H plot at 2.0 K (Fig. 54, right) and the fast increase of M at H about 600 G. Under an applied field greater than 600 G, the interchain antiferromagnetic coupling is overcome and the compound behaves as two ferromagnetic $Fe_2^{III}Co^{II}$ chains.

Three-dimensional magnetic order in this compound is ruled out on the basis of the lack of a λ-peak in the heat capacity measurements in the temperature range 290–1.8 K both at $H = 0$ and 800 G. The magnetization at saturation per $Fe_2^{III}Co^{II}$ unit, at 2.0 K and 5 T, is 4.1 BM [ca. 1.0 BM per Fe^{III} and 2.0 BM per Co^{II} (assuming and effective $S_{Co} = 1/2$ and $g_{Co} = 4$)] supports the intrachain ferromagnetic coupling. The magnetic behavior of the double chain compound $\{[Fe^{III}(bipy)(CN)_4]_2Co^{II}(H_2O)\}\cdot 1/2H_2O\cdot CH_3CN$ under $H \geq 600$ G is similar to that observed for the related 4,2-ribbon like chain $\{[Fe^{III}(bipy)(CN)_4]_2Co^{II}(H_2O)_2\}\cdot 4H_2O$ (single nanowire) which exhibits SCM behavior. The two condensed chains can be viewed as an example of double nanowire. Frequency-dependence of the out-of-phase suceptibility of the double nanowire under an applied field of 800 G is observed (inset of Fig. 54, right). The relaxation time follows an Arrhenius plot with an energy barrier $E_a = 105.5\,cm^{-1}$ and a pre-exponential factor $\tau_0 = 1.5 \times 10^{-17}$ s. The value of this last parameter is much smaller than those reported for the previous $Fe^{III}Co^{II}$ bimetallic chains but since it is obtained under an applied field, the comparison cannot be made.

The condensation of two 4,2-ribbon like bimetallic chains is also observed in the compounds of formula $\{[Fe^{III}(phen)(CN)_4]_2Cu^{II}\}\cdot H_2O$ (Fig. 55) and $\{[Fe^{III}(bipy)(CN)_4]_2Cu^{II}\}\cdot 2H_2O$ (Fig. 56) [126]. The mononuclear precursor $[Fe(L)(CN)_4]^-$ (L = phen and bipy) exhibits bismonodentate [Fe(2)] and trismonodentate [Fe(1)] bridging modes toward the copper atom through two (*cis* positions) and three (*fac* positions) of its four cyanide groups, respectively. The copper atom is five-coordinate with five cyanide-nitrogen atoms building a distorted CuN_5 square pyramid. All the Cu–N–C angles for the phen-containing compound are significantly bent, the minimum and maximum values being 161.0(4) and 171.4(5)°. However, in the structure of the double chain with bipy, only two of the five Cu–N–C angles deviate significantly from linearity [159.4(2) and 168.2(2)°] whereas the other three vary in a narrow range close to 180° [173.1(3)–179.5(2)°]. The CN stretching region of the infrared spectra of these compounds provides evidence of the presence of bridging [doublet at 2175s and 2157m cm^{-1} (L = phen) and

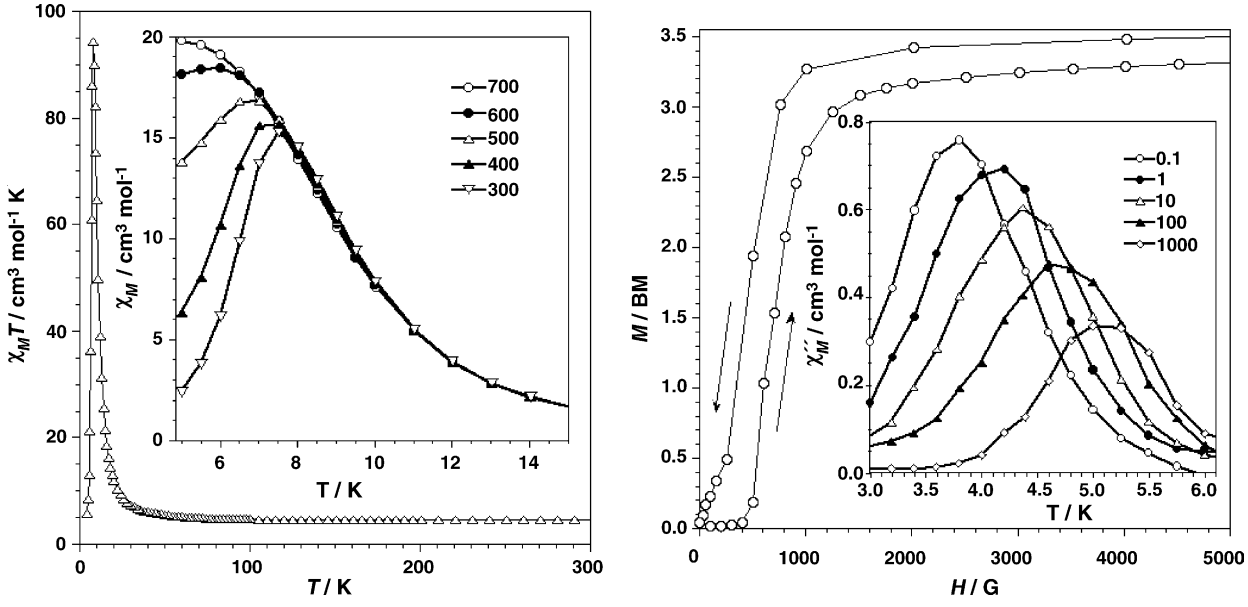

Fig. 54. Temperature dependence of the $\chi_M T$ product per $Fe_2^{III}Co^{II}$ unit under an applied field 100 G (the solid line is an eye-guide). The inset shows the field dependence (H covering the range 300–700 G) of χ_M at very low temperatures (left). Magnetization versus H plot at 2.0 K. The inset shows the out-of-phase component of the ac susceptibility in a 1 G field oscillating at different frequencies (0.1–1000 Hz) and under a dc magnetic field of 800 G. Reprinted from Toma et al. [128]. Copyright ©The Royal Society of Chemistry.

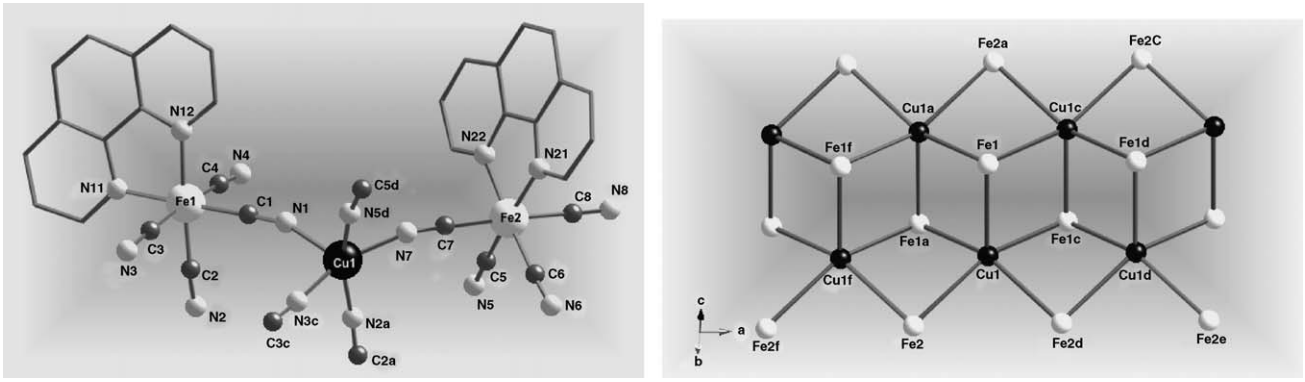

Fig. 55. Structure of the double chain $\{[Fe^{III}(phen)(CN)_4]_2Cu^{II}\}\cdot H_2O$: perspective view of the asymmetric unit (left); a schematic view of a fragment of the double chain skeleton (the full lines represent the cyanide bridges) (right). Adapted from Toma et al. [126]. Copyright ©The Royal Society of Chemistry.

2172s and 2158m cm^{-1} (L = bipy)] and terminal [single peak at 2125m (L = phen) and 2121m cm^{-1} (L = bipy)] cyanide ligands. The iron-copper separation through bridging cyanide are 5.112(2) [Fe(1)···Cu(1)], 5.016(2) [Fe(1)···Cu(1a)], 5.025(2) [Fe(1)···Cu(1c)], 5.031(2) [Fe(2)···Cu(1)] and 5.041(2) Å [Fe(2)···Cu(1f)] for L = phen and 5.0293(7) [Fe(1)···Cu(1c)], 5.0875((7) [Fe(1)···Cu(1)], 5.1892(9) [Fe(1)···Cu(1d)], 5.1004(7) [Fe(2)···Cu(1)] and 4.9381(7) Å [Fe(2)···Cu(1c)] for L = bipy.

These double chains exhibit metamagnetic-like behavior: significant intrachain ferromagnetic coupling between the low-spin iron(III) and the copper(II) ions and weak interchain antiferromagnetic coupling, the values of the critical field being $H_c = 1100$ (L = phen) and 900 G (L = bipy). The H_c values give the order of magnitude of the interchain interactions, ca. $-0.1\ cm^{-1}$. The values of the magnetization at saturation per $Fe^{III}_2Cu^{II}$ unit, at 2.0 K and 5 T, are close to 3.2 BM [ca. 1.0 BM per each Fe^{III} and 1.0 BM per Cu^{II} (assuming $g_{Fe} = g_{Cu} = 2.0$)], in agreement with an intrachain ferromagnetic coupling. No ac signals are observed for these double chains under a dc applied field $H = 0$ G, as expected for a non-magnetic ground state caused by the interchain antiferromagnetic coupling. However, frequency-dependent out-of-phase ac signals occur below 4.0 K under the applied field $H > H_c$. The maximum of the out-of-phase signal occurs at too low a temperature ($T < 1.8$ K) in the case of L = phen, precluding the evaluation of the energy barrier. However, in the case of L = bipy the range of temperatures is somewhat higher (Fig. 57) and values of $E_a = 35\ cm^{-1}$ and $\tau_0 = 4.0 \times 10^{-13}$ s could be calculated through the corresponding Arrhenius plot. The value of τ_0 is close to that observed in the related double chain magnet $\{[Fe^{III}(bipy)(CN)_4]_2Co^{II}(H_2O)\}\cdot 1/2H_2O\cdot CH_3CN$ [128] but that of E_a is smaller in agreement with the lower local anisotropy of the copper(II) ion.

DFT type calculations were performed on the mononuclear $[Fe^{III}(phen)(CN)_4]$ and $[Cu^{II}(NC)_5]$ units and on heterodinuclear single cyanide-bridged Fe^{III}–Cu^{II} fragments in order to analyze the exchange pathways and to get an orbital picture accounting for the magnetic interactions in these double chains. As shown in the spin density map of the low-spin $[Fe(phen)(CN)_4]^-$ unit (Fig. 58, left), its unpaired electron is described by a t_{2g} orbital which corresponds to the combination $d_{xz} - d_{yz}$ [the x and y axes being roughly defined by the Fe–N(phen) bonds]. The spin density is mostly localized at the iron atom, the carbon and nitrogen atoms of the cyanide ligands presenting small spin densities whose sign is determined by the spin polarization mechanism. As far as the copper(II) ion is concerned, the corresponding spin density map (Fig. 58, right) shows that the unpaired electron of this cation is of the e_g type and it lies mainly in the equatorial plane [$d_{x^2-y^2}$ type orbital

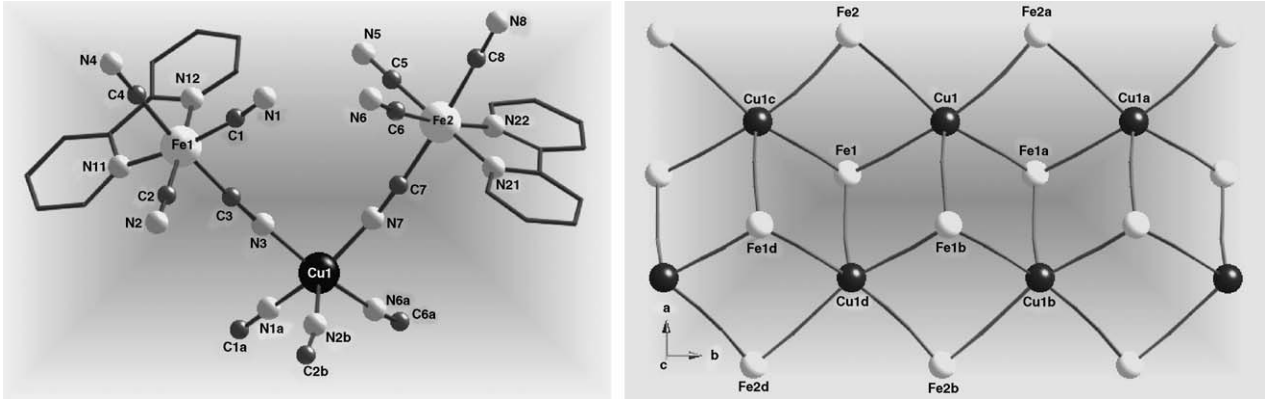

Fig. 56. Structure of the double chain $\{[Fe^{III}(bipy)(CN)_4]_2Cu^{II}\}\cdot 2H_2O$: (left) perspective view of the asymmetric unit; (right) a schematic view of a fragment of the double chain skeleton (the full lines represent the cyanide bridges). Adapted from Toma et al. [126]. Copyright ©The Royal Society of Chemistry.

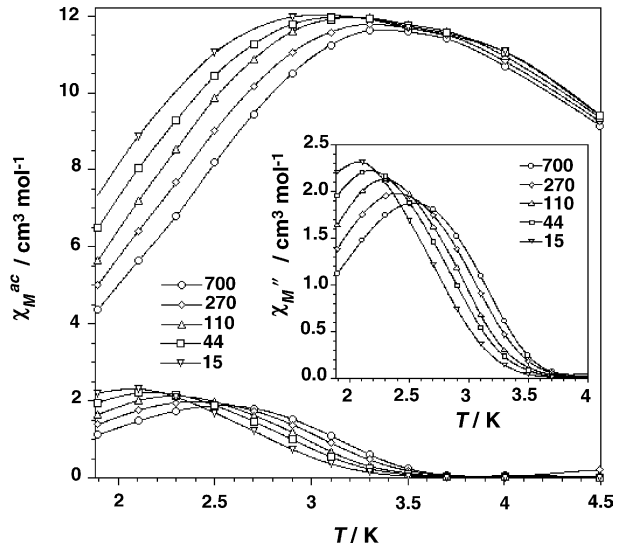

Fig. 57. In-phase and out-of-phase components of the ac susceptibility of $\{[Fe^{III}(bipy)(CN)_4]_2Cu^{II}\}\cdot 2H_2O$ in a 1 G field oscillating at different frequencies and under a dc magnetic field of 1000 G. Reprinted from Toma et al. [126]. Copyright ©The Royal Society of Chemistry.

with the x and y axes defined by the equatorial Cu–N(cyanide) bonds]. A significant spin delocalization on the equatorially bound cyanide-nitrogen atoms is observed, the sign of the spin density of the atoms around the copper being determined by the spin delocalization.

With these orbital pictures in mind, it is easy to visualize the exchange pathways through the cyanide bridge in the double chain structure: two of them (J_1 and J_2) within one of the two parallel chains (Fig. 59, left) an the other one (J_3) between the two parallel chains through the axial copper to cyanide bond (Fig. 59, right). Simple symmetry considerations allow one to predict ferromagnetic coupling for J_1 and J_2 (case of strict orhogonality between the interacting magnetic orbitals). Under ideal conditions (strict linearity of the two bridging cyanides and $\alpha = 0^\circ$), $J_1 = J_2$. As the value of α in $\{[Fe^{III}(phen)(CN)_4]_2Cu^{II}\}\cdot H_2O$ is 45°, J_2 is expected to be greater than J_1. The value of J_3 whatever its sign could be, has to be very small compared with those of J_1 and J_2 because of the weak spin density on the axial nitrogen–cyanide atom. Structural parameters such as the values of α and β will determine the sign of J_3.

The best set of computed coupling parameters were +61.1, +31.7 and +3.4 cm^{-1} for J_1, J_2 and J_3, respectively. The signs of the two former parameters are as expected but their respective values exhibit the opposite trend to that predicted. Most likely, the lower linearity of the Fe–C–N–Cu linkage corresponding to J_2 accounts for its weakening. The calculations show that J_3 is also ferromagnetic. Given that the value of β is close to 90°, even small deviations of γ from 90° would cause ferromagnetic interaction due to the strict orthogonality between the interacting magnetic orbitals. With these calculations in mind, the metamagnetic behavior of the double chains $\{[Fe^{III}(phen)(CN)_4]_2Cu^{II}\}\cdot H_2O$ and $\{[Fe^{III}(bipy)(CN)_4]_2Cu^{II}\}\cdot 2H_2O$ can be understood as a result of dipolar interchain interactions within the double chain motif. The short separation between the two parallel $Fe^{III}_2Cu^{II}$ chains and the large spin of each chain at low temperatures would allow the dipolar ineractions to overcome the very weak J_3 coupling. In summary, these two last metamagnetic compounds are additional examples of double nanowires, the very low value of the blocking temperatures being most likely due to the small anisotropy of the copper(II) ion.

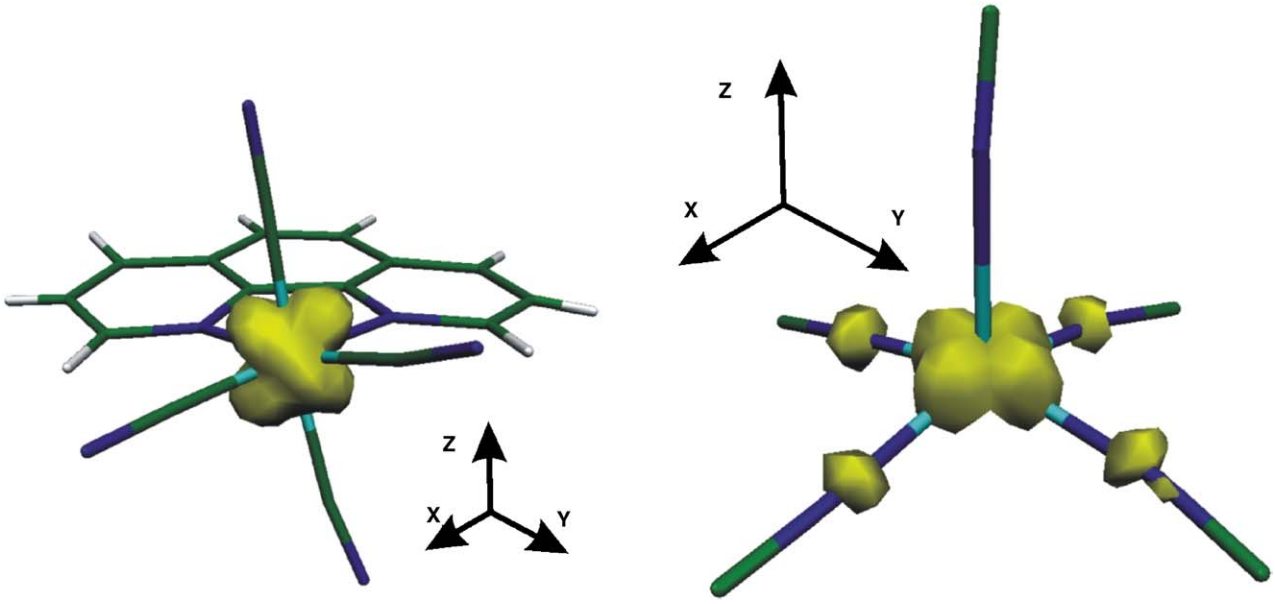

Fig. 58. Spin density maps for $[Fe^{III}(phen)(CN)_4]^-$ (left) and $[Cu^{II}(NC)_5]$ (right), the spin density (in electron units) being plotted with cutoff at 0.015 e. The values of the spin density for the iron unit are: +1.129 (Fe), −0.018 (N_{bipy}), −0.059 (C_{cyano}) and +0.038 (N_{cyano}) [average values are given for the atoms other than iron]. The values of the spin density at the copper unit are: +0.676 (Cu), +0.090 (equatorial N_{cyano}), −0.009 (equatorial C_{cyano}), +0.001 (axial N_{cyano}) and −0.002 (axial C_{cyano}) [average values are given for the atoms of the equatorially bound cyanide ligands]. Reprinted from Toma et al. [126]. Copyright© The Royal Society of Chemistry.

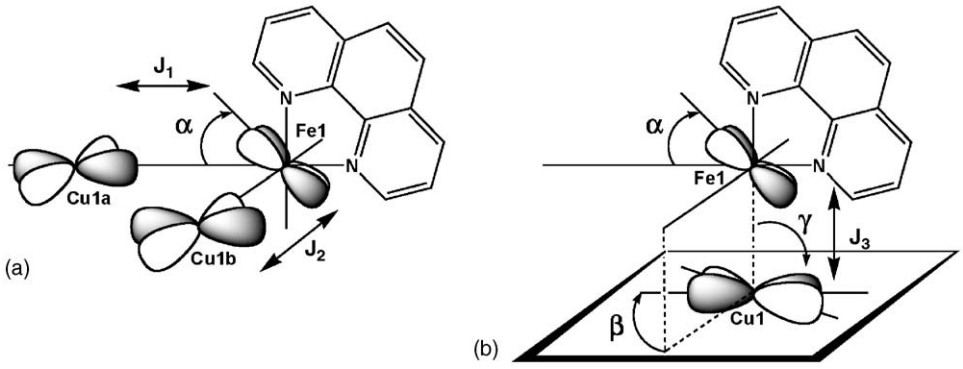

Fig. 59. Orbital pictures of fragments of $\{[Fe^{III}(phen)(CN)_4]_2Cu^{II}\}\cdot H_2O$: (a) in one of the two parallel chains showing the two exchange pathways through the equatorially bound cyanide to copper bonds; (b) between the two parallel chains through the axial cyanide to copper bond. Reprinted from Toma et al. [126]. Copyright ©The Royal Society of Chemistry.

5. Concluding remarks

In the present contribution we have shown how the use of specifically tailored cyano-bearing units of general formula $[M^{III}(L)(CN)_x]^{(x+l-m)-}$ (M = trivalent transition metal ion and L = polydentate blocking ligand) are suitable building blocks to design new magnetic objects whose nuclearity, topology and magnetic properties can be modulated. They are examples of how the creativity of the synthetic chemists in preparing new stable complexes that can be used as ligands is highly rewarding. Although the use of these building blocks as ligands in the cyanide research field is just at the beginning, their use as ligands has made possible the achievement of ferromagnetically coupled single (magnetic nanowires) and double (double magnetic nanowires) 4,2-ribbon like bimetallic chains which behave as SCMs, high-spin species and a large variety of low-dimensional heterometallic species exhibiting intramolecular ferro- and antiferromagnetic coupling. In the very near future, they will provide magnetochemists and scientists working in materials science with a large family of new metal assemblies with original molecular architectures and new spin toplogies.

Acknowledgements

This work is supported by the Spanish Ministry of Science and Technology (Project CTQ2004-03633), the Agencia Valenciana de Ciencia y Tecnología de la Generalitat Valencia (Grupos 03/19), the French CNRS through national research projects and the European Union through the projects MAGMANet (Contract 515767-2) and QueMolNa (MRTN-CT-2003-504880). Two of us (L.M.T. and F.S.D.) thank the Spanish Ministry of Education (L.M.T.) and the Gobierno Autónomo de Canarias for predoctoral fellowships. We are also grateful to the coworkers whose names appear in the references.

References

[1] K.R. Dunbar, R.A. Heintz, Prog. Inorg. Chem. 45 (1997) 283.
[2] M. Verdaguer, A. Bleuzen, V. Marvaud, J. Vaissermann, M. Seuleiman, C. Desplanches, A. Scuiller, C. Train, R. Garde, G. Gelly, C. Lomenech, I. Rosenman, P. Veillet, C. Cartier, F. Villain, Coord. Chem. Rev. 190–192 (1999) 1023.
[3] M. Ohba, H. Okawa, Coord. Chem. Rev. 198 (2000) 313.
[4] J. Cernák, M. Orendác, I. Potocnák, J. Chomic, A. Horendacová, J. Skorsepa, A. Feher, Coord. Chem. Rev. 224 (2002) 51.
[5] M. Pilkington, S. Decurtins, Comprehensive Coordination Chemistry II, in: J.A. MacCleverty, T.J. Meyer (Eds.), From Biology to Nanotechnology, Vol. 7, Elsevier, Amsterdam, 2004, p. 177.
[6] D.J. Darensbourg, A.L. Phelps, Inorg. Chim. Acta 357 (2004) 1603, and references therein.
[7] R. Brahmi, C. Kappenstein, J. Cernák, D. Duprez, A. Sadel, J. Phys. Chem. 96 (1999) 487.
[8] M. Kämper, M. Wagner, A. Weiss, Angew. Chem. 91 (1979) 517.
[9] D. William, J. Kouvetakis, M. O'Keefe, Inorg. Chem. 37 (1998) 4617.
[10] M.P. Shores, L.G. Beauvais, J.R. Long, J. Am. Chem. Soc. 121 (1999) 775.
[11] M.P. Shores, L.G. Beauvais, J.R. Long, Inorg. Chem. 38 (1999) 1648.
[12] M.V. Bennett, L.G. Beauvais, M.P. Shores, J.R. Long, J. Am. Chem. Soc. 123 (2001) 8022.
[13] K.K. Klausmeyer, T.B. Rauchfuss, S.R. Wilson, Angew. Chem. Int. Ed. 37 (1998) 1694.
[14] A.M.A. Ibrahim, Polyhedron 18 (1999) 2111.
[15] S. Ferrere, Chem. Mater. 12 (2000) 1083.
[16] T. Mallah, S. Thiébault, M. Verdaguer, P. Veillet, Science 262 (1993) 1554.
[17] S. Ferlay, T. Mallah, R. Ouhaès, P. Veillet, M. Verdaguer, Nature (London) 378 (1995) 701.
[18] R. Garde, F. Villain, M. Verdaguer, J. Am. Chem. Soc. 124 (2002) 10531.
[19] W.R. Entley, G.S. Girolami, Science 268 (1995) 397.
[20] S.M. Holmes, G.S. Girolami, J. Am. Chem. Soc. 121 (1999) 5593.
[21] Ø. Hatlevik, W.E. Buschmann, J. Zhang, J.L. Manson, J.S. Miller, Adv. Mater. 11 (1999) 914.
[22] O. Sato, T. Iyoda, A. Fujishima, K. Hashimoto, Science 271 (1996) 49.
[23] O. Sato, S. Hayami, Y. Einaga, Z.Z. Gu, Bull. Chem. Soc. Jpn. 76 (2003) 443.
[24] O. Sato, T. Iyoda, A. Fujishima, K. Hashimoto, Science 272 (1996) 704.
[25] Z.Z. Gu, O. Sato, T. Iyoda, K. Hashimoto, A. Fujishima, Chem. Mater. 9 (1997) 1082.
[26] A. Bleuzen, C. Lomenech, V. Escax, F. Villain, F. Varret, C. Cartier dit Moulin, M. Verdaguer, J. Am. Chem. Soc. 122 (2000) 6648.
[27] C. Cartier dit Moulin, F. Villain, A. Bleuzen, M.A. Arrio, P. Sainctavit, C. Lomenech, V. Escax, F. Baudelet, E. Dartyge, J.J. Gallet, M. Verdaguer, J. Am. Chem. Soc. 122 (2000) 6653.
[28] D.A. Pejakovic, J. Manson, J.S. Miller, A. Epstein, J. Phys. Rev. Lett. 85 (2000) 1994.
[29] V. Escax, A. Bleuzen, C. Cartier dit Moulin, F. Villain, A. Goujon, F. Varret, M. Verdaguer, J. Am. Chem. Soc. 123 (2001) 12536.

[30] G. Champion, V. Escax, C. Cartier dit Moulin, A. Bleuzen, F. Villain, F. Baudelet, E. Dartyge, M. Verdaguer, J. Am. Chem. Soc. 123 (2001) 12544.
[31] R. Garde, F. Villain, M. Verdaguer, J. Am. Chem. Soc. 124 (2002) 10531.
[32] M. Mizuno, S. Ohkoshi, K. Hashimoto, Adv. Mater. 12 (2000) 1855.
[33] S. Ohkoshi, M. Mizuno, G. Hung, K. Hashimoto, J. Phys. Chem. B 104 (2000) 8365.
[34] See ref. [2] and references therein.
[35] O. Kahn, Molecular Magnetism, VCH, New York, 1993.
[36] W. Dong, L.N. Zhu, H.B. Song, D.Z. Liao, Z.H. Jiang, S.P. Yan, P. Cheng, S. Gao, Inorg. Chem. 43 (2004) 2465.
[37] A.K. Sra, M. Andruh, O. Kahn, S. Golhen, L. Ouahab, J.V. Yakhmi, Angew. Chem. Int. Ed. 38 (1999) 2606.
[38] B. Nowicka, M. Hagiwara, Y. Wakatsuki, H. Kisch, Bull. Chem. Soc. Jpn. 72 (1999) 441.
[39] R. Kania, B. Sieklucka, Polyhedron 19 (2000) 2225.
[40] G. Rombaut, S. Golhen, L. Ouahab, C. Mathonière, O. Kahn, J. Chem. Soc., Dalton Trans. (2000) 3609.
[41] U. Schröder, F. Scholz, Inorg. Chem. 39 (2000) 1006.
[42] B. Sieklucka, J. Szklarzewicz, T.J. Kemp, W. Errington, Inorg. Chem. 39 (2000) 5156.
[43] G. Rombaut, C. Mathonière, P. Guionneau, S. Golhen, L. Ouahab, M. Verelst, P. Lecante, Inorg. Chim. Acta 326 (2001) 27.
[44] G. Rombaut, M. Verelst, S. Golhen, L. Ouahab, C. Mathonière, O. Kahn, Inorg. Chem. 40 (2001) 1151.
[45] J.M. Herrera, D. Armentano, G. De Munno, F. Lloret, M. Julve, M. Verdaguer, New J. Chem. 27 (2003) 128.
[46] P. Przychodzen, K. Lewinski, M. Balanda, R. Pelka, M. Rams, T. Wasiutynski, C. Guyard-Duhayon, B. Sieklucka, Inorg. Chem. 43 (2004) 2967.
[47] J. Larionova, M. Gross, M. Pilkington, H. Andres, H. Stoeckli-Evans, H.U. Güdel, S. Decurtins, Angew. Chem. Int. Ed. 39 (2000) 1605.
[48] F. Bonadio, M. Gross, H. Stoeckli-Evans, S. Decurtins, Inorg. Chem. 41 (2002) 5891.
[49] T. Korzeniak, R. Podgajny, N.W. Alcock, K. Lewinski, M. Balanda, T. Wasiutynski, B. Sieklucka, Polyhedron 22 (2003) 2183.
[50] B. Sieklucka, T. Korzeniak, R. Podgajny, M. Balanda, Y. Nakazawa, Y. Miyazaki, M. Soria, T. Wasiutynski, J. Magn. Magn. Mater. 272–276 (2004) 1058.
[51] Y.S. You, D. Kim, Y. Do, S.J. Oh, C.S. Hong, Inorg. Chem. 43 (2004) 6899.
[52] F.T. Chen, D.F. Li, S. Gao, X.Y. Wang, Y.Z. Li, L.M. Zheng, W.X. Tang, Dalton Trans. (2003) 3283.
[53] R. Podgajny, T. Korzeniak, K. Stadnicka, Y. Dromzée, N.W. Alcock, W. Errington, K. Kruczala, M. Balanda, T.J. Kemp, M. Verdaguer, B. Sieklucka, Dalton Trans. (2003) 3458.
[54] J.M. Herrera, A. Bleuzen, Y. Dromzée, M. Julve, F. Lloret, M. Verdaguer, Inorg. Chem. 42 (2003) 7052.
[55] Z.J. Zhong, H. Seino, Y. Mizobe, M. Hidai, A. Fujishima, S.I. Ohkshi, K. Hashimoto, J. Am. Chem. Soc. 122 (2000) 2952.
[56] Z.J. Zhong, H. Seino, Y. Mizobe, M. Hidai, M. Verdaguer, S.I. Ohkoshi, K. Hashimoto, Inorg. Chem. 39 (2000) 5095.
[57] D.F. Li, S. Gao, L.M. Zheng, W.I. Sun, T.A. Okamura, N. Ueyama, W.X. Tang, New J. Chem. 26 (2002) 485.
[58] D.F. Li, S. Gao, L.M. Zheng, K.B. Yu, W.X. Tang, New J. Chem. 26 (2002) 1190.
[59] Y. Arimoto, S.I. Ohkoshi, Z.J. Zhong, H. Seino, Y. Mizobe, K. Hashimoto, J. Am. Chem. Soc. 125 (2003) 9240.
[60] R. Pradhan, C. Desplanches, P. Guionneau, J.P. Sutter, Inorg. Chem. 42 (2003) 6607.
[61] J.M. Herrera, Ph.D. Thesis, University of Valencia, 2004.
[62] M.V. Bennett, J.R. Long, J. Am. Chem. Soc. 125 (2003) 2394.
[63] J. Larionova, R. Clérac, J. Sanchiz, O. Kahn, S. Golhen, L. Ouahab, J. Am. Chem. Soc. 120 (1998) 13088.
[64] O. Kahn, J. Larionova, L. Ouahab, Chem. Commun. (1999) 945.
[65] J. Larionova, O. Kahn, S. Golhen, L. Ouahab, R. Clérac, J. Am. Chem. Soc. 121 (1999) 3349.
[66] J. Larionova, O. Kahn, S. Golhen, L. Ouahab, R. Clérac, Inorg. Chem. 38 (1999) 3621.
[67] A.K. Sra, G. Rombaut, F. Lahitête, S. Golhen, L. Ouahab, C. Matonière, J.V. Yakhmi, O. Kahn, New J. Chem. 24 (2000) 871.
[68] J. Larionova, R. Clérac, B. Donnadieu, C. Guérin, Chem. Eur. J. 8 (2002) 2712.
[69] S. Tanase, F. Tuna, P. Guionneau, T. Maris, G. Rombaut, C. Mathonière, M. Andruh, O. Kahn, J.P. Sutter, Inorg. Chem. 42 (2003) 1625.
[70] X.F. Le Goff, S. Willemin, C. Coulon, J. Larionova, B. Donnadieu, R. Clérac, Inorg. Chem. 43 (2004) 4784.
[71] V. Marvaud, C. Decroix, A. Scuiller, C. Guyard-Duhayon, J. Vaissermann, F. Gonnet, M. Verdaguer, Chem. Eur. J. 9 (2003) 1678.
[72] V. Marvaud, C. Decroix, A. Scuiller, F. Tuyèras, C. Guyard-Duhayon, J. Vaissermann, J. Marrot, F. Gonnet, M. Verdaguer, Chem. Eur. J. 9 (2003) 1692.
[73] A. Scuiller, T. Mallah, M. Verdaguer, A. Nivorozkhin, J.L. Tholence, P. Veillet, New J. Chem. 20 (1996) 1.
[74] J.J. Sokol, A.G. Hee, J.R. Long, J. Am. Chem. Soc. 124 (2002) 7656.
[75] (a) C.P. Berlinguette, D. Vaughn, C. Cañada-Vilalta, J.R. Galán-Mascarós, K.R. Dunbar, Angew. Chem. Int. Ed. 42 (2003) 1523;
(b) A.V. Palii, S.M. Ostrovsky, S.I. Klokishner, B.S. Tsukerblat, C.P. Berlinguette, K.R. Dunbar, J.R. Galán-Mascarós, J. Am. Chem. Soc. 126 (2004) 16860.
[76] H.J. Choi, J.J. Sokol, J.R. Long, Inorg. Chem. 43 (2004) 1606.
[77] S. Wang, J.L. Zuo, H.C. Zhou, H.J. Choi, Y. Ke, J.R. Long, X.Z. You, Angew. Chem. Int. Ed. 43 (2004) 5940.
[78] D. Gatteschi, R. Sessoli, Angew. Chem. Int. Ed. 42 (2003) 269.
[79] J.M. Herrera, V. Marvaud, M. Verdaguer, J. Marrot, M. Kalisz, C. Mathonière, Angew. Chem. Int. Ed. 43 (2004) 5468.
[80] (a) K.K. Klausmeyer, S.R. Wilson, T.B. Rauchfuss, J. Am. Chem. Soc. 121 (1999) 2705;
(b) S.M. Contakes, K.K. Klausmeyer, T.B. Rauchfuss, Inorg. Chem. 39 (2000) 2069.
[81] (a) J.L. Heinrich, P.A. Berseth, J.R. Long, Chem. Commun. (1998) 1231;
(b) P.A. Berseth, J.J. Sokol, M.P. Shores, J.L. Heinrich, J.R. Long, J. Am. Chem. Soc. 122 (2000) 9655;
(c) J.J. Sokol, M.P. Shores, J.R. Long, Angew. Chem. 113 (2001) 236;
(d) M.P. Shores, J.J. Sokol, J.R. Long, J. Am. Chem. Soc. 124 (2002) 2279;
(e) J.J. Sokol, M.P. Shores, J.R. Long, Inorg. Chem. 41 (2002) 3052;
(f) J.Y. Yang, M.P. Shores, J.J. Sokol, J.R. Long, Inorg. Chem. 42 (2003) 1403.
[82] (a) H. Oshio, O. Tamada, H. Onodera, T. Ito, T. Ikoma, S.T. Kubota, Inorg. Chem. 38 (1999) 5686;
(b) H. Oshio, H. Onodera, O. Tamada, H. Mizutani, T. Hikichi, T. Ito, Chem. Eur. J. 6 (2000) 2523;
(c) H. Oshio, M. Yamamoto, T. Ito, Inorg. Chem. 41 (2002) 5817.
[83] Z.N. Chen, R. Appelt, H. Vahrenkamp, Inorg. Chim. Acta 309 (2000) 65.
[84] J.A. Smith, J.R. Galán-Mascarós, R. Clérac, J.S. Sun, X. Ouyang, K.R. Dunbar, Polyhedron 20 (2001) 1727.
[85] (a) W.F. Yeung, W.L. Man, W.T. Wong, T.C. Lau, S. Gao, Angew. Chem. Int. Ed. 40 (2001) 3031;
(b) Y.Z. Zhang, S. Gao, H.L. Sun, G. Su, Z.M. Wang, S.W. Zhang, Chem. Commun. (2004) 1906;
(c) S. Wang, J.L. Zuo, S. Gao, Y. Song, H.C. Zhou, Y.Z. Zhang, X.Z. You, J. Am. Chem. Soc. 126 (2004) 8900.
[86] (a) R. Lescouëzec, F. Lloret, M. Julve, J. Vaissermann, M. Verdaguer, R. Llusar, S. Uriel, Inorg. Chem. 40 (2001) 2065;
(b) R. Lescouëzec, F. Lloret, M. Julve, J. Vaissermann, M. Verdaguer, Inorg. Chem. 41 (2002) 818;
(c) L.M. Toma, R. Lescouëzec, L.D. Toma, F. Lloret, M. Julve, J. Vaissermann, M. Andruh, J. Chem. Soc., Dalton Trans. (2002) 3171;
(d) R. Lescouëzec, J. Vaissermann, F. Lloret, M. Julve, M. Verdaguer, Inorg. Chem. 41 (2002) 5943;
(e) R. Lescouëzec, J. Vaissermann, L.M. Toma, R. Carrasco, F. Lloret, M. Julve, Inorg. Chem. 43 (2004) 2234;

(f) L. Toma, R. Lescouëzec, J. Vaissermann, F.S. Delgado, C. Ruiz-Pérez, R. Carrasco, J. Cano, F. Lloret, M. Julve, Chem. Eur. J. 10 (2004) 6130;
(g) L. Toma, R. Lescouëzec, J. Vaissermann, P. Herson, V. Marvaud, F. Lloret, M. Julve, New J. Chem. 29 (2005) 210.
[87] J. Kim, S. Han, I.K. Cho, K.Y. Choi, M. Heu, S. Yoon, B.J. Suh, Polyhedron 23 (2004) 1333.
[88] D.J. Darensbourg, A.L. Phelps, Inorg. Chim. Acta 357 (2004) 1603.
[89] H. Ojima, K. Nonoyama, Coord. Chem. Rev. 92 (1988) 85.
[90] O. Kahn, Adv. Inorg. Chem. 43 (1995) 179.
[91] R. Ruiz, J. Faus, F. Lloret, M. Julve, Y. Journaux, Coord. Chem. Rev. 193–195 (1999) 1069.
[92] J. Cano, E. Ruiz, P. Alemany, F. Lloret, S. Alvarez, J. Chem. Soc., Dalton Trans. (1999) 1669.
[93] (a) I. Fernández, R. Ruiz, J. Faus, M. Julve, F. Lloret, J. Cano, X. Ottenwaelder, Y. Journaux, M.C. Muñoz, Angew. Chem. 113 (2001) 3129;
(b) E. Pardo, J. Faus, M. Julve, F. Lloret, M.C. Muñoz, J. Cano, X. Ottenwaeder, Y. Journaux, R. Carrasco, G. Blay, I. Fernández, R. Ruiz-García, J. Am. Chem. Soc. 125 (2003) 10770;
(c) E. Pardo, K. Bernot, M. Julve, F. Lloret, J. Cano, R. Ruiz-García, F.S. Delgado, C. Ruiz-Pérez, X. Ottenwaelder, Y. Journaux, Inorg. Chem. 43 (2004) 2768;
(d) E. Pardo, K. Bernot, M. Julve, F. Lloret, J. Cano, R. Ruiz-García, J. Pasán, C. Ruiz-Pérez, X. Ottenwaelder, Y. Journaux, Chem. Commun. (2004) 920;
(e) E. Pardo, R. Ruiz-García, F. Lloret, J. Faus, M. Julve, Y. Journaux, F. Delgado, C. Ruiz-Pérez, Adv. Mater. 16 (2004) 1597.
[94] (a) H. Tamaki, Z.J. Zhong, N. Matsumoto, S. Kida, M. Koikawa, N. Achiwa, Y. Hashimoto, H. Okawa, J. Am. Chem. Soc. 114 (1992) 6974;
(b) S.G. Carling, C. Mathonière, P. Day, K.M. Abdul Malik, S.J. Coles, M.B. Hursthouse, J. Chem. Soc., Dalton Trans. (1996) 1839;
(c) C. Mathonière, C.J. Nuttal, S.G. Carlin, P. Day, Inorg. Chem. 35 (1996) 1201;
(d) P. Day, J. Chem. Soc., Dalton Trans. (1997) 701.
[95] (a) L.O. Atovmyan, G.V. Shilov, R.N. Lyubovskaya, E.I. Zhilyaeva, N.S. Ovanesyan, S.I. Pirumova, G. Gusakovskaya, JEPT Lett. 58 (1993) 766;
(b) J. Larionova, B. Mombelli, J. Sanchiz, O. Kahn, Inorg. Chem. 37 (1998) 679.
[96] (a) S. Decurtins, H.W. Schmalle, P. Schneuwly, H.R. Oswald, Inorg. Chem. 32 (1993) 1888;
(b) S. Decurtins, H.W. Schmalle, H.R. Oswald, A. Linden, J. Ensling, P. Gütlich, A. Hauser, Inorg. Chim. Acta 216 (1994) 65;
(c) S. Decurtins, H.W. Schmalle, P. Schneuwly, J. Ensling, P. Gütlich, J. Am. Chem. Soc. 116 (1994) 9521;
(d) S. Decurtins, H.W. Schmalle, R. Pellaux, P. Schneuwly, A. Hauser, Inorg. Chem. 35 (1996) 1451;
(e) S. Decurtins, H.W. Schmalle, R. Pellaux, R. Huber, P. Fisher, B. Ouladdiaf, Adv. Mater. 8 (1996) 647;
(f) R. Pellaux, H.W. Schmalle, R. Huber, P. Fischer, T. Hauss, B. Ouladdiaf, S. Decurtins, Inorg. Chem. 36 (1997) 2301;
(g) S. Decurtins, M. Gross, H.W. Schmalle, S. Ferlay, Inorg. Chem. 37 (1998) 2443;
(h) S. Decurtins, S. Ferlay, R. Pellaux, M. Gross, H. Schmalle, Supramolecular engineering of synthetic metallic materials, in: J. Veciana, C. Rovira, D.B. Amabilino (Eds.), NATO ASI Ser. C518, Kluwer, Dordrecht, 1999, p. 175;
(i) M. Hernández-Molina, F. Lloret, C. Ruiz-Pérez, M. Julve, Inorg. Chem. 37 (1998) 4131.
[97] (a) R. Andrés, M. Gruselle, B. Malézieux, M. Verdaguer, J. Vaissermann, Inorg. Chem. 38 (1999) 4637;
(b) R. Andrés, M. Brissard, M. Gruselle, C. Train, J. Vaissermann, B. Malézieux, J.P. Jamet, M. Verdaguer, Inorg. Chem. 40 (2001) 4633.
[98] (a) E. Coronado, J.R. Galán-Mascarós, C.J. Gómez-García, J.M. Martínez-Agudo, Adv. Mater. 11 (1999) 558;
(b) E. Coronado, J.R. Galán-Mascarós, C.J. Gómez-Gracía, V. Laukhin, Nature 408 (2000) 447;
(c) E. Coronado, J.R. Galán-Mascarós, C.J. Gómez-García, J. Ensling, P. Gütlich, Chem. Eur. J. 6 (2000) 552;
(d) E. Coronado, J.R. Galán-Mascarós, C.J. Gómez-García, J.M. Martínez-Agudo, Inorg. Chem. 40 (2001) 113.
[99] R. Clément, S. Decurtins, M. Gruselle, C. Train, Monatsch. Chem. 134 (2003) 1.
[100] (a) R.J. Parker, L. Spiccia, K.J. Berry, G.D. Fallon, B. Moubaraki, K.S. Murria, Chem. Commun. (2001) 333;
(b) H.Z. Kou, S. Gao, O. Bai, Z.M. Wang, Inorg. Chem. 40 (2001) 6287;
(c) M.S. El Fallah, J. Ribas, X. Solans, M. Font-Bardía, J. Chem. Soc., Dalton Trans. (2001) 247;
(d) H.Z. Kou, B.C. Zhou, S. Gao, R.J. Wang, Angew. Chem. Int. Ed. 42 (2003) 3288;
(e) K. Inoue, K. Kikuchi, M. Ohba, H. Okawa, Angew. Chem. Int. Ed. 42 (2003) 4810;
(f) X.P. Shen, S. Gao, G. Yin, K.B. Yu, Z. Xu, New J. Chem. 28 (2004) 996.
[101] (a) R.J. Parker, L. Spiccia, S.R. Batten, J.D. Casio, G.D. Fallon, Inorg. Chem. 40 (2001) 4696;
(b) N. Mondal, S. Mitra, G. Rosair, Polyhedron 20 (2001) 2473;
(c) E. Colacio, M. Ghazi, H. Stoeckli-Evans, F. Lloret, J.M. Moreno, C. Pérez, Inorg. Chem. 40 (2001) 4876;
(d) F. Bellouard, M. Clemente-León, E. Coronado, J.R. Galán-Mascarós, C.J. Gómez-García, F. Romero, K.R. Dunbar, Eur. J. Inorg. Chem. (2002) 1603;
(e) H.Z. Kou, B.C. Zhou, D.Z. Liao, R.J. Wang, Y. Li, Inorg. Chem. 41 (2002) 6887;
(f) Y.P. Shek, W.T. Wong, S. Gao, T.C. Lau, New J. Chem. 26 (2002) 1099;
(g) S. Tanase, M. Andruh, M. Stanica, C. Mathonière, G. Rombaut, S. Goleen, L. Ouahab, Polyhedron 22 (2003) 1315;
(h) J.E. Koo, D.H. Kim, Y.S. Kim, Y. Do, Inorg. Chem. 42 (2003) 2983;
(i) C.P. Berlinguette, J.R. Galán-Mascarós, K.R. Dunbar, Inorg. Chem. 42 (2003) 3416;
(j) H. Miyasaka, H. Ieda, N. Matsumoto, K.I. Sugiura, M. Yamashita, Inorg. Chem. 42 (2003) 3509;
(k) E. Colacio, J.M. Domínguez-Vera, F. Lloret, A. Rodríguez, H. Stoeckli-Evans, Inorg. Chem. 42 (2003) 6962;
(l) M.K. Saha, F. Lloret, I. Bernal, Inorg. Chem. 43 (2004) 1969;
(m) P. Alborés, L.D. Slep, T. Weyhermüller, L.M. Baraldo, Inorg. Chem. 43 (2004) 6762;
(n) C.S. Hong, Y.S. You, Inorg. Chim. Acta 357 (2004) 3271.
[102] (a) J. Bendix, P. Steenberg, I. Stofte, Inorg. Chem. 42 (2003) 4510;
(b) I.P.Y. Shek, W.F. Yeung, T.C. Lau, J. Zhang, S. Gao, L. Szeto, W.T. Wong, Eur. J. Inorg. Chem. 2 (2005) 364.
[103] V. Marvaud, J.M. Herrera, T. Barrilero, F. Tuyeras, R. Garde, A. Scuiller, C. Decroix, M. Cantuel, C. Desplanches, Monastch. Chem. 134 (2003) 149.
[104] T.H. Lu, H.Y. Kao, D.I. Wu, K.C. Kong, C.H. Cheng, Acta Crystallogr. C44 (1988) 1184.
[105] J.C. Revee, J. Chem. Educ. 62 (1985) 44.
[106] L.M. Toma, J. Vaissermann, F. Lloret, M. Julve, in preparation.
[107] A.A. Schildt, J. Am. Chem. Soc. 82 (1960) 3000.
[108] L.M. Toma, J. Vaissermann, F. Lloret, M. Julve, in preparation.
[109] L.M. Toma, J. Vaissermann, F. Lloret, M. Julve, in preparation.
[110] L.M. Toma, C. Ruiz, F. Lloret, M. Julve, in preparation.
[111] K. Wieghardt, W. Schmidt, W. Herrmann, H.J. Küppers, Inorg. Chem. 22 (1983) 2953.
[112] C.K. Ryu, R.B. Lessard, D. Lynch, J.F. Endicott, J. Phys. Chem. 93 (1989) 1752.
[113] L.M. Toma, R. Lescouëzec, C. Ruiz-Pérez, F. Lloret, M. Julve, in preparation.
[114] S. Trofimenko, Inorg. Synth. 12 (1970) 1254.
[115] T. Kajiwara, T. Ito, Acta Crystallogr. C56 (2000) 22.

[116] A. Kamiyama, T. Noguchi, T. Kajiwara, T. Ito, Inorg. Chem. 41 (2002) 507.
[117] M. Verdaguer, Polyhedron 20 (2001) 1115.
[118] F. Lloret, R. Ruiz, M. Julve, J. Faus, Y. Journaux, I. Castro, M. Verdaguer, Chem. Mater. 4 (1992) 1150.
[119] R.L. Carlin, Magnetochemistry, Springer, Berlin, 1986, p 148.
[120] D. Armentano, G. De Munno, F. Lloret, A.V. Palii, M. Julve, Inorg. Chem. 41 (2002) 2007.
[121] S. Ferrer, F. Lloret, I. Bertomeu, G. Alzuet, J. Borrás, S. García-Granda, M. Liu-González, J.G. Haasnoot, Inorg. Chem. 41 (2002) 5851.
[122] B.S. Tsukerblat, M.I. Belinskii, V.E. Fainzil'berg, Sov. Sci. Rev. B Chem. 8 (1987) 337.
[123] R. Lescouëzec, Rosa Lllusar, F. Lloret, M. Julve, in preparation.
[124] L.M. Toma, J. Vaissermann, F. Lloret, M. Julve, in preparation.
[125] L. Toma, L.M. Toma, R. Lescouëzec, D. Armentano, G. De Munno, M. Andruh, J. Cano, F. Lloret, M. Julve, Dalton Trans. (2005) 1357.
[126] L.M. Toma, F.S. Delgado, C. Ruiz-Pérez, R. Carrasco, J. Cano, F. Lloret, M. Julve, Dalton Trans. (2004) 2836.
[127] R. Lescouëzec, J. Vaissermann, C. Ruiz-Pérez, F. Lloret, R. Carrasco, M. Julve, M. Verdaguer, Y. Dromzee, D. Gatteschi, W. Wernsdorfer, Angew. Chem. Int. Ed. 42 (2003) 1483.
[128] L.M. Toma, R. Lescouëzec, F. Lloret, M. Julve, J. Vaissermann, M. Verdaguer, Chem. Commun. (2003) 1850.
[129] O. Kahn, Struct. Bonding (Berlin) 68 (1987) 89.
[130] R. Lescouëzec, R. Llusar, S. Uriel, F. Lloret, M. Julve, in preparation.
[131] R. Lescouëzec, R. Llusar, S. Uriel, F. Lloret, M. Julve, in preparation.
[132] (a) G. De Munno, R. Ruiz, F. Lloret, J. Faus, R. Sessoli, M. Julve, Inorg. Chem. 34 (1995) 408;
(b) G. De Munno, T. Poerio, M. Julve, F. Lloret, G. Viau, A. Caneschi, J. Chem. Soc., Dalton Trans. (1997) 601;
(c) G. De Munno, G. Viau, M. Julve, F. Lloret, J. Faus, Inorg. Chim. Acta 257 (1997) 121.
[133] P. Román, C. Guzmán-Miralles, A. Luque, J.I. Beitia, J. Cano, F. Lloret, M. Julve, S. Alvarez, Inorg. Chem. 35 (1996) 3741.
[134] A. Rodríguez-Fortea, P. Alemany, S. Alvarez, E. Ruiz, A. Scuiller, C. Decroix, V. Marvaud, J. Vaissermann, M. Verdaguer, I. Rosenman, M. Julve, Inorg. Chem. 40 (2001) 5868.
[135] R. Lescouëzec, R. Llusar, S. Uriel, F. Lloret, M. Julve, in preparation.
[136] L.M. Toma, C. Ruiz, F. Delgado, F. Lloret, M. Julve, in preparation.
[137] L.M. Toma, R. Lescouëzec, J. Pasán, C. Ruiz-Pérez, J. Vaissermann, J. Cano, R. Carrasco, W. Wernsdorfer, F. Lloret, M. Julve, J. Am. Chem. Soc., submitted for publication.
[138] R. Lescouëzec, S. Uriel, R. Llusar, F. Lloret, M. Julve, in preparation.
[139] R. Lescouëzec, D. Armentano, G. De Munno, F. Lloret, M. Julve, in preparation.
[140] R. Lescouëzec. L.M. Toma, C. Ruiz-Pérez, J. Pasán, F. Lloret, M. Julve, in preparation.
[141] R. Ruiz, J. Faus, F. Lloret, M. Julve, Y. Journaux, Coord. Chem. Rev. 193–195 (1999) 1069, and references therein.
[142] O. Rotthaus, S. Le Roy, A. Tomas, K.M. Barkigia, I. Artaud, Inorg. Chim. Acta 357 (2004) 2211.
[143] F.M. Crean, K. Schug, Inorg. Chem. 23 (1984) 853.
[144] R. Lescouëzec, F. Khöeler, Angew. Chem. Int. Ed. 43 (2004) 2571.
[145] T. Hasegawa, T.C. Lau, H. Taube, W.P. Schaefer, Inorg. Chem. 30 (1991) 2921.
[146] L.M. Toma, L.D. Toma, F.S. Delgado, C. Ruiz-Pérez, J. Sletten, J. Cano, J.M. Clemente-Juan, F. Lloret, M. Julve, Coord. Chem. Rev., in press.
[147] R.E.P. Winpenny, Adv. Inog. Chem. 52 (2001) 1.
[148] D. Gatteschi, L. Sorace, J. Solid State Chem. 159 (2001) 253.
[149] N.E. Chakov, W. Wernsdorfer, K.A. Abboud, D.N. Hendrickson, G. Christou, Dalton Trans. (2003) 2243.
[150] E.C. Sañudo, W. Wernsdorfer, K.A. Abboud, G. Christou, Inorg. Chem. 43 (2004) 4137.
[151] M. Murugesu, J. Raftery, W. Wernsdorfer, G. Christou, E.K. Brechin, Inorg. Chem. 43 (2004) 4203.
[152] S.T. Ochsenbein, M. Murrie, E. Rusanov, H. Stoeckli-Evans, C. Sekine, H.U. Gudel, Inorg. Chem. 41 (2002) 5133.
[153] E. Coronado, A. Forment-Aliaga, A. Gaita-Ariño, C. Jiménez-Saiz, F.M. Romero, W. Wernsdorfer, Angew. Chem. Int. Ed. 43 (2004) 6152.
[154] E. Pardo, I.M. Osorio, M. Julve, F. Lloret, J. Cano, R. Ruiz-García, J. Pasán, C. Ruiz-Pérez, X. Ottenwaelder, Y. Journaux, Inorg. Chem. 43 (2004) 7594.
[155] S. Osa, T. Kido, N. Matsumoto, N. Re, A. Pochaba, J. Mrozinski, J. Am. Chem. Soc. 126 (2004) 420.
[156] C.M. Zaleski, E.C. Depperman, J.W. Kampf, M.L. Kirk, V.L. Pecoraro, Angew. Chem. Int. Ed. 43 (2004) 3912.
[157] A. Mishra, W. Wernsdorfer, K.A. Abboud, G. Christou, J. Am. Chem. Soc. 126 (2004) 15648.
[158] H. Miyasaka, R. Clérac, W. Wernsdorfer, L. Lecren, C. Bonhomme, K.I. Sugiura, M. Yamashita, Angew. Chem. Int. Ed. 43 (2004) 2801.
[159] (a) A. Caneschi, D. Gatteschi, R. Sessoli, P. Rey, Acc. Chem. Res. 22 (1989) 392;
(b) A. Caneschi, D. Gatteschi, P. Rey, Prog. Inorg. Chem. 39 (1991) 331.
[160] R.J. Glauber, J. Math. Phys. 4 (1963) 294.
[161] A. Caneschi, D. Gatteschi, N. Lalioti, C. Sangregorio, R. Sessoli, G. Venturi, A. Vindigni, A. Rettori, M.G. Pini, M.A. Novak, Angew. Chem. Int. Ed. 40 (2001) 1760.
[162] A. Caneschi, D. Gatteschi, N. Lalioto, R. Sessoli, L. Sorace, V. Tangoulis, A. Vindigni, Chem. Eur. J. 8 (2002) 286.
[163] A. Caneschi, D. Gatteschi, N. Lalioti, C. Sangregorio, R. Sessoli, G. Venturi, A. Vindigni, A. Rettori, M.G. Pini, M.A. Novak, Europhys. Lett. 58 (2002) 771.
[164] L. Bogan, A. Caneschi, M. Fedi, D. gatteschi, M. Massi, M.A. Novak, M.G. Pini, A. Rettori, R. Sessoli, A. Vindigni, Phys. Rev. Lett. 90 (20) (2004) 207204.
[165] K.S. Cole, R.H. Cole, J. Chem. Phys. 9 (1941) 341.
[166] C. Dekker, A.F.M. Arts, H.W. Wijn, A.J. Van Duyneveldt, J.A. Mydosh, Phys. Rev. B 40 (1989) 11243.
[167] A. Caneschi, D. Gatteschi, P. Rey, R. Sessoli, Inorg. Chem. 30 (1991) 3936.
[168] R. Clérac, H. Miyasaka, M. Yamashita, C. Coulon, J. Am. Chem. Soc. 124 (2002) 12387.
[169] H. Miyasaka, R. Clérac, K. Mizushima, K.I. Sugiura, M. Yamashita, W. Wernsdorfer, C. Coulon, Inorg. Chem. 42 (2003) 8203.
[170] T.F. Liu, D. Fu, S. Gao, Y.Z. Zhang, H.L. Sun, G. Su, Y.J. Liu, J. Am. Chem. Soc. 125 (2003) 13976.
[171] J. Ribas, A. Escuer, M. Monfort, R. Vicente, R. Cortés, L. Lezama, T. Rojo, Corrd. Chem. Rev. 193–195 (1999) 1027, and references therein.
[172] P.J. Van Kroningsbruggen, O. Kahn, K. Nakatani, Y. Pei, J.P. Renard, M. Drillon, P. Legoll, Inorg. Chem. 29 (1990) 3325.
[173] N.E. Chakov, W. Wernsdorfer, K.A. Abboud, G. Christou, Inorg. Chem. 43 (2004) 5919.
[174] H.J. Gerritsen, E.S. Sabisky, Phys. Rev. 132 (1963) 1507.
[175] M. Ferbinteanu, H. Miyasaka, W. Wernsdorfer, K. Nakata, K.I. Sugiura, M. Yamashita, C. Coulon, R. Clérac, J. Am. Chem. Soc. 127 (2005) 3090.
[176] (a) G. De Munno, M. Julve, F. Lloret, J. Faus, A. Caneschi, J. Chem. Soc., Dalton Trans. (1994) 1175;
(b) J. Brunzelle, A. Fitch, Y. Wang, S.F. Pavkovic, Acta Crystallogr. C 52 (1996) 2984.
[177] P.V. Bernhardt, B.P. Macpherson, M. Martínez, Inorg. Chem. 39 (2000) 5203.